

**EXAMINING THE BINDING OF RADIONUCLIDES WITH MARINE
BIOPOLYMERS, A COMPARATIVE STUDY ON TH, PA, BE, PO AND PB
ISOTOPES**

A Dissertation

by

CHIA-YING CHUANG

Submitted to the Office of Graduate and Professional Studies of
Texas A&M University
in partial fulfillment of the requirements for the degree of

DOCTOR OF PHILOSOPHY

Chair of Committee,
Committee Members,

Head of Department,

Peter H. Santschi
Antonietta Quigg
Bruce Herbert
Thomas Bianchi
Rkgtu'Ej cr o cp

December 2013

Major Subject: Oceanography

Copyright 2013 Chia-Ying Chuang

ABSTRACT

Natural radioisotopes, Th, Pa, Pb, Po and Be, have been used as important proxies in oceanographic investigations for decades. Biopolymers, produced by both phytoplankton and bacteria, play an important role in the scavenging of these radionuclides, thus regulating the particulate organic carbon (POC)/isotope ratios in different oceanographic regions, which have been used to calculate POC flux.

To study the binding mechanisms of colloidal organic material to these radionuclides, marine colloids isolated by cross-flow ultrafiltration from seawater, together with dissolved exopolymeric substances (EPS) produced by laboratory cultured diatoms were collected. By separating, identifying and characterizing radiolabeled organic carriers, the most efficient binding of many of these nuclides likely occurs to acid polysaccharide- and Fe-related protein-containing biomolecules.

To differentiate between uptake to amorphous silica or associated biopolymers, radionuclides were incubated with diatom cultures of *Phaeodactylum tricoratum*. Partition coefficients (K_d) of radionuclides to different fractions of diatom cells, and the role of diatom related biopolymers were examined. More than 50% of selected radionuclides were bound to all-inclusive biopolymer fractions, and $\log K_d$ values of radioisotopes to whole diatom cells with or without silica frustules were similar, but $\log K_d$ values for cleaned silica frustules were orders of magnitude lower. Results from isoelectric focusing showed the most efficient binding sites occurring in acid-polysaccharides and iron-binding proteins. As revealed by 2D HSQC NMR spectra, the

biopolymers in the HF insoluble fraction were mainly composed of carboxyl-rich, aliphatic-phosphoproteins.

The concentrations of potential carrier phases for radionuclides and their K_d values were determined for particles collected by sediment traps deployed at the Oceanic Flux Program site off Bermuda. Chemical considerations, as well as factor analysis and correlations of $\log K_d$ values with chemical parameters, indicate that hydroxamate-siderophores (HS) are major classes of biopolymers that have a role in binding Po and Pa. MnO_2 and FeO_2 , whose presence is closely related to that of HS, are also involved in binding of Pa and Po. The carbonate and biogenic silica phases are identified to be important in predicting removal and fractionation of Th and Be in the ocean.

DEDICATION

To my parents

ACKNOWLEDGEMENTS

I would like to express my greatest appreciation to my committee chair, Dr. Peter Santschi, for his generous support, encouragements, and endless knowledgeable advices, guiding and enlightening me the way of science research. I am also deeply grateful to my committee member at Galveston, Dr. Antonietta Quigg, for her advice, comments, and immeasurable supports to my needs in this research. My grateful thanks also go out to my committee members at College Station, Dr. Bruce Herbert and Dr. Thomas Bianchi, for their guidance throughout this study.

I am also thankful for my outstanding colleagues, Dr. Kathy Schwehr, Dr. Saijin Zhang, Dr. Chen Xu, Dr. Hsiu-Ping Li, Dr. Yuelu Jiang, Yi-Fang Ho, and people in the LOER lab for their kind helps and friendships. Special thanks also go to Dr. Yuan-Hui Li, Dr. Liang-Saw Wen, Dr. Laodong Guo, Dr. Chin-Chang Hung, Dr. Maureen Conte and Dr. Dorothea Schumann, from for their significant advice and supports on this research.

I would like to also express my deep gratitude to Sherry Parker, Mary Howley, Nicole Kinslow, Holly Richard, Missy Mathews and Wendy Gamble, and other staff in Department of Marine Sciences at Texas A&M University at Galveston and Department of Oceanography at Texas A&M University, who helped me a lot throughout my study.

This research was supported by grants from the National Science Foundation (OCE#0851191). My grateful thanks also go for the financial support through Sharps Fellowships from Department of Oceanography, Texas A&M University.

Finally, wholehearted thanks to my dearest family and friends for their selfless and endless love at all time.

TABLE OF CONTENTS

	Page
ABSTRACT	ii
DEDICATION	iv
ACKNOWLEDGEMENTS	v
TABLE OF CONTENTS	vii
LIST OF FIGURES.....	ix
LIST OF TABLES	xii
CHAPTER I INTRODUCTION	1
1.1 Background	1
1.2 Hypothesis and objectives.....	12
CHAPTER II ORGANIC LIGANDS FOR STRONGLY BINDING IONS OF RADIONUCLIDES, Th, Pa, Pb, Po AND Be, IN COLLOIDAL MACROMOLECULES IN THE OCEAN	14
2.1 Overview	14
2.2 Introduction.....	15
2.3 Material and methods.....	18
2.4 Results and discussion.....	26
2.5 Conclusions	38
CHAPTER III ROLE OF DIATOMS IN THE SCAVENGING OF PARTICLE REACTIVE RADIONUCLIDES, Th, Pa, Pb, Po AND Be, IN THE OCEAN: A CASE STUDY WITH <i>PHAEODACTYLUM TRICORNUTUM</i>	40
3.1 Overview	40
3.2 Introduction.....	41
3.3 Methods and materials	44
3.4 Results.....	50
3.5 Discussion	61
3.6 Conclusion.....	67
CHAPTER IV THE MOLECULAR LEVEL CHARACTERIZATION OF ORGANIC CARRIERS OF Th, Pa, Pb AND Be RADIONUCLIDES FROM DIATOM FRUSTULES	69

4.1 Overview	69
4.2 Introduction	70
4.3 Materials and methods	72
4.4 Results and discussion.....	79
4.5 Conclusions	90
CHAPTER V ROLE OF BIOPOLYMERS AS MAJOR CARRIER PHASES OF Th, Pa, Pb, Po, AND Be RADIONUCLIDES IN SETTLING PARTICLES FROM THE ATLANTIC OCEAN	91
5.1 Overview	91
5.2 Introduction	92
5.3 Methods	95
5.4 Results	108
5.5 Discussion	121
5.6 Conclusions	134
CHAPTER VI SUMMARY	136
REFERENCEU.....	140

LIST OF FIGURES

FIGURE	Page
1.1 A conceptual diagram showing how the pathways of particle reactive radionuclides interact with the carbon flux in the ocean.	1
1.2 Conceptual flow diagram that details the proposed work.	4
2.1 Percentage distribution of amino acid groups in marine colloids and diatom extracted EPS.	31
2.2 Results from Isoelectric focusing electrophoresis of a) ^{234}Th ; b) ^{233}Pa ; c) ^{210}Pb ; d) ^{210}Po and e) ^7Be radiolabeled EPS and colloids.	36
2.3 Percentage distribution of a) Proteins (mg/g); b) total carbohydrates (TCHO, mg/g); c) Fe contents (ppb) in isoelectric focusing electrophoresis of radiolabeled EPS and colloids.	37
3.1 a) Comparisons of $\log K_d$ values of ^{234}Th , ^{233}Pa , ^{210}Pb , ^{210}Po and ^7Be on different type of particles, including pure silica, acid cleaned diatom frustule (w/ $\text{OC}\% < 0.1$), diatom cell with or without Si frustule; b) Variations in $\log K_d$ values of ^{234}Th , ^{233}Pa , ^{210}Pb , ^{210}Po and ^7Be with the four different types of particles.	51
3.2 ATR-FTIR spectra of different EPS samples extracted from diatom, <i>Phaeodactylum tricornutum</i> . a) EPS Si+ and b) EPS Si-. c) The difference FTIR spectrum (by EPS Si- minus EPS Si+). Arrows indicate the signature bands of amide I ($1652\text{-}1648\text{ cm}^{-1}$), amide II ($1550\text{-}1548\text{ cm}^{-1}$) and carbohydrate ($800\text{-}1200\text{ cm}^{-1}$).	55
3.3 Variation of concentrations of classified amino acid groups between a) EPS Si+ and b) EPS Si-.	56
3.4 Size distribution pattern of proteins in EPS Si+ and EPS Si- harvested from <i>P. tricornutum</i> grown in seawater media with and without Si respectively. (Lane 1: EPS Si+; Lane 2: EPS Si-; Lane 3: standard molecular weight markers).	57
3.5 Isoelectric focusing (IEF) electrophoresis of radiolabeled EPS Si+ and EPS Si- harvested from <i>P. tricornutum</i> grown in seawater media with and without Si respectively: a) ^{234}Th , b) ^{233}Pa , c) ^{210}Po , d) ^{210}Pb and e) ^7Be . Note: y-axis is specific to percentage of each radionuclide measured.	58

3.6 Percentage distribution of a) proteins (mg/g); b) total polysaccharides (mg/g); c) Fe (ppb) content in Isoelectric focusing (IEF) electrophoresis of ^{234}Th , ^{233}Pa , ^{210}Pb , ^{210}Po and ^7Be radiolabeled EPS Si+ and EPS Si- harvested from <i>P. tricornutum</i> grown in seawater media with and without Si respectively.	60
4.1 Scheme of chemical separation of individual biopolymers responsible for binding of different radionuclides, from radiolabeled diatom incubations.....	76
4.2 Comparisons of $\log K_d$ values of ^{234}Th , ^{233}Pa , ^{210}Pb and ^7Be with different fractions of diatom cells.....	80
4.3 Percentage activities of ^{234}Th , ^{233}Pa , ^{210}Pb and ^7Be in different biopolymer fractions of diatom cell.	83
4.4 Size distribution pattern of proteins in different biopolymer fractions harvested from <i>P. tricornutum</i> grown in seawater media with (L1-4) and without Si (L5, L6) respectively. (Lane 1: SDS extractable fraction, EPS Si+; Lane 2: EDTA extractable fraction, EPS Si+; Lane 3: AEPS Si+; Lane 4: NAEPS Si+; Lane 5: AEPS Si-; Lane 6: NAEPS Si-; Lane 7: standard molecular weight markers)	85
4.5 2D HSQC NMR spectrum of the biopolymer residues from HF insoluble fraction in DMSO- d_6 . Assignment of regions: 1. aliphatics; 2. specific methines from intact cyclic terpenoids; 3. Carboxyl-rich alicyclic molecule (CRAM); 4. DMSO- d_6 (NMR solvent); 5. amino-acid α -proton in peptide chains; 6. Non-conjugated double bonds.	86
4.6 2D HSQC NMR spectra of biopolymer representatives: (A) lignin (aromatic biopolymer), (B) albumin bovine serum (protein), (C) amylopectin (carbohydrate), and (D) tomato cuticle (aliphatic biopolymer). Assignments of the major structural classes as follows: (1) aliphatic linkers (and aliphatic coproducts extracted from wood in lignin isolation), (2) methoxyl, (3) linkers between aromatic rings, (4) aromatic rings, (5) aliphatic side chain residues, (6) amino acid α -protons in peptide chains, (7) aromatic side chain residue, (8) CH_2 in carbohydrate, (9) CH in carbohydrate, (10) anomeric units, (11) residues in main aromatic chain, and (12) esters and ethers linkers. *Reprinted from Sambrook et al. (1989).....	88
5.1 Graphic representation of Factor Analysis (FA) carried out with all three depths samples (open circle: radionuclides; filled circle: possible carrier phases/proxies). a) Distribution of factors according to their loadings of F1 and F2; b) Distribution of factors according to their loadings of F3 and F4. ...	118

5.2 Correlations of particulate concentration (in wt/wt unit) of a) Mn with Fe; b) OC with HS-C/OC; c) OC with TCHO; d) URA with TCHO; e) OC with HQ; f) URA with Protein; in three different depths.....	119
5.3 Correlations of a) particulate Mn concentration with $\log K_d^{210}\text{Po}$; b) particulate HS concentration with $\log K_d^{210}\text{Po}$; c) particulate Mn concentration with $\log K_d^{233}\text{Pa}$; d) particulate HS concentration with $\log K_d^{233}\text{Pa}$; e) particulate Si concentration with $\log K_d^7\text{Be}$; f) particulate CaCO_3 concentration with $\log K_d^{234}\text{Th}$; in three different depths.	120

LIST OF TABLES

TABLE	Page
2.1 Sampling locations and ancillary data.....	20
2.2 Chemical Composition of colloids and extracted EPS.	27
2.3 Concentrations of classified amino acid groups in marine colloids and EPS samples.	28
2.4 Partition coefficient of radionuclides with marine colloids and EPS.	30
2.5 Rotated Component Matrix derived from the Covariance Matrix (n=11 for all factors).	32
3.1 Elemental and Biochemical composition of EPS Si+ and EPS Si- harvested from <i>P. tricornutum</i> grown in seawater media with and without Si respectively.	52
4.1 LogK _d values of ²³⁴ Th, ²³³ Pa, ²¹⁰ Pb and ⁷ Be for different diatom cells fractions.....	81
4.2 Percentages of radionuclide activities in different biopolymer (BP) fractions of diatom cells.	83
4.3 2D HSQC NMR spectral assignments in Fig. 5.5.....	87
5.1 LogK _d values for ²³⁴ Th, ²³³ Pa, ²¹⁰ Pb, ²¹⁰ Po and ⁷ Be, as well as chemical composition of the <125 μm fraction of OFP sediment trap samples.	103
5.2 Averages of logK _d values of radionuclides, particulate organic and elemental concentrations and the total particle fluxes at three depths at the Oceanic Flux Program (OFP) site off Bermuda.	109
5.3 Comparisons of logK _d values among ²³⁴ Th, ²³³ Pa, ²¹⁰ Po, ²¹⁰ Pb and ⁷ Be from different aquatic environments.	111
5.4 R-values for each two crossed factors by 2-tailed Pearson Product Moment Correlation (pair-wise deletion for missing data).	113
5.5 Rotated structure matrix derived from the covariance matrix with logK _d of selected radionuclides with data from all three depths.	115
5.6 Elemental composition and their possible % shale contribution in OFP sediment trap particles.....	128
5.7 Concentration of selected elements in their estimated forms.....	129

CHAPTER I

INTRODUCTION

1.1 Background

Radionuclides from both natural and anthropogenic sources have been used for decades as important proxies to understand oceanic processes, such as boundary scavenging and paleocirculation (e.g., Broecker and Peng, 1982), estimation of particle and colloid fluxes in the water column, as well as residence times of different water masses.

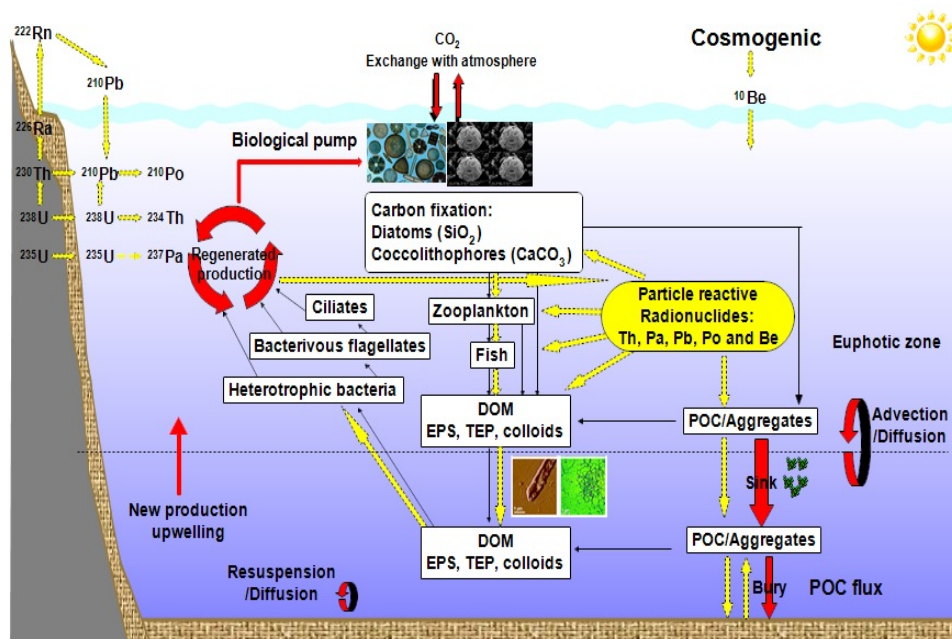


Fig. 1.1 A conceptual diagram showing how the pathways of particle reactive radionuclides interact with the carbon flux in the ocean.

Fig. 1.1 is a conceptual diagram showing how the pathways of particle reactive radionuclides interact with the carbon flux in the ocean. Quantification of these processes is important for predicting global carbon budgets used to assess the extent of global climate change. Different isotopic techniques were applied to understand the sources, pathways, dynamics, and fate of carbon, as well as pollutants and particles from different origins in the oceans. Natural radioactivity in seawater is primarily derived from the three primordial radioactive parents, uranium-238, uranium-235 and thorium-232, which produce three decay series. Some soluble mother nuclides, such as uranium, decay to particle reactive daughter nuclides, such as thorium and protactinium. Particle reactive radionuclides are removed from the water column by “scavenging”: adsorption on particles and subsequent removal with these particles to the sediments at the sea floor. Differences in particle reactivity lead to different distributions and disequilibrium patterns of mother and daughter radionuclides in the water column. Oceanographers have exploited the reactions of these particle-scavenged radionuclides to derive quantitative information on sources and fluxes of marine and terrestrial particles, carbon, and gases as well as their residence times in the present and past ocean. A conceptual diagram showing how the pathways of particle reactive radionuclides interact with the carbon flux in the ocean.

However, the interactions and binding relationships between radionuclides and marine organic matter, especially biopolymers, are largely unknown. The molecular mechanisms of tracer applications to marine particle cycling remain poorly understood (Santschi et al., 2006). Generally, the speciation and transport of these low concentration

natural radionuclides (present at ~pico- to femto- or atto- molar concentrations) in the ocean is controlled by thermodynamic and kinetic processes, e.g., adsorptive uptake and transport by organic or inorganic colloids and particles. Given that the concentrations of organic and inorganic colloids (i.e., micro- and nanoparticles) and macro-particles in surface waters are of the order of micromolar concentrations (Santschi et al., 1995, 2002), and the ions of natural radionuclides in the sub-picomolar range, these ions are unlikely to form their own hydrolytic species but tend to associate with a carrier phase, e.g., colloids or particles. There is considerable evidence that the speciation and transport of natural radionuclides such as Pu, Th and Pa in aquatic environments are controlled by particles and colloids, e.g., Si-Al-hydroxides (Doucet et al., 2001; Kim et al., 2003; Panak et al., 2003), Fe-organic colloids (Santschi et al., 2002) and polysaccharide-rich exopolymeric substances (Quigley et al., 2002; Roberts et al., 2009; Xu et al., 2009, 2011b). Understanding the mechanisms that control the adsorption onto colloids and particles is important in the assessment of the limitations of their uses and applications. A conceptual flow diagram that details the proposed work is shown in Fig. 1.2, and further detailed below.

1.1.1 Organic carrier phases in the ocean

A major fraction of global organic carbon exists as dissolved substances in seawater, including reactive substances categorized broadly as proteins, polysaccharides and lipids, as well as humic substances and their degradation products (e.g. colloids and exopolymeric substances) of these primary constituents. These dissolved (i.e., filter-passing) substances have many charged sites that can bind natural radionuclides.

Colloids (defined here as material with at least one dimension in the size range 1 nm-0.2 μm), consisting of organic carbon that makes up 30 to 50% of the dissolved organic carbon pool in the ocean (Santschi, 1997), play an important role in controlling the speciation of natural radionuclides, thus influencing their fate, transport and bioavailability in seawater and freshwater systems.

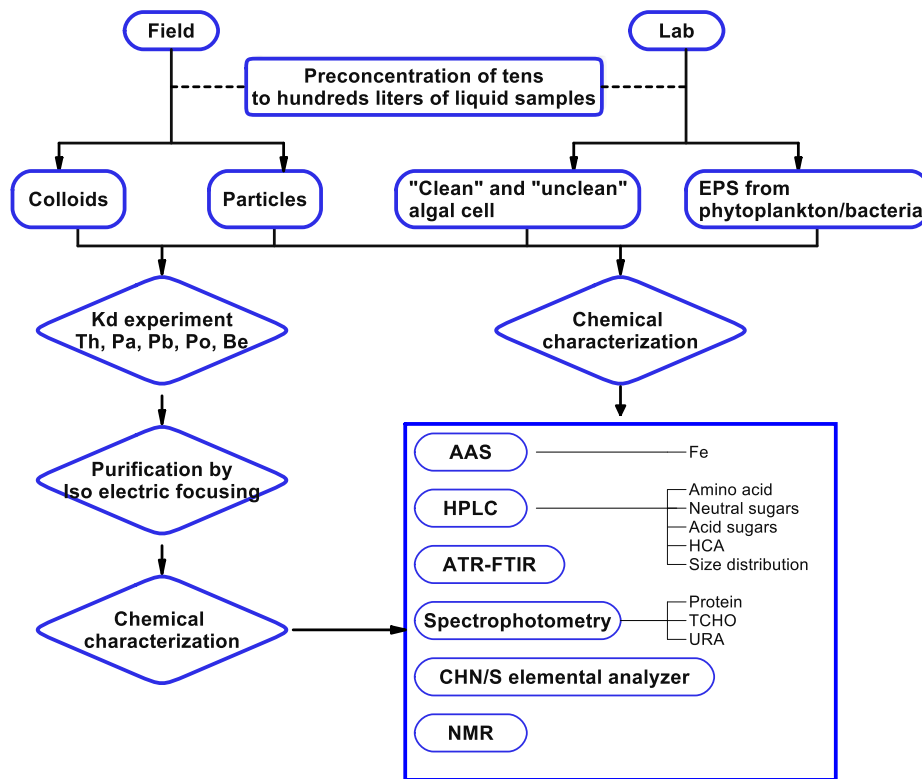


Fig. 1.2 Conceptual flow diagram that details the proposed work.

About half of the global primary production takes place in the oceans (Longhurst et al., 1995; Field et al., 1998). Photosynthetic activity by phytoplankton in surface seawater is a major driving force in sequestering the greenhouse gas CO_2 (Falkowski et

al., 1998). The global net primary production from phytoplankton is estimated as ~45-50 Pg C per annum (Longhurst et al., 1995; Field et al., 1998), driven by a phytoplankton biomass of ~ 1 Pg C, which is roughly 0.2% of the photosynthetically active carbon biomass on the Earth (Field et al., 1998). A significant portion of photosynthetic production of phytoplankton is released as exopolymeric substances (EPS) into the dissolved organic carbon (DOC) pool (Fogg, 1983; Baines and Pace, 1991), contributing significantly to the primary marine organic carbon reservoir. EPS produced by bacteria and phytoplankton form an important fraction of the dissolved organic matter (DOM) (Bhaskar et al., 2005) and are usually regarded as the precursors of transparent exopolymer particles (TEP) (Passow and Alldredge, 1994; Passow et al., 1994), which play a decisive role in aggregation processes (Bhaskar et al., 2005) and gel formation (Verdugo et al., 2004; Verdugo and Santschi, 2010; Verdugo, 2012). Due to the presence of charged functional groups and their amphiphilic, adsorptive and adhesive properties (Arce et al., 2004), EPS also serve as a natural ligand source, providing abundant binding sites for many other molecules including trace metals, nanoparticles, and radionuclides (Decho and Lopez, 1993; Bhaskar et al., 2005; Doucet et al., 2007; Roberts et al., 2009; Xu et al., 2009, 2011b; Chen et al., 2011).

Diatoms are one of the most important contributors to the global carbon fixation and the cycling of all biological elements. This microscopic, eukaryotic phytoplankton group conducts out about one-fifth of the photosynthesis on Earth (Armbrust, 2009) and is estimated to contribute up to 45 to 48 % of the global oceanic primary production (Nelson et al., 1995; Mann, 1999). The cell wall of diatoms is composed of an

architecturally elegant, siliceous frustule encased in an organic coating (Reimann et al., 1965). Those frustules, sink to the bottom of the ocean, after the diatom cell dies and is often preserved in the sediments, are believed to be responsible to the fractionation of many of the particle reactive radionuclides, such as $^{231}\text{Pa}/^{230}\text{Th}$ (Chase et al., 2002). However, a series of field and laboratory studies both showed a selective and compound specific interaction of ^{234}Th with marine organic matter (Guo et al., 2002a; Quigley et al., 2002; Roberts et al., 2009; Xu et al., 2009, 2011b) that is partly originating from diatoms. Recently, a set of phosphoproteins and long chain polyamines, called silaffins, isolated from diatom cell walls were shown to assemble and generate networks of silica nanospheres within seconds when added to a solution of silicic acid (Kröger et al., 1999; Kröger and Poulsen, 2008; Kröger and Sandhage, 2010). Knowledge of the chemical composition of this organic template present as inner and outer coatings of diatom cells may be responsible for implied role of diatom frustules in the scavenging particle reactive radionuclides. Therefore, understanding the molecular nature of these organic coatings and embedded substances and their probable fate in aquatic environments has important consequences for the interpretations of the geochemical cycling of particle reactive radionuclides and for paleo-oceanography studies. While experimental data are highly suggestive, determining the true organic carrier phase remains a challenge and more research into this question is clearly warranted.

1.1.2 Evidence for special organic carrier molecules of selected natural radionuclides

1.1.2.1 Thorium and Protactinium

Thorium has only one oxidation state, IV, in the natural radioactive decay series as either a daughter of uranium (e.g., ^{230}Th , ^{234}Th), radium (e.g., ^{228}Th), or as thorium, the parent of a decay series (^{232}Th). As Th (IV), it is known to be strongly particle-reactive. Reviewed by Santschi et al. (2006), chemical studies on the behavior of thorium in natural waters show that it is either complexed with organic ligands (e.g., Choppin, 1983, 1989) or present as $\text{Th}(\text{OH})_4^0$ and $\text{Th}(\text{OH})_3\text{CO}_3^-$ complex (Langmuir and Herman, 1980; Bruno, 1990; Östhols et al., 1994; Murphy et al., 1999; Fanghänel and Neck, 2002; Kim et al., 2003; Panak et al., 2003). A series of laboratory (Quigley et al., 2002; Alvarado Quiroz et al., 2006) and field experiments (Guo et al., 2002a, b; Hung et al., 2003a, b; Santschi et al., 2003; Hung et al., 2004a, b; Roberts et al., 2009) reported a strong association of thorium with colloidal carbohydrate- and uronic acid-rich substances. Those materials showed low isoelectric point and were about 10 kDa molecular weight. These findings resulted in close correlations between $^{234}\text{Th}/\text{POC}$ ratios and acid polysaccharide or uronic acid (URA) content of the suspended or sinking particles. Santschi et al. (2003) proposed that the contribution of bacteria to ^{234}Th and POC removal is to cause the break up of sinking aggregates and thus, decreasing ^{234}Th and/or POC fluxes, based on inverse relationships between $^{234}\text{Th}/\text{POC}$ ratios with bacterial biomass and other relationships between field parameters. This hypothesis is confirmed by data from Gulf of Mexico (GOM) (Hung et al., 2010). Though the cumulative

evidence from the analysis of the combined data sets from GOM cruises clearly indicates that the uronic acid (URA) content can predict Th-234 flux (Hung et al., 2010; Xu et al., 2011a), there the correlation between URA and polysaccharide contents in sediment trap material was significant (Xu et al., 2011a).

Like thorium, protactinium is also a highly particle reactive element. However, the chemistry of protactinium is more complex, in large part because protactinium has two possible oxidation states (IV, V) in natural waters (Alhassanieh et al., 1999). The predominant form in oceanic systems is likely Pa(V) (Choppin, 1983), which is quite soluble, similarly to the Pu(V) ion, and sorbs to particle surfaces to a much lower extent than the four-valent oxidation state ion of Pa(IV). What is known is the redox potential for Pa(V) to Pa(IV) reduction is -0.05V (Greenwood and Earnshaw, 1998). From this redox potential at pH of 7, and using other values from Stumm and Morgan (1996), a number of microbially produced molecules as well as simple polysaccharides could abiotically reduce Pa(V) to Pa(IV). It is likely that Pa(V) is firstly reduced to Pa(IV) before adsorption and removal from natural waters can take place, as has been seen for Np(V), which is reduced in the presence of natural organic matter such as humics (Zeh et al., 1999). Organic ligands such as extracellular polymeric substances (EPS) produced by phytoplankton and bacteria are another possible source of reductants and this will therefore be one of the focal areas of this study.

Both ^{231}Pa ($T_{1/2} = 32800$ yr) and ^{230}Th ($T_{1/2} = 75400$ yr) are particle reactive and are produced to give a constant activity ratio of 0.093. The interesting thing is that Th is somewhat more reactive than Pa so that the two isotopes are fractionated. The residence

time of Th in the ocean is about 30 years, whereas the residence time of Pa is about 150 years. As a consequence the Th that is produced in the water column is usually deposited on the seafloor in the same basin, not very distant from where it originated, whereas Pa is further advected by currents and eddy-diffusive mixing before it is deposited. ^{231}Pa produced in the open ocean thus has a greater chance than ^{230}Th to reach productive coastal seas where particle fluxes and scavenging rates are higher. Thus, $^{231}\text{Pa} / ^{230}\text{Th}$ ratios higher than 0.093 are found in sediments underlying productive coastal seas, whereas lower ratios occur in the sediments of the open ocean. The original application of the $^{231}\text{Pa} / ^{230}\text{Th}$ ratio was therefore as a proxy for paleoproductivity studies. Field studies showed that the contents of polysaccharides and calcium carbonate are significantly correlated to particle–water partition coefficients (K_d) of Th and Pa in sediment trap material collected from the GOM and Sargasso Sea. Moreover, $\log K_d$ of Th (and Pa) values are correlated to the polysaccharide content, while no correlation was apparent with CaCO_3 , MnO_2 , Fe_2O_3 and SiO_2 (Roberts et al., 2009). Since polysaccharides are not generally regarded as strongly chelating agents for actinides, other co-occurring organic phases originating from the matrix of carbohydrate-rich EPS, could be responsible for the binding.

1.1.2.2 Lead and Polonium

The two main routes of supply of ^{210}Pb ($T_{1/2}=22.3$ yr) to the oceans are deposition from the atmosphere and in situ production by radioactive decay of ^{226}Ra . Once in the surface ocean, most of the ^{210}Pb is removed via sorption onto particulate matter in the upper ocean and driven downwards by the flux of biogenic material from surface

productivity (Fisher et al., 1988). Pb is an oxygen-seeking metal that was observed to frequently associate with mineral (e.g., bone, shell, and structure) fractions of organisms, and with cell walls in single-celled organisms that provide the largest surface area to bind to (Fisher and Reinfelder, 1995). However, in sediment traps it is found in proportion to POC. Recent studies found that ^{210}Pb showed strong similarities to those of ^{210}Po (Stewart et al., 2007), as both isotopes were correlated with freshly produced material. In coastal marine systems, Pb in colloids and suspended particles has also been shown to be strongly related to the cycling of Fe (Wen et al., 1999; Wen et al., 2008), similar to the case of the class B metal Ag, which also showed a strong relationship to Fe (Wen et al., 2002).

^{210}Po ($T_{1/2}=138.4$ d), the last radioactive member of the uranium family, is formed by decay of ^{210}Pb via ^{210}Bi ($T_{1/2}=5.01$ d). The distribution of Po has direct relevance to global biogeochemical cycling of other oxygen Group VI elements (S, Se and Te). It appears to behave similarly to Se, either acting as an S analogue or binding to S ligands, primarily associating with proteins in living organisms (Stewart and Fisher, 2003a, b). Field studies showed a correlation between particulate ^{210}Po activity to chlorophyll, suggesting that most of the scavenging is controlled by oceanic phytoplankton (Stewart et al., 2005; Du et al., 2011 and references therein). ^{210}Po is strongly associated with organic matter and concentrated mostly in the carbon-based flux of oceanic particles (Rutgers van der Loeff and Geibert, 2008). Furthermore, results from laboratory experiments showed a lowered ^{210}Po binding in the presence of acid polysaccharides

(Quigley et al., 2002) but an enhancement by the presence of proteins (Fisher et al., 1983; Cherrier et al., 1995; LaRock et al., 1996; Stewart and Fisher, 2003a, b).

Po can also penetrate into the cytoplasm of cells and can be bioconcentrated to higher trophic levels in older organisms (Stewart and Fisher, 2003a, b). Po can bioaccumulate in marine food chains and shows a slow loss rate from organic material and a biological recycling similar to POC, whereas ^{210}Pb is not accumulated in organisms. Hence, this results in different extents of $^{210}\text{Po}/^{210}\text{Pb}$ disequilibria in the oceanic water column (Bacon et al., 1976; Nozaki et al., 1976; Cochran et al., 1983; Stewart et al., 2005). Most importantly, the disequilibrium between ^{210}Po and ^{210}Pb has been widely used to trace particle dynamics and export fluxes of organic carbon and particles from the upper ocean.

1.1.2.3 Beryllium

Similar to ^{210}Po and ^{210}Pb , cosmogenic ^7Be and ^{10}Be have also been widely used as proxies in oceanographic and geochemical investigations (Kumar et al., 1995, 1998; Feng et al., 1999; Kim et al., 2000; Matisoff et al., 2005; Baskaran, 2011; Kaste and Baskaran, 2011). The scavenging of Be in the ocean is also dependent on particulate composition, with biogenic silica, CaCO_3 , lithogenic material and organic matter as the main components, yet no consistent conclusions could be made up till now as to the nature of the controlling phase (Chase et al., 2002; Chase and Anderson, 2004; Li, 2005; Kretschmer et al., 2011).

1.1.2.4 Multiple isotopic ratios

Although the use of isotope ratios may help eliminating the effects of particle composition (Baskaran et al., 1997; Feng et al., 1999; Matisoff et al., 2005; Baskaran and Swarzenski, 2007), the exact causes for fractionation effects among different radioisotopes remains largely unknown. It points to the urgent need for studying the role of chemical composition and types of organic functional groups in the fractionation of natural radionuclides in the ocean to validate the applications of natural radionuclides as geochemical and oceanographic proxies.

1.2 Hypothesis and objectives

***Hypothesis 1:* Carrier phases for the selected radionuclides will be mostly organic rather than inorganic. The organic coatings or embedded organic templates in the biogenic particles are the main phases responsible for scavenging of natural radionuclides in the ocean.**

Objective 1-1: To develop method to clean the biogenic particle (e.g. diatom frustules) to eliminate most of the outer organic coatings.

Objective 1-2: To assess the partitioning coefficients of the selected radionuclides, including ^{234}Th , ^{233}Pa , ^{210}Pb , ^{210}Po and ^7Be , with these biogenic particles with different organic contents.

Objective 1-3: To separate, purify and chemically identify, at the molecular level, the radionuclide binding biopolymers associated with biogenic particles (e.g., diatom frustule).

***Hypothesis 2:* There will be different types of organic biopolymeric carrier molecules for each of the different radionuclides.**

Objective 2-1: To purify EPS and natural organic biopolymers from both large scale algae and bacteria cultures in the lab and aquatic samples in the field.

Objective 2-2: To chemically characterize different organic matter fractions at the molecular level from dissolved organic material of different origins.

Objective 2-3: Develop separation and characterization methods to determine the chemical composition, at the molecular level, of those radionuclides binding organic biopolymers.

Objective 2-4: Develop an understanding of the relationship between biopolymer composition and its binding properties to selected radionuclides (e.g., if the content of natural reducing agent that can enhance or depress the binding affinity of multi-valent radionuclides, e.g., Pa(VI, V) and Po(-II, II, IV)).

CHAPTER II

ORGANIC LIGANDS FOR STRONGLY BINDING IONS OF RADIONUCLIDES, Th, Pa, Pb, Po AND Be, IN COLLOIDAL MACROMOLECULES IN THE OCEAN

2.1 Overview

Natural colloidal organic material (COM), including phytoplankton exopolymeric substances (EPS) and marine colloids, are able to strongly bind ions of different natural radioisotopes that are used as geochemical tracers in marine systems, e.g., for particulate organic material flux dynamics and organic carbon cycling in the ocean, and aggregation. To study the binding mechanisms of COM to ions of natural radionuclides, marine colloids (1 kDa – 0.2 μm) isolated by cross-flow ultrafiltration from seawater of the west Pacific Ocean and the Gulf of Mexico, together with dissolved EPS produced by laboratory cultured diatoms were collected. The organic compositions of different biopolymers were investigated to determine partitioning coefficients of five radionuclides: ^{234}Th , ^{233}Pa , ^{210}Pb , ^{210}Po and ^7Be , to individual chelating biomolecules. By separating, identifying and characterizing radiolabeled organic carriers, we found that the most efficient binding of many of these nuclides likely occurs to acid polysaccharide- and Fe-related protein-containing biomolecules, i.e., proteoglycans, glycoproteins, and hydroxamate siderophoric moieties, thus providing new insights into the relative importance of specific organic phases that exist in marine colloidal material to the

binding and possible removal of specific radionuclides in the ocean.

2.2 Introduction

A major fraction, 30-50%, of global dissolved organic carbon exists as colloidal substances in seawater (Santschi et al., 1994; Benner et al., 1997; Wells, 1998). The change in the bulk composition of these colloidal substances from estuarine to shelf and offshore waters is a progressive increase in organic content and decrease in mineralogical content, e.g., clays and metal oxyhydroxides (Sigleo and Means, 1990; Wells and Goldberg, 1992; Wells and Goldberg, 1994; Benner et al., 1997; Leppard et al., 1997; Santschi et al., 2005). The main organic carbon composition of dissolved organic carbon are reactive substances categorized broadly as proteins, polysaccharides and lipids, as well as humic substances, including many polar sites, e.g., $-\text{COOH}$, $-\text{OH}$, $-\text{O}=\text{POOO}-$, $-\text{CONHO}-$, $\text{R}-\text{N}-\text{R}$ and $\text{R}-\text{S}-\text{R}$ groups. In most cases cations such as trace metals and radionuclides are trace constituents that accompany this bulk colloidal carrier phase due to electronegative or negatively charged functional groups of these molecules distributed within the colloidal macromolecular organic matrix.

Various studies have found colloidal organic material (COM) plays an important role in controlling the speciation, transport and bioavailability of natural trace elements in seawater and freshwater systems. However, the correlations differ distinctly among the nuclides and areas (e.g., oceans versus coasts). It is clear that the colloidal fraction of any

given nuclide is not necessarily coupled tightly to the abundance of bulk colloidal carbon, but to the specific ligands or functional groups distributed within the colloidal organic matrix (e.g., Lieser et al., 1986; Honeyman and Santschi, 1991; Guo and Santschi, 1997a; Guo et al., 1997; Santschi, 1997, 2002; Wen et al., 1997a, b, 1999).

Most natural radionuclides have metal characteristics, and organic ligands, such as siderophores, are the major classes of metal chelators in the aquatic environment (Vraspir and Butler, 2009). The direct source of strong complexing ligands that control trace element speciation in seawater is still not well understood. However, it is very likely that colloidal organic ligands are released in relation to microorganism activities in the ocean. A handful of marine prokaryotes are well known to release siderophores, a group of high-affinity metal-binding ligand compounds, in response to their need for soluble Fe, which is present at very low concentrations in oceanic waters (Reid et al., 1993; Neilands, 1995; Winkelmann, 2002). EPS produced by bacteria and phytoplankton also form an important fraction of dissolved organic matter (Bhaskar et al., 2005) and are usually regarded as the precursors of transparent exopolymer particles (Passow and Alldredge, 1994; Passow et al., 1994), which play a decisive role in aggregation processes (Bhaskar et al., 2005) and gel formation (Verdugo et al., 2004; Verdugo and Santschi, 2010; Verdugo, 2012). These EPS, composed mainly of polysaccharides and glycoproteins, and containing charged functional groups and amphiphilic, adsorptive and adhesive properties (Arce et al., 2004),

provide a substantial pool of organic carbon available to serve as a natural ligand source for many other molecules, including trace metals, nanoparticles, and radionuclides (e.g., Lieser et al., 1986; Decho and Lopez, 1993; Guo et al., 1997,a; Wen et al., 1997a, 1999, 2011; Santschi et al., 2002, 2005; Bhaskar et al., 2005; Doucet et al., 2007; Zhang et al., 2008, 2013; Roberts et al., 2009; Xu et al., 2009, 2011; Chen et al., 2011).

To evaluate specific functional groups in colloidal macromolecular matter controlling the chelation of ions of particle-reactive radionuclides, $^{234}\text{Th(IV)}$, $^{233}\text{Pa(IV)}$, $^{210}\text{Po(IV)}$, $^{210}\text{Pb(II)}$ and $^7\text{Be(II)}$, we have examined comprehensively the composition of marine colloids collected from the West Pacific Ocean and the Gulf of Mexico, as well as those extracted from laboratory diatom cultures. The abundance of potential organic carriers in colloids and EPS, including proteins, individual amino acids, total polysaccharides, uronic acids, hydroquinones, and hydroxamate-type and catechol-type siderophores were quantified. The purpose of this study was to examine their possible relationships with experimentally determined partitioning coefficients of ^{234}Th , ^{233}Pa , ^{210}Po , ^{210}Pb and ^7Be between colloidal (1 kDa to 0.2 μm) and truly dissolved phases (<1 kDa). Results from the separation of radiolabeled colloids and EPS by isoelectric focusing, as well as chemical relationships and statistical analyses provide new insights into the relative importance of specific organic carrier phases to the binding and removal of specific radionuclides by marine biopolymers.

2.3 Material and methods

2.3.1 Colloidal organic matter collected from field site

Since concentrations of marine colloids are very low, large scale pre-concentration needs to be carried out to characterize them. Cross-flow ultrafiltration is particularly useful for the pre-concentration of macromolecular organic matter from large volumes of seawater (e.g., Wen et al., 1996, 1997a, b; Guo et al., 1997). Seawater was collected from coastal sites in the Gulf of Mexico (July, 2010) and from open ocean sites in the west Pacific Ocean (March, 2009 and May, 2010). Briefly, tens to hundreds liters of seawater were pre-filtered through a 0.2 μm Millipore® cartridge (in-line set-up) into an enclosed reservoir. The colloidal fraction ($<0.2 \mu\text{m}$ and $>1 \text{ kDa}$) was then desalted and freeze-dried for later use. The laboratory-made ultrafiltration system (Wen et al., 1996, 1997a, b; Guo et al., 1997) was composed of four 1 kDa cutoff cartridges (Millipore®) with a peristaltic pump and Teflon tubing. Cartridges, tubing and reservoirs were all thoroughly cleaned before sampling with detergent (Micro®), 0.1 N NaOH and 0.1 N HCl. All cartridges were checked for their integrity before use with vitamin B₁₂ (1.3 kDa). The details of sampling times, depths, locations, water depths and surface water temperature, salinity values are given in Table 2.1.

2.3.2 Culturing and separation EPS from marine algae

Marine phytoplankton, *Phaeodactylum tricoratum* (UTEX646) and *Skeletonema costatum* (CCMP 2092), were cultivated in f/2 (with Si) media (salinity of 26) at a temperature of $19 \pm 1^\circ\text{C}$ with a light cycling of 14h: 10h under a saturating irradiance of $100 \mu\text{mol quanta m}^{-2} \text{s}^{-1}$ for EPS production. The growth status of algae was monitored by changes in optical density at 750 nm. As the diatom *P. tricoratum* can grow in the absence of silicate (that is, the biogenesis of silicified frustules is facultative), two different kinds of EPS were collected: from *P. tricoratum* cultured in f/2 and f/2-Si media. EPS was separated from these cultures once they reached stationary phase using procedures developed in Zhang and Santschi (2009). Briefly, tens of liters of laboratory cultures were centrifuged (2694 g, 30 min) and filtered (0.2 μm). The filtrate was desalted and collected with a 1kDa cutoff cross-flow ultrafiltration/diafiltration membrane and followed by freeze-drying for later use.

Table 2.1 Sampling locations and ancillary data.

Sample ID	Cruise	Station	Location		Water depth (m)	Sampling depth (m)	Salinity	Temperature (°C)
West Pacific Ocean								
C1	ORI-925 (May, 2010)	ST 26	22°12.0'N,	119°05.4'E	20	5	30.23	17.05
C2		ST 28	22°45.0'N,	119°46.8'E	60	5	34.67	22.18
C3		ST 30	22°32.4'N,	120°03.6'E	130	5	34.50	24.80
C7		ST W16	21°45.0'N,	121°07.8'E	1025	80	34.86	23.89
Gulf of Mexico								
C11	MCH* (Aug, 2010)	A14	28°47.5'N,	95°10.5'E	20	5	32.42	31.70

*Cruise of NOAA/TAMU Mechanisms Controlling Hypoxia (MCH).

2.3.3 Composition analysis of marine biopolymers

Three laboratory produced EPS and eight natural marine colloids samples (Table 2.1) were analyzed for individual chemical components. Elemental content of carbon (C), nitrogen (N) and sulfur (S), was determined using a Perkin Elmer CHNS 2400 analyzer, with cysteine as a standard (Guo and Santschi, 1997b). Total carbohydrate (TCHO) concentration was determined by the TPTZ (2, 4, 6-tripyridyl-s-triazine, Sigma) method using glucose as the standard and uronic acids (URA) were measured by meta-hydroxyphenyl method, using glucuronic acid as the standard (Hung and Santschi, 2001).

Protein content was determined using a modified Lowry protein assay with bovine serum albumin (BSA) as the standard (Pierce, Thermo Scientific).

Hydroquinone (HQ) determination was adopted from Sirajuddin et al. (2007), using hydroquinone as the standard. Briefly, 1 mg freeze-dried sample was dissolved in Milli-Q water, and the solution was sonicated for an hour. A 300 μ l aliquot of 100 μ M KMnO₄ was added to 100 ml of the sample solution and reacted for 15 min under room temperature. The hydroquinone concentration was then determined by UV-VIS spectrophotometry at 288 nm. Hydroxamate type- siderophores (HS) was measured by the Csaky's assay (1948), using acetohydroxamic acid (AHA) as the standard. Catechol types of siderophore was analyzed by Arnow's method (1937), using catechol as the standard.

Individual amino acids were analyzed by a reverse-phase HPLC with an Alltech Alltima C18 column (5 μ m, 250 \times 4.6 mm), using an pre-column O-phthaldialdehyde (OPA) derivatization methods (Duan and Bianchi, 2007). Individual amino acids were identified and quantified with a fluorescence detector (excitation/emission wavelength: 330/418 nm) on the basis of internal standard, norvaline, and 17 individual standards (Sigma). For all HPLC work, Waters EmpowerTM 2 software was employed to operate the system and to acquire and integrate the chromatograms.

2.3.4 Sorption experiments

Natural seawater, collected from the Gulf of Mexico with a salinity of 35.0, was sequentially filtered through a 0.2 μm polycarbonate cartridge and ultra-filtered with a 1 kDa cutoff ultrafiltration membrane to remove particulate and colloidal organic matter (Guo et al., 1995; Roberts et al., 2009). The <1 kDa ultrafiltrate fraction was then used for all sorption experiments. The ^{234}Th tracer was purified and extracted from a ^{238}U stock solution (Quigley et al., 2002; Alvarado Quiroz et al., 2006); ^{233}Pa , in equilibrium with ^{237}Np , obtained from Pacific Northwest National Laboratory; ^{210}Pb and ^{210}Po , in 1 N HNO_3 and 2 N HCl , respectively, were purchased from Eckert & Ziegler Isotope Products and the ^7Be tracer solution (in 0.5 N HCl) was manufactured at the Paul Scherrer Institute, Switzerland (Schumann et al., 2013).

The design of sorption experiments was modified from Roberts et al. (2009). Specifically, non-complexing 20 mM/10 mM Tris-HCl buffer was transferred into acid cleaned experimental tubes to precondition the container walls for at least 24 h to reduce tracer adsorption. The buffer capacity of Tris-HCl was sufficient to neutralize the acidic radionuclide tracer solutions, which helped to avoid pseudo colloids generation by NaOH , and maintain the pH at 8.0 ± 0.2 .

Each experiment was performed in duplicate. Seawater (10 ml) was added to the preconditioned tubes, and then between 10 to 15 Bq of each of the radionuclide tracers (at

equilibrium) was added. Solutions were gently shaken and left to equilibrate overnight. Pre-weighed marine biopolymers (marine colloids and diatom extracted EPS) were added to the seawater/radionuclide mix, resulting in a final particulate concentration of 5 mg/L. This concentration is within the range of colloid concentrations, ~0.2 to 5.1 mg/L, in our study areas (data not shown). This also allowed for accurate weighing and quantitative recovery of particulate matter from our experimental system. The mixture was gently stirred for 1 week to reach partitioning equilibrium of nuclides between marine biopolymers and dissolved phases. The $^{233}\text{Pa}/^{237}\text{Np}$ decay and ingrowth correction were based on the assumption that ^{237}Np would only exist in the truly dissolved phase. At the end, the experimental solution was filtered through 1kDa cutoff MicrosepTM centrifugal devices (Pall Life Sciences), and the colloidal (<0.2 μm and >1 kDa) and truly dissolved (<1 kDa) fractions retained for measurements of radionuclide activity (see below). All related tubing and containers were pretreated with ultrafiltered seawater to reduce the tracer adsorption.

The acid recoverable tracer from the container walls was usually less than 10% of the total adsorbed tracer. This tracer fraction was irreversibly lost and thus ignored in the calculations as it did not participate in the solution reactions. This behavior justified using the sum of the measured fractions as the total amounts participating in the reactions that were studied.

2.3.5 Measurements, partition coefficient, and fractionation factor of selected radionuclides: ^{234}Th , ^{233}Pa , ^{210}Pb , ^{210}Po and ^7Be

Activity concentrations of ^{234}Th , ^{233}Pa , ^{210}Pb and ^7Be were measured by gamma counting the 63.5 keV, 312 keV, 46.5 keV and 477.6 keV lines, respectively, on a Canberra ultra-high purity germanium well type detector. The ^{210}Po activity was analyzed by liquid scintillation counting (Beckman Model 8100 Liquid Scintillation Counter). Both colloidal and dissolved phases samples were counted. All activities of selected radionuclides were corrected for decay and normalized to the same geometry for ease of comparison and further evaluation.

Partition coefficients (K_c) between dissolved and colloidal phases were determined to quantify the interactions between radionuclides and marine biopolymers in experimental systems. K_c is defined as:

$$K_c = A_c / (A_d * C_c) \quad (1)$$

where A_c and A_d represents colloidal and dissolved activities of radionuclides (Bq/L), respectively, and C_c is the colloidal concentration (g/ml) (Honeyman and Santschi, 1989; Guo et al., 1997).

2.3.6 Isoelectric focusing of radiolabeled marine colloids and EPS

In order to examine the specific binding ligands to five different radionuclides in the marine colloids and diatom extracted EPS (Alvarado Quiroz et al., 2006; Zhang et al.,

2008; Xu et al., 2009), radiolabeled biopolymers E1, E3, C9 and C11 (high OC content and available sample amount; see Table 2.1) were subjected to Isoelectric Focusing (IEF) separation with a Gel Electrophoresis apparatus (Amersham Biosciences, Multiphor Electrophoresis System). Briefly, radiolabeled biopolymers and a 140 μ l of rehydration solution were loaded onto an IPG strip (GE healthcare immobilineTM Drystrip, pH 3-10, 11cm) and were re-swelled overnight. Afterward, the strip was loaded for isoelectric focusing for 17.5 hr. The strip was then cut into 11 1cm-pieces and followed by 1% SDS extraction overnight. Activity of the five radionuclides in each fraction were subsequently analyzed. Due to the limited amount of material, only selected chemical components (TCHO, Proteins and Fe) in individual fractions were characterized by methods described above.

2.3.7 Determination of relationship between biopolymer composition and its binding properties to selected radionuclides by statistical analysis

The whole data set obtained from composition analysis and partition coefficient experiments of all selected radionuclides (n=11; 13 variables) is summarized in Table 2.2, and Table 2.4. A serial statistical analysis was performed on this unique data matrix, using SPSS software® package (Version 17.0). Factor analysis was performed to evaluate possible relationships among the compositional variables and the partition coefficients (K_c) in the eleven samples. Factors were extracted by principle component

analysis, and rotated by the varimax method with Kaiser normalization. In a generalized adsorption/desorption reaction: $C \leftrightarrow X$, where X = concentration of a given species in colloidal phase (g or mole per gram biopolymers), and C = concentration of a given species in liquid phase (g or mole per cm^3 of liquid), the equilibrium constant K_c is defined as:

$$K_c = X/C = \exp \left(\frac{-\Delta G_r}{RT} \right) \quad (2)$$

Therefore, $\log K_c$ is proportional to $-\Delta G_r$, which is the Gibbs free energy change of the sorption reaction (Li, 2000). Hence, $\log K_c$ values were used for all statistical analyses to evaluate the possible carrier phases for radionuclides.

2.4 Results and discussion

2.4.1 Chemical characterization of marine biopolymers

The organic composition (carbon, nitrogen, sulfur, proteins, total carbohydrates, uronic acids, hydroquinones and hydroxamate siderophores) of eight marine colloids and three diatom extracted EPS samples are given in Table 2.2. Maximum 1 standard deviations (SD) for each analysis were 1% (relative). Interestingly, no catechol-type siderophores could be detected in these samples.

Table 2.2 Chemical Composition of colloids and extracted EPS.

Cruise	Station	Depth	ID	OC	ON	OS	Protein	TCHO	URA	HS	HQ		
		(m)				(%)	(mg/g)						
Colloids	ORI-925	ST 26	5	C1	5.1	0	9.9	21.4	23.2	2.7	3.3	1.5	
		ST 28	5	C2	12.6	0.33	10.7	49.8	61.6	13.5	4.0	1.4	
		ST 30	5	C3	9.6	0.50	7.8	39.3	50.4	10.5	1.5	0.84	
		ST W16	80	C7	6.9	0	9.9	16.1	13.6	0.0	0.53	0.19	
			5000	C8	9.7	0.57	5.3	24.5	49.0	11.5	0.33	1.3	
	ORI-892	ST 30	20	C9	41.0	4.2	3.8	89.9	187.1	62.7	0.63	3.6	
			95	C10	38.8	4.0	2.8	77.0	125.0	46.0	0.57	4.6	
	GOM	A14	5	C11	31.7	3.0	0	89.9	188.8	48.4	0.17	5.9	
	EPS	Algae Species		Media	ID								
		<i>Phaeodactylum</i>		f/2	E1	36.2	4.7	2.7	203.9	191.5	41.7	0.28	9.1
		<i>tricornutum</i>		f/2-Si	E3	37.5	2.7	1.7	196.7	258.6	48.3	0.22	8.8
<i>Skeletonema costatum</i>		f/2	E8	45.3	10.6	2.1	439.3	89.7	31.1	0.36	18.8		

*Maximum 1 standard deviations (SD) for each analysis were 1% (relative).

Table 2.3 Concentrations of classified amino acid groups in marine colloids and EPS samples.

Class	Aliphatic (nonpolar alkyl)	Sulfur	Hydroxyl	Aromatic	Basic(Amino group)	Carboxylic acid	Total
Name of the amino acids	Glycine, Alanine, Valine, Leucine, Isoleucine	Cysteine, Methionine	Serine, Threonine	Phenylalanine, Tyrosine, Tryptophan	Histidine, Lysine, Arginine	Aspartic acid, Glutamic acid	
Abbreviation	Gly, Ala, Val, Leu, Ile	Cys, Met	Ser, Thr	Phe, Tyr, Trp	His, Lys, Arg	Asp, Glu	
Sample ID	mg/g						
C1	5.4	1.2	1.9	2.7	3.5	3.6	18.4
C2	6.6	1.6	2.6	3.4	2.5	4.7	21.4
C3	7.3	1.4	2.7	3.4	3.9	3.2	21.8
C7	2.3	0.6	2.3	2.2	1.1	3.6	12.0
C8	6.1	2.1	8.9	3.3	3.3	8.6	32.2
C9	16.9	4.1	25.3	5.5	8.8	19.6	80.1
C10	10.3	3.7	14.4	5.0	6.0	14.0	53.4
C11	18.7	5.1	20.3	10.8	8.8	23.0	86.7
E1	70.2	14.0	17.4	14.0	13.6	71.1	200.3
E3	84.7	17.6	21.3	17.7	13.0	110.4	264.7
E8	86.0	32.6	45.2	33.5	64.4	210.1	471.8

* Maximum 1 standard deviations (SD) for each analysis were 1% (relative). Categories of amino acids based on the nature of their side groups.

Results from amino acid analysis also support the observation that EPS samples had a higher amount of total protein-containing biomolecules than marine colloid samples (Table 2.3). Based on the nature of their side groups, amino acids were classified into six categories (Table 2.3 and Fig. 2.1). The average amount of each category in marine colloids followed some general trends: Carboxylic \approx Hydroxyl \approx Aliphatic $>$ Amino \approx Aromatic $>$ Sulfur containing groups. For the EPS, the trends were in the order of Carboxylic $>$ Aliphatic $>$ Amino \approx Hydroxyl $>$ Aromatic \approx Sulfur containing groups. Notably, carboxylic amino acids were the most abundant category, comprising more than one third, in both colloids and EPS samples, suggesting a high percentage of proteins existing as glycoproteins or proteoglycans in marine biopolymers and EPS.

Considering the binding site provided by these side groups of amino acids, including carboxyl ($-\text{COO}^-$), hydroxyl ($-\text{OH}$), amino group ($-\text{NH}$), sulfate ester ($-\text{O}-\text{SO}_3^-$), disulfide bond ($-\text{S}-\text{S}-$) and sulfhydryl ($-\text{SH}$) functional groups, these negatively charged ligands in marine colloids and EPS (present at micromolar concentrations) could favor their binding with positively charged radionuclide ions (present at sub-picomolar concentrations) to some different extent in seawater. In addition, in terms of the amounts, EPS samples had significantly higher average amounts of each group of amino acids than colloids (consistent with other compositional analysis), indicating more degraded properties of marine colloids than the EPS samples.

Table 2.4 Partition coefficient of radionuclides with marine colloids and EPS.

	Cruise	Station	Depth (m)	ID	LogK _c					
					Pb	Th	Pa	Be	Po	
Colloids	ORI-925	ST 26	5	C1	4.68	5.69	5.57	4.54	5.17	
		ST 28	5	C2	4.63	5.11	5.61	4.51	5.04	
		ST 30	5	C3	4.44	5.18	5.54	4.59	5.31	
		ST W16	80	C7	4.67	5.18	5.67	4.58	5.15	
	ORI-892	ST 30	5000	C8	4.58	5.59	5.40	4.57	4.84	
			20	C9	4.72	5.35	5.43	4.52	4.95	
			95	C10	4.59	4.90	5.35	4.43	5.16	
	GOM	A14	5	C11	4.40	5.78	5.19	4.67	5.68	
	EPS	Algae Species		Media	ID					
		<i>Phaeodactylum tricornutum</i>		f/2	E1	4.34	4.98	5.20	4.81	5.44
				f/2-Si	E3	4.54	5.33	5.34	4.50	5.36
<i>Skeletonema costatum</i>		f/2	E8	4.48	5.08	4.94	4.66	5.37		

* Maximum 1 standard deviations (SD) for each analysis were 10% (relative).

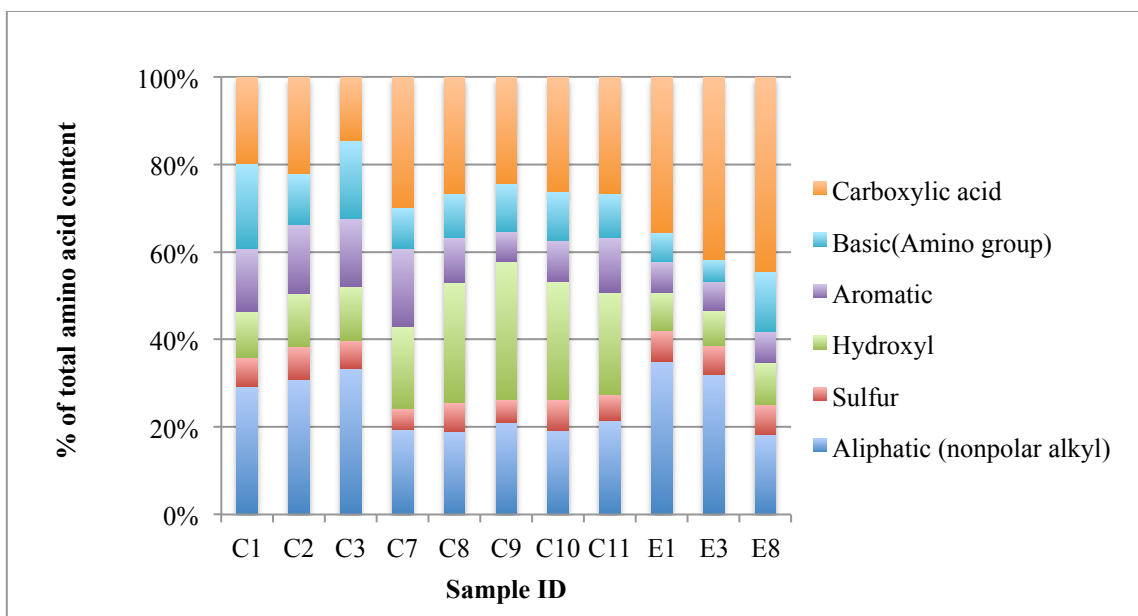


Fig. 2.1 Percentage distribution of amino acid groups in marine colloids and diatom extracted EPS.

2.4.2 Partitioning between dissolved and colloidal phases of ^{234}Th , ^{233}Pa , ^{210}Pb , ^{210}Po and ^7Be

Averaged $\log K_c$ values of the colloids and EPS samples were 5.35 and 5.13 for ^{234}Th , 5.47 and 5.16 for ^{233}Pa , 5.16 and 5.39 for ^{210}Po , 4.59 and 4.45 for ^{210}Pb and 4.55 and 4.66 for ^7Be , respectively (Table 2.4). Reported $\log K_c$ values here are comparable with those found in the field and laboratory studies, around 5 to 6 for ^{234}Th , ^{233}Pa and ^{210}Po , 4 to 5 for ^{210}Pb and ^7Be (e.g., Baskaran et al., 1992; Guo et al., 1997; Steinmann et al., 1999; Wen et al., 1999; Quigley et al., 2002; Yang et al., 2013a), suggesting the sorption experiments here produce similar partitioning for the selected radionuclides in marine environment. No statistical differences of $\log K_c$ values between colloids and EPS

were observed, except for $\log K_c$ of ^{233}Pa , which was higher for colloids than for EPS.

The average $\log K_c$ values of these radionuclides followed the order of $\text{Pa} \approx \text{Th} \approx \text{Po} > \text{Pb} \approx \text{Be}$. $\log K_c$ values of Pb were correlated positively with those of Pa and inversely with those of Be.

Table 2.5 Rotated Component Matrix derived from the Covariance Matrix (n=11 for all factors).

	Component		
	1	2	3
% of Variance	56.2%	14.4%	12.3%
Uronic acid (URA)	0.95	0.18	-0.02
Total carbohydrate (TCHO)	0.91	0.04	0.15
Organic carbon (OC)	0.81	0.57	0.08
Organic nitrogen (ON)	0.43	0.84	0.24
Hydroquinone (HQ)	0.38	0.79	0.40
$\log K_c(\text{Po})$	0.31	0.05	0.79
Protein	0.29	0.84	0.36
$\log K_c(\text{Th})$	0.10	-0.67	0.16
$\log K_c(\text{Be})$	-0.03	0.15	0.87
$\log K_c(\text{Pb})$	-0.21	-0.13	-0.88
$\log K_c(\text{Pa})$	-0.53	-0.59	-0.52
Hydroxamate siderophore (HS)	-0.65	-0.14	-0.30
Organic sulfur (OS)	-0.88	-0.23	-0.36

* Bold value denotes loadings with a significance level of ± 0.4 .

2.4.3 Effects of COM composition on the partitioning of ^{234}Th , ^{233}Pa , ^{210}Po , ^{210}Pb and ^7Be between dissolved and colloidal phases

Limited by the numbers of available samples and the 3-dimensional architecture of COM (including colloids and EPS), definitive relationships between functional groups of biomolecules and $\log K_c$ values of radionuclides were difficult to obtain. Factor analysis

(varimax) was used to help explore the effects of COM composition on radionuclide partitioning and find the most likely carrier biomolecules for radionuclides binding in the colloids and EPS samples. With all samples analyzed, three factors explain 82.9% of the total variance present in the original data set. We adopted the symbol $\log K_c(X, Y, Z)$ to represent $\log K_c$ values of X, Y and Z (X, Y, Z represent radionuclides). Table 2.5 lists the loadings of variables on factors 1 to 3 (F1 to F3). Factor loadings (fl) of $fl \leq -0.4$ or $fl \geq 0.4$ are considered here to be significant (bold numbers in Table 2.5). Members of F and -F groups are inversely correlated. Particularly, factor 1 (F1) is represented by URA, TCHO, OC and ON. The negative factor 1 (-F1) is represented by $\log K_c(\text{Pa})$, HS and OS. F2 is represented by OC, ON, HQ and protein; -F2 represents $\log K_c(\text{Th, Pa})$. F3 is represented by $\log K_c(\text{Po, Be})$, HQ and -F3 by $\log K_c(\text{Pb, Pa})$.

Overall, though bulk organic material was not found to be a good proxy for prediction of radionuclide binding, the same can be said for TCHO, URA, protein and ON, which reflect the degraded properties of carrier biomolecules, OS and HS phases, for Pa. Similar results were also shown in our other studies (Chuang et al., 2013, under review) that hydroxamate siderophores (HS) appear to be a main component of recalcitrant organic carbon in the sinking particles and play an important role in the fractionation and scavenging of Pa in the water column. Additionally, HQ showed a positive correlation with $\log K_c(\text{Po, Be})$ and inverse correlation with $\log K_c(\text{Th, Pa, Pb})$. The control mechanisms behind these relationships are not quite clear. But as a common redox regulator with phenolic hydroxyl functional group present in humic substances (e.g., Kalmykov et al., 2008, and references therein), HQ might relate to the redox

changes of multi-valent radionuclides (Zeh et al., 1999; Kalmykov et al., 2008), e.g., Pa and Po in this study, by further changing their affinities to organic biomolecules; or, direct complexing by hydroxyl (-OH⁻) functional group to nuclides (Thakur et al., 2006) with A-type metal properties, e.g., Th, Pa and Be in this study.

2.4.4 Isoelectric focusing of radiolabeled marine biopolymers

By using isoelectric focusing electrophoresis, the specific carrying biomolecules for radionuclides were further separated on the basis of their different isoelectric points. Four selected radiolabeled EPS and colloids samples (E1 and E3, C9 and C11) were investigated. The results are shown in Figure 2.2, in terms of % activity in each fraction vs. corresponding pH. In Fig. 2.2a, about 30% of the ²³⁴Th was concentrated below pH of 4 in all tested EPS and COM samples. ²³³Pa showed higher pH_{IEF} peak at about pH 4 to 5, especially for the E1 sample, with more than about 35% of ²³³Pa that was concentrated here (Fig. 2.2b). In Fig. 2.2c, ²¹⁰Pb-labeled EPS and COM similarly showed the major peak at pH<3 with a sub peak at pH around 6. Sample E3 showed a second minor peak at pH>8. Even for ²¹⁰Pb/²¹⁰Po, as a pair of mother-daughter radionuclides, ²¹⁰Po-labeled EPS and COM showed different IEF profiles from those of ²¹⁰Pb. In Fig. 2.2d, ²¹⁰Po showed the main pH_{IEF} peak at about pH 6.5 in all samples. ⁷Be showed the highest abundance at a basic pH of 8.5, and some minor pH_{IEF} peaks at lower pH values, e.g, pH 5.5 for E3; pH 3.5 and 7.5 for C9; pH 5.5 to 6.5 for C11 (Fig. 2.2d). Overall, results from the IEF profiles indicate that different functional groups in EPS and COM respond differently to the different radionuclides. Similar IEF spectra of ²¹⁰Po further demonstrate the specificity of the carrier biomolecules, no matter if the sample

was EPS or colloid. In contrast, ^7Be showed the least specific pH_{IEF} of its carrier biomolecules, and was also different among samples.

Further compositional analyses results of IEF fragments are shown in Fig. 2.3. For proteins, in EPS samples, ~25% were concentrated at pH of 5 with a minor peak at pH of 3; in colloids, major peaks were at around pH of 6.5 and 9. Total carbohydrates (TCHO) had a major peak at pH of 5 and a minor peak at $\text{pH} < 4$ and a pH of 3 in EPS sample; and TCHO showed less specific peaks at pH of 4-5 and 8-9 in colloids. For Fe, two distinct peaks were showed up at pH of 8 and 3.

Overall, ^{234}Th and ^{233}Pa and ^{210}Pb were mainly complexed by positively charged organic macromolecules, with low isoelectric points around 2-5 (Fig. 2.2a-c), where also Fe, proteins and acid polysaccharides accumulated (Fig. 2.3). Most of ^7Be activities, with relatively high amounts of proteins and Fe (Fig. 2.2e, 2.3a and 2.3c), were found at pH values higher than 8, suggesting their carriers were mainly composed of negatively charged Fe-related carrier biomolecules. Last, ^{210}Po -labelled EPS was immobilized at around pH 6 in the electric field (Fig. 2.2d), a pH value close to the isoelectric points where proteins mostly accumulate (Fig. 2.3a), possibly due to a preponderance of weakly acid residues.

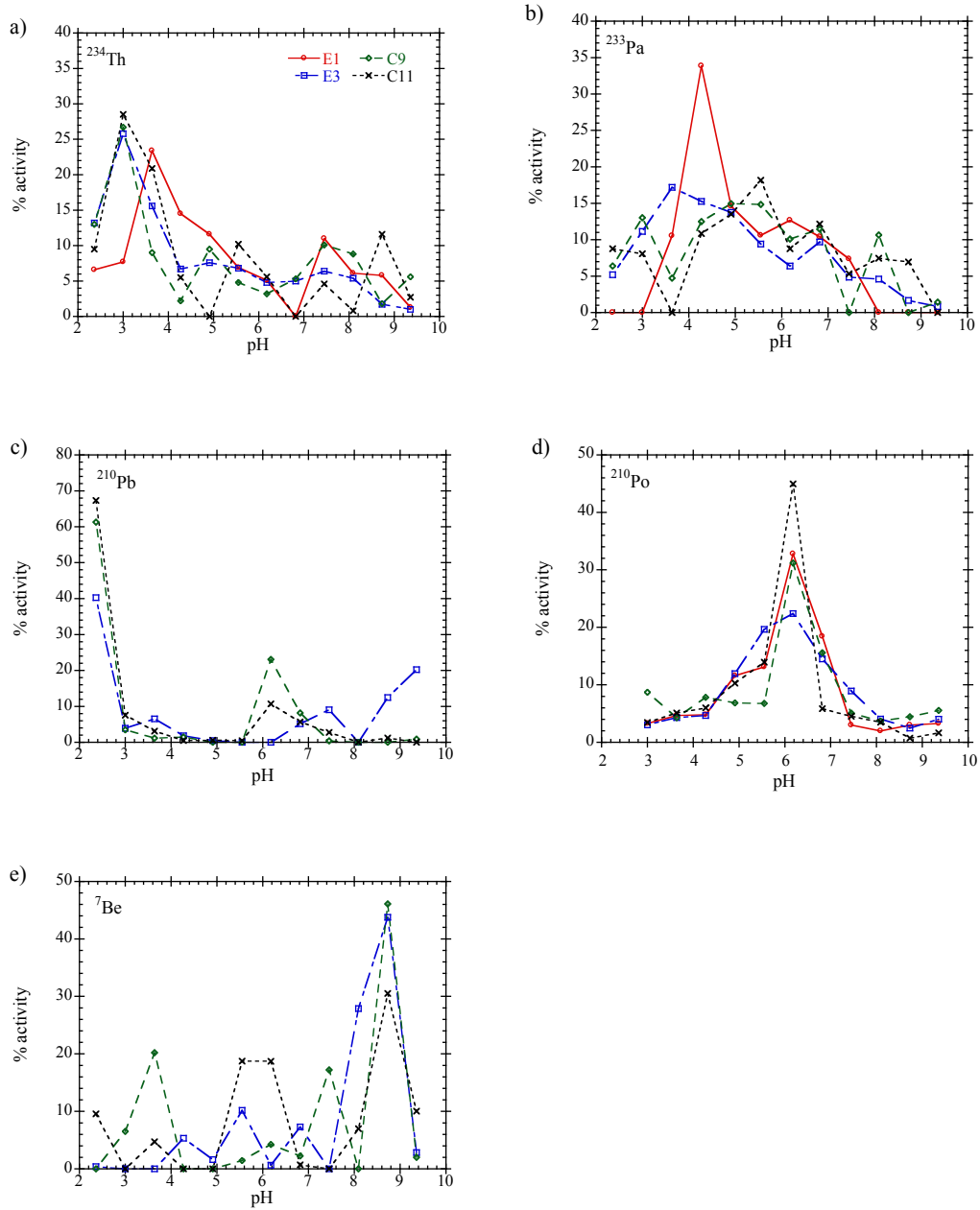


Fig. 2.2 Results from Isoelectric focusing electrophoresis of a) ^{234}Th ; b) ^{233}Pa ; c) ^{210}Pb ; d) ^{210}Po and e) ^7Be radiolabeled EPS and colloids.

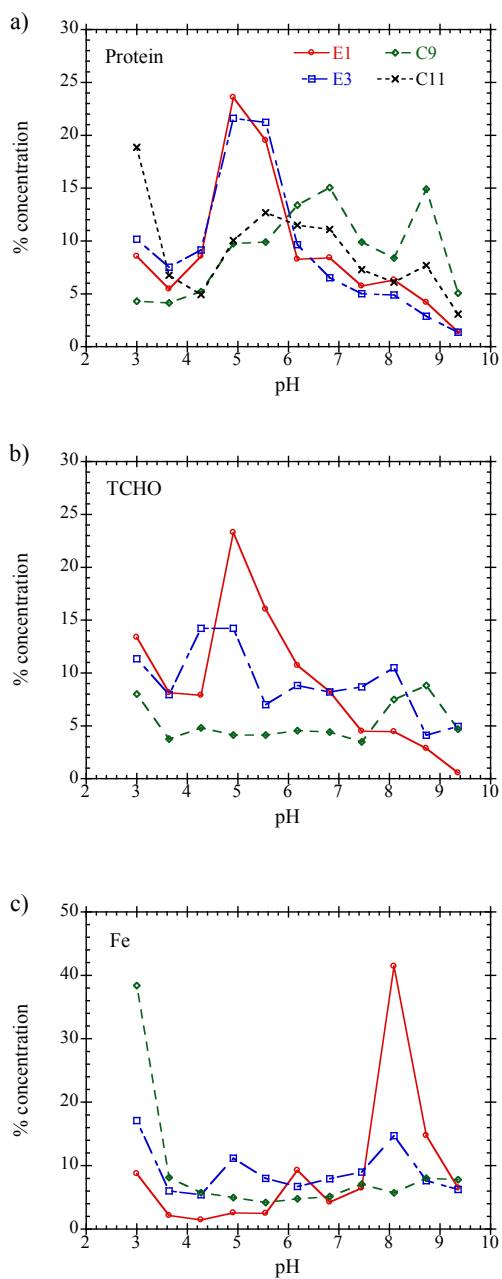


Fig. 2.3 Percentage distribution of a) Proteins (mg/g); b) total carbohydrates (TCHO, mg/g); c) Fe contents (ppb) in isoelectric focusing electrophoresis of radiolabeled EPS and colloids.

While Quigley et al. (2002) first reported a strong association of ^{234}Th with URA-rich substances of low isoelectric points, Alvarado Quiroz et al. (2006) further confirmed that strongly ^{234}Th -binding amphiphilic biomolecules showed varied functional group composition, including carboxylic acid, phosphate and sulfate groups, depending on the COM sources. This also implies that the abilities of radionuclides consist of strong polydentate chelating metal complexes in clustered structures of different organic carrier molecules.

Similarly, a structural study reported that marine hydroxamate siderophore exochelin *MS* (the extracellular siderophore from *Mycobacterium smegmatis*, Dhungana et al., 2004) have seven protonation sites for metal binding, one on a carboxylic acid, three on hydroxamate sites, and three on primary amine groups. The binding of radionuclides with natural hydroxamate siderophores might also form a similar configuration. As a consequence of the heterogeneity of the binding sites, the isoelectric point of any extracted radionuclide-binding molecule would be expected to show different pH_{IEF} patterns due to the different pK_a values of different binding sites, as was found in this study. Thus, a more in-depth evaluation of these organic carrying biomolecules from different COM sources at the molecular level is clearly warranted.

2.5 Conclusions

Combined the results from the factor analysis of radionuclide partitioning and chemical composition data as well as isoelectric focusing data provide a basis to evaluate possible biopolymeric macromolecular carrier phases for selected radionuclides. It becomes evident that specific organic biomolecules in marine colloids and EPS are the

main carrier phases for selected radionuclides in the ocean, consistent with results from previous field and laboratory studies. In particular, acid polysaccharides and uronic acids appear to be organic ligands for ^{234}Th binding; hydroxamate siderophores and organic sulfur containing biomolecules are important in the binding of ^{233}Pa ; ^{210}Pb -binding is associated to acid polysaccharides- and/or Fe-related protein-containing biomolecules; proteins-containing biomolecules are shown to be major classes of ^{210}Po binding biopolymers; for ^7Be , the strongest binding biomolecules seem to contain hydroquinones and/or Fe-containing biomolecules.

In our study area, marine colloids with concentrations ranging from ~ 0.2 to 5.1 mg/L, comprised a major organic carbon pool comparable or higher than particulate organic carbon (Guo and Santschi, 1997b; Hung et al., 2004a; 2012). These results help to obtain a better understanding of the control mechanisms by colloids in the fractionation of radionuclides in the ocean. This in turn is important in the assessment of the use of radionuclides to assess organic matter cycling. To further identify the specific binding ligands for the different radionuclides, molecular level studies of these biomolecules is needed.

CHAPTER III

ROLE OF DIATOMS IN THE SCAVENGING OF PARTICLE REACTIVE RADIONUCLIDES, Th, Pa, Pb, Po AND Be, IN THE OCEAN: A CASE STUDY WITH *PHAEODACTYLUM TRICORNUTUM*

3.1 Overview

Laboratory studies have been conducted to examine the sorption of selected radionuclides (^{234}Th , ^{233}Pa , ^{210}Po , ^{210}Pb , and ^7Be) onto inorganic (pure silica and acid-cleaned diatom frustules) and organic (diatom cells, with or without silica frustules) particles in natural seawater, and the role of exopolymeric substances (EPS), extracted from the same species of diatom, *Phaeodactylum tricornutum*. The partition coefficients (K_d values, reported as $\log K_d$) of radionuclides between water and particles ranged from 4.78 to 6.69 for ^{234}Th , from 5.23 to 6.71 for ^{233}Pa , from 4.44 to 5.86 for ^{210}Pb , from 4.47 to 4.92 for ^{210}Po , and from 4.93 to 7.23 for ^7Be . In general, the sorption of all radionuclides can be enhanced significantly by organic particles, resulting in K_d values 1-2 orders of magnitude higher than on inorganic particles. Results of particulate chemical composition indicated that EPS and frustule embedded biomolecules in the diatom cells are responsible for the sorption enhancement rather than the silica shell itself. Variations in K_d values of different radionuclides suggest that sorption affinity is likely controlled by specific organic functional groups. In addition, by separating

radiolabeled EPS via isoelectric focusing, we found that isoelectric points are radionuclide specific, suggesting that radionuclides bind to specific biopolymer functional groups with the most efficient binding sites occurring in acid polysaccharides and iron-binding proteins. Further progress in radionuclides controlling mechanisms of diatoms requires improved understanding of the molecular level characterization of these diatom related biopolymers.

3.2 Introduction

The chemical interactions between trace elements, dissolved and particulate chemical constituents in the ocean, as well as particle scavenging by organic and inorganic reactions, is one of the important factors controlling the trace elemental composition of seawater (Hurd and Spencer, 1991). The major part of oceanic particulate matter is biogenic organic matter, although suspended particles may also contain clay minerals, especially in estuaries and near-shore environments. About half of the global primary production takes place in the oceans (Longhurst et al., 1995; Field et al., 1998). Photosynthetic activity by phytoplankton in the surface ocean is a major driving force in sequestering the greenhouse gas carbon dioxide (Falkowski et al., 1998). The global net primary production from phytoplankton is estimated as ~45-50 Pg C per annum (Carr et al., 2006), driven by a phytoplankton biomass of ~1 Pg C, which is roughly 0.2% of the photosynthetically active carbon biomass on the Earth.

Diatoms are arguably one of the most important contributors to the global carbon fixation and the cycling of all biological elements. These microscopic, eukaryotic phytoplankton carry out about one-fifth of the photosynthesis on Earth (Armbrust 2009) and are estimated to contribute up to 45 to 48 % of the global oceanic primary production (Nelson et al. 1995; Mann 1999). The cell wall of diatoms is composed of an architecturally elegant, siliceous frustule encased in an organic coating (Reimann et al. 1965). Those frustules, sink to the bottom of the ocean after cell death, and are often preserved in the sediments. Biogenic silica derived from diatoms is also believed to be responsible for the scavenging and fractionation of many of the particle reactive radionuclides, such as ^{231}Pa , ^{230}Th and their ratio (Walter et al. 1997; Chase et al. 2002). The original application of the $^{231}\text{Pa}/^{230}\text{Th}$ ratio was used as a proxy for paleoproductivity studies, and the ratio is also used to assess boundary scavenging and ocean circulation (e.g., Anderson et al. 1983; Kumar et al. 1995; Walter et al. 1997). However, results from both field and laboratory studies found Thorium to Protactinium ratios in suspended or sinking particles can vary as a function of particulate chemical composition, sampling location, depth and size (Li 2005, and references therein).

Both field and laboratory studies have shown selective and compound specific interactions of ^{234}Th with marine organic matter (e.g., Guo et al. 2002; Roberts et al. 2009; Xu et al. 2011) that is partly originating from diatoms. Recently, a set of

phosphoproteins and long chain polyamines (LCPA), e.g., silaffins and cingulin, isolated from diatom frustules, were shown to be responsible for the assembly from nanoparticulate opal that is then generating networks of silica nanospheres (e.g., Kröger et al. 1999; Kröger and Poulsen 2008; Scheffel et al. 2011). Knowledge of the chemical composition of this organic template present as inner and outer coatings of diatom cells is important for identifying the biomolecules responsible for the scavenging particle reactive radionuclides. Therefore, understanding the molecular nature of these organic coatings, their embedded substances and probable fate in aquatic environments could have important consequences for the interpretation of the geochemical cycling of particle reactive radionuclides and for paleo-oceanography studies.

The aim of the present study was to examine the role of biogenic silica related biomolecules on the sorption of ^{234}Th , ^{233}Pa , ^{210}Pb , ^{210}Po and ^7Be radionuclides. The diatom species selected for the present study is *Phaeodactylum tricornutum*. Unlike most diatoms, *P. tricornutum* can grow in the absence of dissolved silicate, and the biogenesis of silicified frustules is facultative. This provides a unique opportunity to explore whether the silicified frustules or the organic matter attached or embedded on the diatom frustules, such as exopolymeric substances (EPS) or silaffins, are the main carrier phases responsible for the radionuclide uptake. Partition coefficients (K_d values) of selected radionuclides with these organic and inorganic silica particles, including pure silica,

acid-cleaned diatom frustules (organic matter removed to <1%), and diatom cells grown with or without their silicified frustules, were thus examined. By characterizing the exopolymeric substances (EPS) composition and separating the radiolabeled EPS using isoelectric focusing (IEF), our findings reveal the binding biomolecules are radionuclides specific and also help better understand the role of diatoms in the radionuclide biogeochemistry.

3.3 Methods and materials

3.3.1 Diatom cultures, sample preparation and EPS extraction

Phaeodactylum tricornutum (UTEX 646) was selected for culturing in autoclaved f/2 (with frustle) and f/2-Si (no frustle) media (salinity of 26) at a temperature of $19 \pm 1^\circ\text{C}$ with a light cycling of 14h: 10h under a saturating irradiance of $100 \mu\text{mol quanta m}^{-2} \text{s}^{-1}$. In order to deplete the diatom of Si supply, cultures were transferred into f/2-Si medium over at least 6 generations by harvesting cells (2694g, 30 min, room temperature) and resuspending them in fresh f/2-Si medium. Sterile polycarbonate bottles were also used to prevent Si supply from glassware. The growth status of *P. tricornutum* was monitored by changes in optical density at 750 nm. Cells, frustules and EPS were collected when *P. tricornutum* reached the stationary phase.

Laboratory cultures of *P. tricornutum* were centrifuged (2694 g, 30 min) and filtered (0.2 μm) to collect the whole cells. The frustules were treated repeat cleaning using a

hydrogen peroxide (30%, room temperature) treatment till bubbles were no longer generated, followed by concentrated nitric acid (HNO₃) digestion (85°C, 1 hr) to remove organic matter which was adopted from Robinson et al. (2004). The resulting organic carbon (C), nitrogen (N) and sulfur (S) contents of the cleaned frustules were measured using a Perkin Elmer CHNS 2400 analyzer to ensure the removal of organic materials using cysteine as a standard according to (Guo and Santschi, 1997b).

Procedures developed by Zhang et al. (2008) were used for EPS extraction, which minimize cell rupture and molecular alterations, and maximize extraction efficiency. EPS here is referring to those biopolymers that are attached on the diatom frustules. Hereafter, EPS Si⁺ and EPS Si⁻ denote the EPS extracted from diatoms cultured under Si-replete (i.e. f/2 medium) and Si-depleted (i.e. f/2-Si medium) conditions, respectively. Briefly, laboratory cultures were centrifuged (2694 g, 30 min) and filtered (0.2 µm) when diatoms reached stationary phase. The diatom cells were soaked with 3% sodium chloride (NaCl) solution for 10 min and followed by centrifugation at 2000g, 15 min, to remove the medium and weakly bound organic material on the cells. The pellet from previous step was resuspended in a new 100 ml 3% NaCl solution and stirred gently overnight at 4°C. The resuspended particle solution was ultra-centrifuged at 12000g (30 min, 4°C) and the supernatant was then filtered through a 0.2 µm polycarbonate membrane. The filtrate was desalted and collected with a 1 kDa cutoff cross-flow

ultrafiltration/diafiltration membrane and then freeze-dried for later use.

3.3.2 Characterization of exopolymeric substances

After partitioning EPS collected from lab cultures into aliquots for freeze-drying, subsamples were analyzed for individual components. Concentration of total carbohydrate (TCHO) concentration was determined by the TPTZ (2, 4, 6-tripyridyl-s-triazine) method using glucose as the standard, and uronic acids were measured by meta-hydroxyphenyl method using glucuronic acid as the standard (Hung and Santschi, 2001). Protein content was determined using a modified Lowry protein assay, using bovine serum albumin (BSA) as the standard (Pierce, Thermo Scientific). C, N and S contents were determined as described above. Iron was measured using an atomic absorption spectrometer (Varian) after overnight digestion with 12 mol L⁻¹ HNO₃ at 85°C (Van Loon, 1985).

To evaluate of protein size distribution pattern in EPS Si⁺ and EPS Si⁻, sodium dodecyl sulfate-polyacrylamide gel electrophoresis (SDS-PAGE) was carried out according to Sambrook et al. (1989) using standard molecular weight markers (Dual Xtra Standards, Bio-Rad). Individual amino acids are analyzed by a reverse-phase Waters HPLC system with an Alltech Alltima C18 column (5 µm, 250 × 4.6 mm), using an pre-column O-phthaldialdehyde (OPA) derivatization methods (Duan and Bianchi, 2007). Individual amino acids were identified and quantified with a fluorescence

detector (excitation/emission: 330/418 nm) on the basis of internal standard, norvaline, and 17 individual standards (Sigma). For all HPLC work, Waters Empower™ 2 software was employed to operate the system and to acquire and integrate the chromatograms. Fourier Transform Infrared Spectroscopy (FTIR) was used to characterize samples using a Varian 3100 model interfaced with a single reflection horizontal ATR accessory (PIKE Technologies, Inc., Madison, WI). A diamond plate was used as the internal reflection element. A freeze-dried EPS sample was mounted at the surface of the diamond. Absorbance spectra from 800 to 2000 cm^{-1} were collected and integrated using Varian Resolution Pro 4.0 software.

3.3.3 Sorption experiments

Natural seawater, collected from the Gulf of Mexico with a salinity of 35.0, was sequentially filtered through a 0.2 μm polycarbonate cartridge and ultrafiltered with a 1 kDa cutoff membrane to remove particulate and colloidal organic matter (Guo et al., 1995; Roberts et al., 2009). The <1 kDa ultrafiltrate fraction was then used for all sorption experiments.

The ^{234}Th tracer was purified and extracted from a ^{238}U solution (Quigley et al., 2002; Alvarado Quiroz et al., 2006); ^{233}Pa , in equilibrium with ^{237}Np , was obtained from Pacific Northwest National Laboratory; ^{210}Pb and ^{210}Po , in 1 mol L^{-1} HNO_3 and 2 mol L^{-1} Hydrochloric acid (HCl), respectively, were purchased from Eckert & Ziegler Isotope

Products and the ^7Be tracer solution (in $0.1 \text{ mol L}^{-1} \text{ HCl}$) was manufactured at the Paul Scherrer Institute, Switzerland (Schumann et al., 2013).

Sorption experiments were carried out with all five radionuclides and four different types of particles: pure silica particles (SiO_2 , $\sim 5 \mu\text{m}$, Sigma), acid-cleaned diatom frustules ($\text{OC} < 0.1\%$), whole diatom cells cultured with f/2 and f/2-Si medium.

Non-complexing $50/25 \text{ mmol L}^{-1}$ Tris-HCl buffered seawater ($< 1 \text{ kDa}$) solutions were transferred into acid cleaned experimental tubes to precondition container walls for at least 24 h to reduce tracer adsorption. The buffer capacity of Tris-HCl also neutralized the acidic radionuclide tracer solutions avoiding pseudocolloids generation by sodium hydroxide (NaOH) (Roberts et al., 2009), and maintained the pH at 8.0 ± 0.5 . Then, different types of pre-weighed amounts of particles were added to the seawater, resulting in a final particulate concentration of about 2 mg L^{-1} . The experimental system was stirred for 48 h to reach partitioning equilibrium of nuclides between particulate and dissolved phases. After that, the experimental solution was filtered through a $0.2 \mu\text{m}$ pore size polycarbonate filter (Millipore®). Before sample filtration, the filter and filtration system was pretreated with ultrafiltered seawater to reduce the adsorption of radionuclides (Chuang et al., 2013b). Both the filter and the $< 0.2 \mu\text{m}$ filtrate was collected to measure activities of selected radionuclides.

3.3.4 Partition coefficient of ^{234}Th , ^{233}Pa , ^{210}Pb , ^{210}Po and ^7Be

Activity concentrations of ^{234}Th , ^{233}Pa , ^{210}Pb and ^7Be were measured by gamma counting the 63.5 keV, 312 keV, 46.5 keV and 477.6 keV lines, respectively, on a Canberra ultra-high purity germanium well type detector. The ^{210}Po activity was analyzed by liquid scintillation counting (Beckman Model 8100 Liquid Scintillation Counter). The filter samples ($>0.2\ \mu\text{m}$ particulate phase) were soaked with $1\ \text{mol L}^{-1}$ HCl for 20 min in a counting vial and the filtrate samples ($<0.2\ \mu\text{m}$ dissolved phase) were transferred into counting vials directly. Both filter and filtrate samples were then counted for activities of each radionuclide. All reported activities were decay and geometry corrected.

Traditional partition coefficients (K_d) between dissolved and particulate phases were used to quantify the sorption of radionuclides onto different particles in different experimental systems. K_d was defined here as:

$$K_d = A_p \times (A_d \times C_p)^{-1} \quad (1)$$

where A_p and A_d represented particulate and dissolved activities (Bq L^{-1}) of radionuclides; C_p is the particle concentration (g ml^{-1}) (Honeyman and Santschi, 1989; Guo and Santschi, 1997b).

3.3.5 Isoelectric focusing of radionuclides labeled EPS

EPS Si+ and EPS Si- were incubated with ^{234}Th , ^{233}Pa , ^{210}Pb , ^{210}Po and ^7Be for

isoelectric focusing electrophoresis (IEF) separation to determine the pH_{IEF} of selected radionuclides binding ligands (Alvarado Quiroz et al., 2006; Zhang et al., 2008; Xu et al., 2009). Briefly, radiolabeled biopolymers and a 140 μ l of rehydration solution were loaded onto an IPG strip (GE healthcare immobilineTM Drystrip, pH 3-10, 11cm) and were re-swelled overnight. Afterward, the strip was loaded into the device for isoelectric focusing for 17.5 hr. The strip was then cut into 11 1cm-pieces and followed by 1% sodium dodecyl sulfate (SDS) extraction overnight. Five radionuclide activities of each fraction were subsequently analyzed. Due to the limited amount of each strip fraction, selected chemical compositions (TCHO, Proteins and Fe) of individual fraction were characterized as described above.

3.4 Results

3.4.1 Partitioning of ^{234}Th , ^{233}Pa , ^{210}Pb , ^{210}Po and ^7Be between dissolved and silica particles

Our sorption experimental results indicate that acid-cleaned silica frustules from diatom *P. tricornutum*, $\log K_d$ values were similar to commercially available pure silica for the selected radionuclides (^{234}Th , ^{233}Pa , ^{210}Pb , ^{210}Po and ^7Be), and that they are 1-2 orders of magnitude lower than those of untreated whole diatom cells, regardless of silica-containing or silica-free shells (Fig. 3.1).

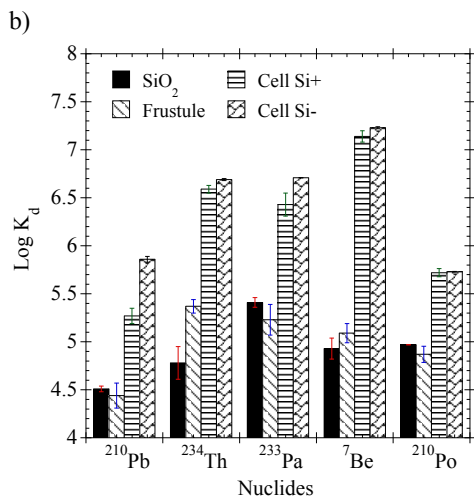
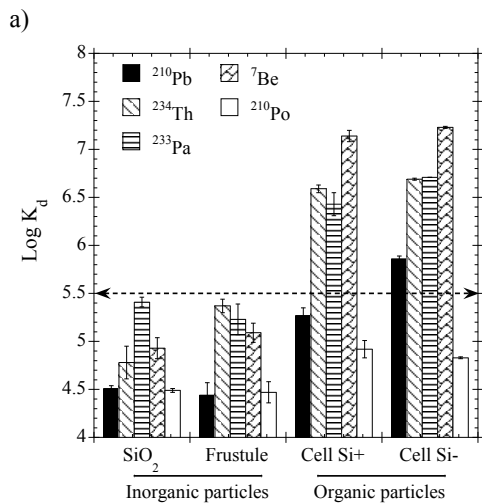


Fig. 3.1 a) Comparisons of $\log K_d$ values of ^{234}Th , ^{233}Pa , ^{210}Pb , ^{210}Po and ^7Be on different type of particles, including pure silica, acid cleaned diatom frustule (w/ OC%<0.1), diatom cell with or without Si frustule; b) Variations in $\log K_d$ values of ^{234}Th , ^{233}Pa , ^{210}Pb , ^{210}Po and ^7Be with the four different types of particles.

Table 3.1 Elemental and Biochemical composition of EPS Si+ and EPS Si- harvested from *P. tricornutum* grown in seawater media with and without Si, respectively.

		Unit	EPS Si+	EPS Si-
Major organic component	C	%	35.1	33.8
	N	%	4.0	0.5
	S	%	1.8	0.0
	Protein	mg g ⁻¹	216.4	131.5
	TCHO	mg g ⁻¹	233.2	263.9
	URA	mg g ⁻¹	87.6	31.2
Amino acid composition	Group	Individual amino acid	nmol mg⁻¹	
	Sulfur	Cys	12.2	3.0
		Met	4.9	2.2
	Basic (amino group)	Arg	20.5	5.8
		Lys	5.7	1.0
	Carboxylic	Asp	76.2	19.5
		Glu	28.5	8.0
	Hydroxyl	Ser	10.6	4.9
		Thr	16.6	3.7
	Aromatic	Tyr	5.2	2.2
		Phe	8.2	3.3
	Aliphatic	Val	17.1	5.1
		Ile	11.4	3.0
		Leu	18.1	4.9
Total			235.1	66.5

*Maximum 1 standard deviations (SD) for each analysis were 1% (relative). Categories of amino acids are based on the nature of their side groups.

No significant differences in logK_d values of all selected radionuclides with organic particles (diatom cells with or without silica frustule) were observed. In particular, logK_d values of selected radionuclides in adsorption experiments with different particle types ranged from 4.78 to 6.69 for ²³⁴Th, 5.23 to 6.71 for ²³³Pa, 4.47 to 4.92 for ²¹⁰Po, 4.44 to

5.86 for ^{210}Pb and 4.93 to 7.23 for ^7Be , respectively (Fig. 3.1). Furthermore, the averaged $\log K_d$ values from our experiments varied among the selected radionuclides, following the order of $\text{Be} > \text{Pa} > \text{Th} > \text{Pb} > \text{Po}$ in these sorption experiments, showing that the affinity to biogenic silica varied among the different radionuclides (Fig. 3.1).

3.4.2 Composition of EPS extracted from *P. tricornutum*, under Si-depleted and Si-replete conditions

The composition (C, N and S, proteins, uronic acids (URA), total carbohydrates (TCHO) and individual amino acids) of two types of diatom EPS (EPS Si⁺ and EPS Si⁻) are given in Table 3.1. Maximum 1 standard deviations (SD) for each analysis were 1% (relative). Categories of amino acids are based on the nature of their side groups. Overall, EPS Si⁺ showed higher concentrations in its organic compounds than EPS Si⁻, except for its TCHO% (Table 3.1). This was also reflected in ATR-FTIR spectra of these two EPS samples (Fig. 3.2). ATR-FTIR spectroscopy provides a non-invasive way to quickly gain information about the contents of major secondary structures of biopolymers (Schmitt et al., 1995; Xu et al., 2011b; Jiang et al., 2012). Major infrared (IR) peaks were assigned according to Xu et al. (2011b) and Jiang et al. (2012). Characteristic bands found in the IR spectra of proteins and polypeptides include the Amide I (1652-1648 cm^{-1}) and Amide II (1550-1548 cm^{-1}). The absorption associated with the Amide I band leads to stretching vibrations of the C=O bond of the amide, absorption associated

with the Amide II band leads primarily to bending vibrations of the N-H and C-N bond. The symmetric stretching peak due to deprotonated carboxyl groups is observed at 1400 cm^{-1} along with the CH_2 bending mode at 1455 cm^{-1} . In the $800\text{-}1200\text{ cm}^{-1}$ regions, given information were about the main polysaccharides present in the complicated systems of polysaccharide mixtures, e.g., responses from C-O, C-O-C, P-O-P, C-O-P and ring vibrations. Specifically, the peaks at 1241 and 1113 cm^{-1} correspond to P-O stretching in phosphate groups. In summary, amide, carboxyl, and phosphoryl functional groups were observed in two different EPS samples. Overall, EPS Si+ sample showed significant higher intensities in peaks in Amide I and Amide II regions while EPS Si- sample had higher polysaccharides, phosphoryl carboxyl functional groups responses. The compositional distinctions are well reflected in the difference spectrum (Fig. 3.2c). The increase in the relative intensity of the band assigned to polysaccharides, and the decrease in the relative intensity of the band assigned to Amide I and II, could thus be referred as marker bands induced by diatom cells underwent Si-deficiency.

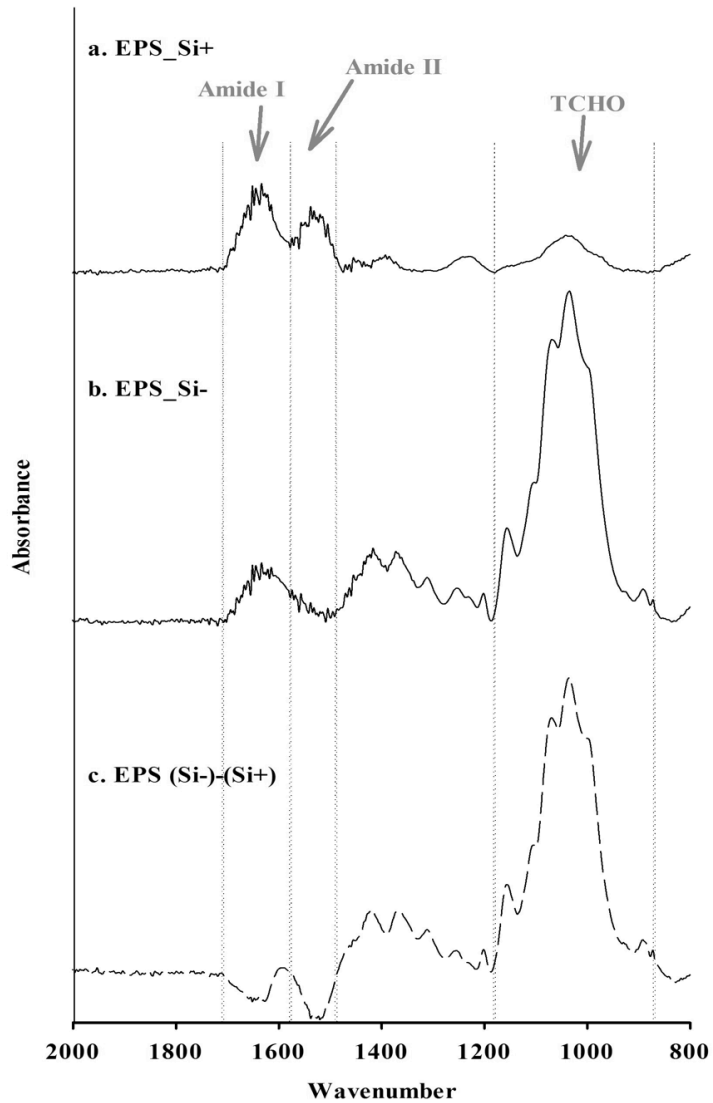


Fig. 3.2 ATR-FTIR spectra of different EPS samples extracted from diatom, *Phaeodactylum tricornutum*. a) EPS Si⁺ and b) EPS Si⁻. c) The difference FTIR spectrum (by EPS Si⁻ minus EPS Si⁺). Arrows indicate the signature bands of amide I (1652-1648 cm⁻¹), amide II (1550-1548 cm⁻¹) and carbohydrate (800-1200cm⁻¹).

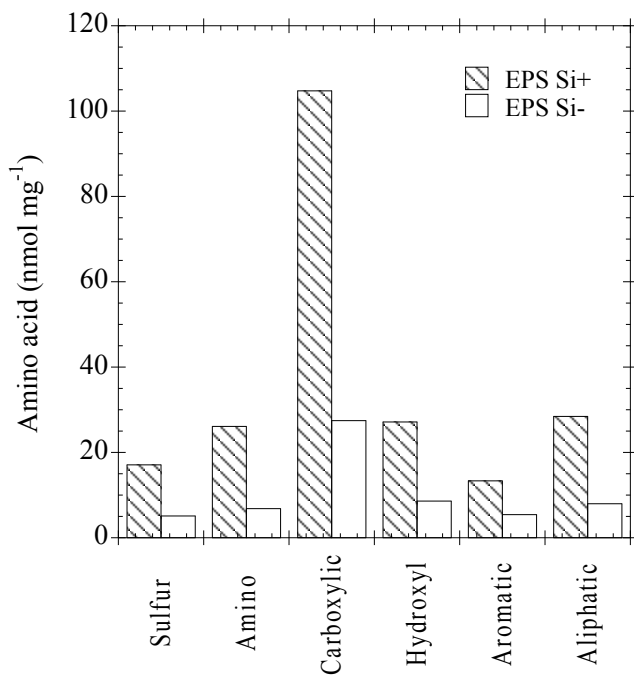


Fig. 3.3 Variation of concentrations of classified amino acid groups between a) EPS Si⁺ and b) EPS Si⁻.

Results from amino acid analysis also support that EPS Si⁺ sample had a higher amount of total protein-containing biomolecules than EPS Si⁻ sample (Table 3.1). In general, as individual amino acids, the amino group and acid group dominate the properties of the molecules. However, when amino acids combine to form proteins it is the properties of the side chains only that determines the properties of the protein. Based on the nature of their side groups, we classified identified amino acids into six categories (Table 3.1 and Fig. 3.3). Results showed the total amount of amino acids in each group

from two different EPS followed the same order of carboxylic >> aliphatic \approx hydroxyl \approx amino > sulfur > aromatic (Fig. 3.3). Two different EPS had the same pattern of amino acid composition but with different amounts in each group (Fig. 3.3). Consistent with other compositional analysis, the EPS Si⁺ sample had higher amounts in each group of amino acids. Moreover, SDS-PAGE results from EPS Si⁺ and EPS Si⁻ samples also showed similar pattern in protein size distribution, and with higher amounts in the EPS Si⁺ sample (Fig. 3.4).

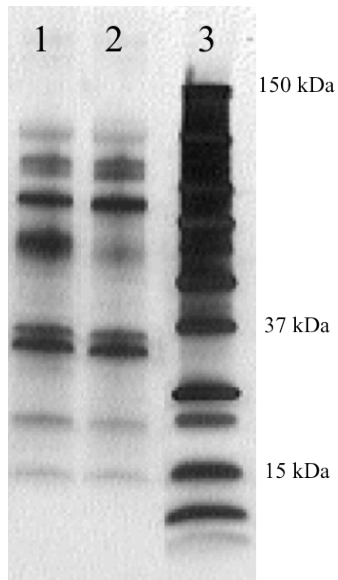


Fig. 3.4 Size distribution pattern of proteins in EPS Si⁺ and EPS Si⁻ harvested from *P. tricornutum* grown in seawater media with and without Si respectively. (Lane 1: EPS Si⁺; Lane 2: EPS Si⁻; Lane 3: standard molecular weight markers).

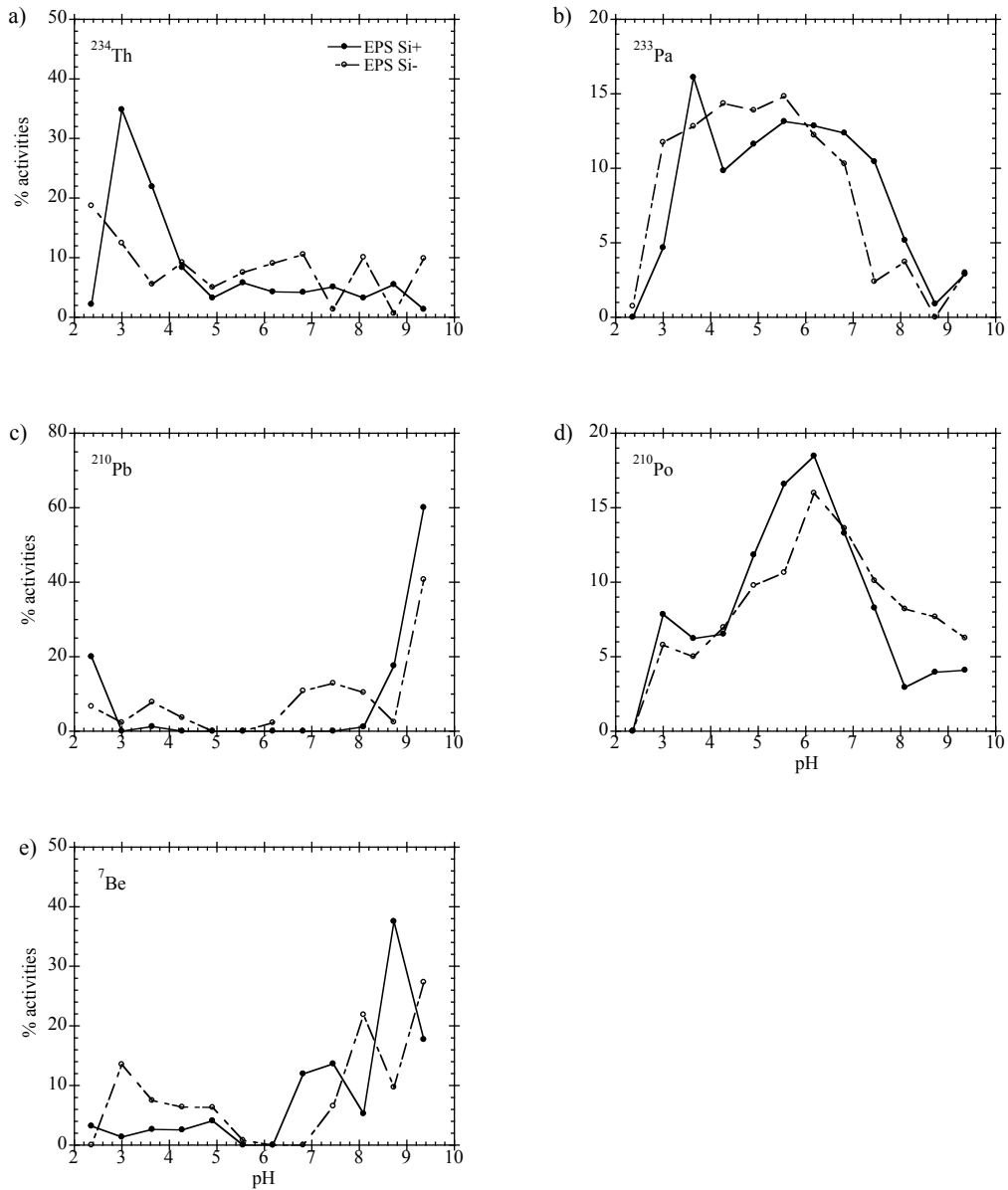


Fig. 3.5 Isoelectric focusing (IEF) electrophoresis of radiolabeled EPS Si+ and EPS Si- harvested from *P. tricornutum* grown in seawater media with and without Si respectively: a) ^{234}Th , b) ^{233}Pa , c) ^{210}Po , d) ^{210}Pb and e) ^7Be . Note: y-axis is specific to percentage of each radionuclide measured.

3.4.3 Isoelectric focusing of radiolabeled EPS

In Fig. 3.5, results from IEF profiles indicate that different functional groups in EPS bind the different radionuclides very selectively. Specifically, more than 30% of the ^{234}Th labeled EPS was concentrated below pH 4, while ^{233}Pa showed a broad pH_{IEF} peak at higher pH of 3 to 6. Even as a pair of mother-daughter radionuclides, ^{210}Pb and ^{210}Po still showed different patterns in their IEF profiles. For ^{210}Pb , more than 40% of labeled EPS was found above pH of 9 with a minor concentrated fraction below pH 3, and ^{210}Po showed main pH_{IEF} peak at pH 6 with a sub-peak at around pH 3. ^7Be showed most abundance at basic pH range > 8 and a minor abundance fraction at acidic pH range of 3.

Results from compositional analysis of IEF sections are shown in Fig. 3.6. For proteins, $\sim 20\%$ were concentrated on the segment with a pH of 5.5 and with a minor peak at $\text{pH} < 4$. Total polysaccharides had a major peak at pH 5 and two minor peaks at $\text{pH} < 4$ and $\text{pH} > 8$. For Fe, two distinct peaks could be identified at pH 4-5 and ~ 8 , respectively. Similar to the results for radionuclides, proteins, total polysaccharides and Fe contents had similar IEF profiles for both EPS Si+ and Si- samples. Consensus IEF spectra further implied that carrier molecules for each nuclide had similar properties of electric charges (Figs. 3.5 and 3.6).

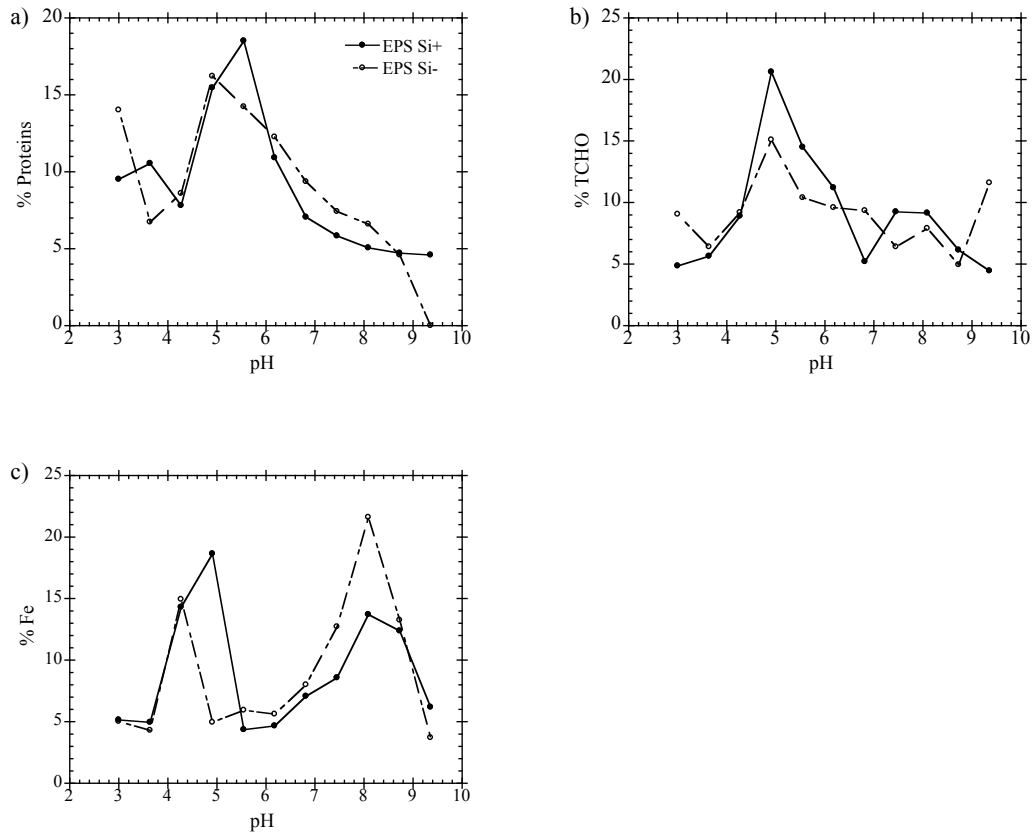


Fig. 3.6 Percentage distribution of a) proteins (mg/g); b) total polysaccharides (mg/g); c) Fe (ppb) content in Isoelectric focusing (IEF) electrophoresis of ^{234}Th , ^{233}Pa , ^{210}Pb , ^{210}Po and ^7Be radiolabeled EPS Si+ and EPS Si- harvested from *P. tricorutum* grown in seawater media with and without Si respectively.

Overall, ^{234}Th and ^{233}Pa were mainly complexed by positively charged organic macromolecules, with low pH_{IEF} around 3-5 (Figs. 3.5a and 3.5b), where also Fe, proteins and acid polysaccharides accumulated (Fig. 3.6). Most of ^{210}Pb and ^7Be

activities, with relatively high amounts of Fe (Figs. 3.5c, 3.5e and 3.6c), were found at pH higher than 8, suggesting their carriers were mainly composed of negatively charged Fe-related carrier molecules. Last, ^{210}Po -labelled EPS was immobilized at around pH 6 in the electric field (Fig. 3.5d), a pH close to the isoelectric points where proteins mostly accumulate (Fig. 3.6a), possibly due to a preponderance of weakly acid residues.

3.5 Discussion

3.5.1 Role of diatoms in scavenging of particle reactive radionuclides

Silica frustules from cells of diatom *P. tricornutum* were extensively acid-washed to remove both surface organic coatings and tightly-bound templating biomolecules embedded in the silica shell (e.g., silaffin) until the final OC concentration was <0.1%, were used for sorption experiments. These silica frustules showed similar $\log K_d$ values to a commercially available pure silica, for five different radionuclides (^{234}Th , ^{210}Pb , ^{233}Pa , ^7Be and ^{210}Po). Besides, $\log K_d$ values of radionuclides on pure silica particles were significantly, by 1-2 orders of magnitude, lower than those of whole diatom frustules in the presence of the templating biomolecules. No significant difference in the $\log K_d$ values of each radioisotope between diatom cells with or without silica frustule was found, attesting that the presence of silica, in this case, was not responsible for enhancing the sorption of radionuclides onto particles (Fig. 1), as is traditionally

assumed. Interactive effects between mineral (silica) phases and associated biopolymers are thus strongly suggested by our data.

Pure silica has previously been shown to be a poor sorbent for selected radionuclides (e.g., ^{234}Th and ^{233}Pa , summarized in Roberts et al., 2009; ^{210}Pb , ^{210}Po and ^7Be , summarized in Yang et al., 2013). In the present laboratory experiments, using pure silica, we obtained relatively low values of K_d . As a matter of fact, if one would want to obtain 10% of a dissolved radionuclide to sorb on pure silica (e.g., opal), this would require $\log K_d$ values of 6-7, given typical particle concentrations of 10-100 $\mu\text{g L}^{-1}$ in the ocean. However, typical $\log K_d$ values for pure opal phases are 5 or less for these radionuclides, corresponding to a A_p to A_d ratio of 0.01-0.001 or 0.1-1% of their dissolved activities for these radionuclides in oceanic environments (Roberts et al. 2009; Yang et al. 2013). This suggests that there must be other carrier phases responsible for radionuclide complexation and scavenging that occur in conjunction with opal production. Furthermore, our observed trend of K_d values of selected radionuclides is also consistent with what was found in the field and laboratory studies. For example, Chase et al. (2002) showed that Be and Pa had higher K_d values than Th when extrapolated to a 100% opal particles. Describing $\log K_d$ values of Th, Pa and Be as a function of %opal in the particulate matter, correlation coefficients ($\gamma_{\text{Th}}=-0.77$, $\gamma_{\text{Pa}}=0.67$ and $\gamma_{\text{Be}}=0.85$) followed the order that $\text{Be} > \text{Pa} > \text{Th}$, suggesting biogenic opal had the

highest impact on the binding of Be onto the oceanic particles. The $\log K_d$ values reported in a controlled laboratory study (Yang et al. 2013) also showed a trend of Be>Pb>Po, similar to our results using pure silica particles.

Diatom frustules should represent an inorganic-organic hybrid material that is mainly composed of inorganic silica to which various specific organic macromolecules (proteins, polysaccharides, long-chain polyamines, etc.) are attached. Several kinds of diatom frustule proteins have been identified and well characterized, including frustulins, pleuralins, silaffins, and cingulins, which are all endowed with silica-forming activity (Kröger et al. 1999; Kröger et al. 2002; Kröger and Poulsen 2008). Some of them, e.g., silaffins and cingulins, appear to be entrapped inside the frustule and could be likely well preserved during their transport and export to deep ocean. This is because they are not easily extracted from frustules, even under harsh extraction conditions (e.g., 2% SDS at 95 °C, 8 mol L⁻¹ urea, or 6 mol L⁻¹ guanidinium-HCl, at room temperature), as long as the silica remains intact (Scheffel et al. 2011). This fact can explain the large and significant differences found in K_d values between inorganic (pure silica and acid-cleaned frustules) and organic silica particles (whole diatom cells with or without silica frustules).

While the K_d value of ⁷Be might look surprisingly high, it had previously been observed that beryllium forms strong complexes with proteins in biological systems,

which is also the chemical basis to its strong toxicity (e.g., Scott et al. 2008).

Furthermore, adenosine diphosphate (ADP) and beryllium fluoride together tend to bind to adenosine triphosphate (ATP) sites and inhibit protein action, making it possible to crystallize proteins in the bound state. In addition, ADP and fluoride form strong ternary complexes (Issartel et al. 1991), thus allowing for the possibility that the Be(II)-binding site might be the multiple phosphate and/or amino and carboxyl groups in silaffin proteins. Through the study of several biologically relevant small molecule complexes of beryllium, it was discovered that beryllium has a high propensity to displace hydrogen atoms in strong hydrogen bonds (Issartel et al. 1991). These bonds, often formed between amino acids containing carboxylate and hydroxyl groups, help provide the framework supporting protein structure and function. Extending this model to real biological systems, it was shown that beryllium in human blood displaced all 12 strong hydrogen bond atoms in transferrin, an iron transport protein found in blood plasma. This presents a potential pathway for beryllium to enter cells with transferrin receptors (Scott et al. 2008). Further separation and analytical work will have to be done to unravel the actual strong binding sites specific for $^7\text{Be(II)}$ and other radionuclides.

3.5.2 Composition of EPS extracted from *P. tricornutum*, under Si-depleted and Si-replete conditions

From all composition analyses, diatom cultured under Si-stressed condition resulted in producing higher amounts of polysaccharides but much lower amounts of protein-containing biomolecules. Interestingly, the protein-containing biomolecules only showed any difference in terms of amounts in two EPS samples, but overall had similar molecular composition. This could be explained by what was found in genetic studies (e.g., Sapriel et al. 2009). Si-starvation up-regulated 13 genes in diatom cells, whereas 210 up-regulated genes were induced by Si-sufficient condition. Among the 13 up-regulated genes in Si-starvation condition, there are genes involved in carbon acquisition and glyoxylate cycle. Isocitrate lyase, an enzyme involved in the conversion of lipids to carbohydrates, is among the proteins whose expression is strongly up-regulated in the absence of Si in *P. tricornutum* (Sapriel et al. 2009). Among the up-regulated genes in Si-replete condition, there are genes involved in carbohydrate, amino groups, glutamate and glutamine metabolism, as well as the S-adenosine methionine cycle, which make a connection to the metabolism of sulfur (Frigeri et al. 2006; Sapriel et al. 2009). These observations support our findings that the EPS Si⁺ sample has a relatively higher amount of proteins and sulfur whereas EPS Si⁻ sample is richer of TCHO content.

3.5.3 Radionuclide-carrying biomolecules in EPS

Activity distributions of different radionuclide-carrying biomolecules along a pH gradient in the electric field revealed that isoelectric points are unique for the different radionuclides, suggesting that specific organic carrier phases are responsible for binding of each of the different radionuclides.

Previous studies using controlled laboratory experiments have identified uronic acids as the major carrier molecules in the ^{234}Th -labeled EPS at acidic pH were mainly composed of uronic acid (Quigley et al. 2002; Zhang et al. 2008; Xu et al. 2009). Alvarado Quiroz et al. (2006) further confirmed that the molecular weight (MW) and specific functional group composition of the strongly ^{234}Th -binding amphiphilic biomolecules can vary, depending on the species of plankton or bacteria, and included carboxylic acid, phosphate and sulfate groups. Hence, different acidic functional groups can, at times, contribute to the binding of ^{234}Th . This implies that the binding environment for these radionuclides, present at total concentrations at least a million times lower than those acid functional groups, consists of strong polydentate chelate complexes in clustered structures of different organic carrier molecules. While experimental data are highly suggestive, further molecular level identification studies are warranted for elucidating the role of those implanted biopolymers in diatom frustules in the scavenging and fractionation of particle reactive radionuclides in the ocean.

3.6 Conclusion

Silica frustules from cells of diatom *Phaeodactylum tricornutum* were extensively acid-washed to remove both surface organic coatings and tightly-bound templating biomolecules embedded in the silica shell (e.g., silaffin) until the final OC concentration was <0.1%, were used for sorption experiments. These silica frustules showed similar $\log K_d$ values to a commercially available pure silica, for five different radionuclides (^{234}Th , ^{210}Pb , ^{233}Pa , ^7Be and ^{210}Po). Besides, $\log K_d$ values of radionuclides on pure silica particles were significantly, by 1-2 orders of magnitude, lower than those of whole diatom frustules in the presence of the templating biomolecules. No significant difference in the $\log K_d$ values of each radioisotope between diatom cells with or without silica frustule was found, providing further evidence that silica cannot be the main carrier phase for these selected radionuclides in the ocean, as is traditionally assumed. Moreover, activity distributions of different radionuclide-carrying biomolecules along a pH gradient in the electric field revealed that isoelectric points are unique for the different radionuclides, suggesting that specific organic carrier phases are responsible for the binding of different radionuclides. Thus, our results not only help in the interpretation of silica as a paleoproductivity proxy but also have significant implications for both oceanography and geochemistry. While experimental data are highly suggestive, further molecular level identification studies are warranted for elucidating the role of

those embedded biopolymers in diatom frustules in the scavenging and fractionation of particle reactive radionuclides in the ocean.

CHAPTER IV

**THE MOLECULAR LEVEL CHARACTERIZATION OF ORGANIC
CARRIERS OF Th, Pa, Pb AND Be RADIONUCLIDES FROM DIATOM
FRUSTULES**

4.1 Overview

Laboratory studies have been conducted to investigate the binding mechanism of ^{234}Th , ^{233}Pa , ^{210}Pb , and ^7Be radionuclides to biogenic silica and its embedded biopolymers (BP). The experiment intended to differentiate between uptake to amorphous silica or associated biopolymers by incubating radionuclides during the growth of the diatoms. Separated fractions were divided after diatom cell death, or cell lysis. Partition coefficients (K_d) of radionuclides to different fractions of diatom cells (with or without silica frustules), and the role of extra/intra-cellular, and frustule embedded biopolymers, extracted from the same diatom species, *Phaeodactylum tricorutum*, were examined. High-resolution solution state 2D NMR approaches were applied to identify the signatures of biomolecules extracted from diatom frustules. More than 50% of selected radionuclides were bound to all-inclusive biopolymer fractions, showing the great importance of these diatom related biopolymers in the scavenging and fractionation of these radionuclides in the ocean. Variations in K_d values of different radionuclides suggest that the sorption affinity is likely controlled by specific organic

functional groups. Revealed by 2D HSQC (Heteronuclear single quantum coherence) NMR spectrum, the HF insoluble fraction biopolymers were mainly composed of carboxyl-rich, aliphatic-phosphoproteins, responsible for the strong binding of radionuclides.

4.2 Introduction

Biogenic silica (BSi) from diatom frustules are preserved to a significant extent in the sedimentary record and have been studied extensively from biological, paleoceanographic and geochemical perspectives. Its biogenic sediment burial rate in marine sediments is second only to that of calcium carbonate. Responsible for as much as 30–50% of the primary production occurring in the surface ocean (e.g., Nelson et al., 1995; Brzezinski et al., 1998; Ragueneau et al., 2000; Coale et al., 2004), diatoms contribute a great percentage to the organic-carbon flux exported from the euphotic zone to the deep ocean (Buesseler, 1998).

The nanostructure of diatom frustules is precisely controlled involving proteins as biocatalysts, e.g., biosilica-associated peptides (silaffins), which act as templates for *in vitro* silica formation from a silicic acid solution (Kröger et al., 1999; Kröger et al., 2002). Frustule proteins have been identified from both pennate and centric diatoms, consisting of several types of proteins, including frustulins, pleuralins, silaffins, and cingulins (Kröger et al., 1999; Kröger et al., 2002; Kröger and Poulsen, 2008).

According to Kröger and Poulsen (2008), silaffins are phosphoproteins that become solubilized upon dissolution of the diatom silica under relatively mild conditions using an acidified ammonium fluoride solution (10 M NH_4F pH 4–5). This solubilization distinguishes silaffins from pleuralins, as the latter can only be solubilized by using anhydrous HF, which not only leads to the removal of silica, but also to deglycosylation and dephosphorylation (Kröger and Poulsen, 2008). Silaffins appear to be entrapped inside the silica, because as long as the silica remains intact, they are not extracted from diatom cell walls even under harsh extraction conditions, such as 2% SDS at 95 °C, 8M urea, or 6M guanidinium-HCl at room temperature. Cingulins are proteins associated with the girdle band region of the diatom frustule and are endowed with silica-forming activity (Scheffel et al., 2011).

Because the silaffin polyamines contain multiple phosphate groups, they can strongly bind not only to the Si-OH group, but also assemble metal nanoparticles. Thus, the templating biomolecules have also been useful in nanotechnology, as in the manufacturing of MgO_2 , TiO_2 , BaTiO_3 , and other materials (Kröger and Poulsen, 2008; Das and Marsili, 2011).

The focus of this chapter is to investigate the binding mechanism of ^{234}Th , ^{233}Pa , ^{210}Pb , and ^7Be radionuclides to biogenic silica and its embedded BP. The experiment intended to differentiate between uptake to amorphous silica or associated biopolymers

by incubating radionuclides during the growth of the diatoms. Separated fractions were separated after diatom cell death, or cell lysis. K_d values of selected radionuclides with diatom cells (grown with and without their silicified frustules, as well as different fractions of diatom cells) were thus examined. Carrier biomolecules are subsequently separated and identified at the molecular level to further uncover the structure and possible binding mechanisms of the carrier phases for different radionuclides.

4.3 Materials and methods

4.3.1 Radiolabeled diatom cultures

Natural seawater of salinity 35, collected from the Gulf of Mexico, was sequentially filtered through a 0.2 μm polycarbonate cartridge and ultrafiltered with a 1 kDa cutoff membrane to remove particulate and colloidal organic matter (Guo et al., 1995; Roberts et al., 2009). The <1 kDa ultrafiltrate fraction was then used for later experiments. The ^{234}Th tracer was purified and extracted from a ^{238}U solution (Quigley et al., 2002; Alvarado Quiroz et al., 2006); ^{233}Pa , in equilibrium with ^{237}Np , was obtained from Pacific Northwest National Laboratory; ^{210}Pb , in 1 N HNO_3 , was purchased from Eckert & Ziegler Isotope Products and the ^7Be tracer solution (in 0.1 N HCl) was manufactured at the Paul Scherrer Institute, Switzerland (Schumann et al., 2013).

Autoclaved f/2 and f/2-Si media was added to the preconditioned clear PE container, and then ~ 10 to 15 Bq of each radionuclide tracer (^{234}Th , ^{233}Pa , ^{210}Pb , and ^7Be , at

equilibrium) was added. Solutions were then gently shaken and left to equilibrate overnight. In each radiolabeled medium, 1 ml of laboratory culture, *Phaeodactylum tricornutum* (UTEX 646), was added to incubate at a temperature of $19 \pm 1^\circ\text{C}$ with a light cycling of 14: 10 h under a saturating irradiance of $100 \mu\text{mol quanta m}^{-2} \text{s}^{-1}$. The growth status of *P. tricornutum* was monitored by changes in optical density at 750 nm in a parallel non-labeled culture. Cells, frustules, EPS and frustule embedded biopolymers were collected when *P. tricornutum* reached the stationary phase. The total growth time was 35 d.

4.3.2 Exopolymeric substance (EPS) extraction

Procedures developed by Zhang and Santschi (2009) were used for EPS extraction, which minimize cell rupture and molecular alterations, and maximize extraction efficiency. Hereafter, EPS Si⁺ and EPS Si⁻ denote the EPS extracted from diatoms cultured under Si-replete (i.e. f/2 medium) and Si-depleted (i.e. f/2-Si medium) conditions, respectively. There are two kinds of EPS, attached-EPS (AEPS) and non-attached-EPS (NAEPS). Both fractions were collected in this study, referred to as ‘biopolymers that are attached on the diatom frustules’, or ‘dissolved in the medium’, respectively. Briefly, for NAEPS, laboratory cultures were centrifuged (2694 g, 30 min) and filtered (0.2 μm). The filtrate was desalted and collected with a 1 kDa cutoff cross-flow ultrafiltration/diafiltration membrane and followed by freeze-drying for later use;

for AEPS extraction, diatom cells were collected after centrifugation from the previous step. Then, the pellet was soaked with 3% sodium chloride (NaCl) solution for 10 min and followed by centrifugation at 2000g, 15 min, to remove the medium and weakly bound organic material on the cells. The pellet was then resuspended in a new 100 ml 3% NaCl solution and stirred gently overnight at 4°C. The resuspended particle solution was ultra-centrifuged at 12000g (30 min, 4°C) and the supernatant was then filtered through a 0.2 µm polycarbonate membrane. The filtrate was desalted and collected with a 1 kDa cutoff cross-flow ultrafiltration/diafiltration membrane and subsequently freeze-dried for later use.

4.3.3 Frustule protein extraction

Scheme of chemical separation of individual biopolymers responsible for binding different radionuclides is given in Fig. 4.1, frustule protein extraction was adapted from Scheffel et al. (2011). Briefly, the clean diatom cells from the previous AEPS extraction step were resuspended in 10 ml 100 mM EDTA (pH 8.0) lysis buffer at 4°C overnight, and the supernatant (defined as **EDTA extractable fraction**) was collected after centrifuging at 3000 g for 10 min. Subsequently, the pellet was placed in 10 ml 1% SDS in 10 mM Tris (pH 6.8) solution and heated at 95 °C for 1 h. The resulting frustules were collected by centrifugation (2500 g, 10 min), washed with 10 ml milli-Q water three times, and then were freeze-dried for later use. The supernatant from this step was

collected and defined as **SDS extractable fraction**. These two fractions represent intracellular biopolymers lysed after cell breakage.

Hydrofluoric acid (HF) digestion was applied to help extract the diatom frustule biopolymers. HF is a non-oxidizing acid commonly used to convert SiO₂ to SiF₄ for wet digestion (Šulcek and Povondra, 1989; Scheffel et al., 2011). Hence, frustule biopolymers could be separated from the digested solution by a 3 kDa cutoff membrane. However, high concentration HF would also liberate A-type metal radionuclides (Th, Pa and Be in this study) from any complex by frustule biopolymers (e.g., Burnett et al., 1997). Furthermore, deglycosylation might be also occurred during the HF digestion (Mort and Lamport, 1977). Therefore, the <3 kDa fraction represents the sum of silica and frustule biopolymer residues.

In detail, a 5 ml of 52 % HF was added to the frustules in a 15 ml plastic centrifugation tube and the mixture solution was incubated on ice for 1 h. Hydrogen fluoride was then evaporated under a N₂ stream to reduce the volume to dryness. The remaining material was neutralized with a 3 ml Tris-HCl (250 mM, pH 8.0) and followed by centrifugation at 11000 g for 15 min with 3 kDa Microsep™ Centrifugal Devices (Milipore).

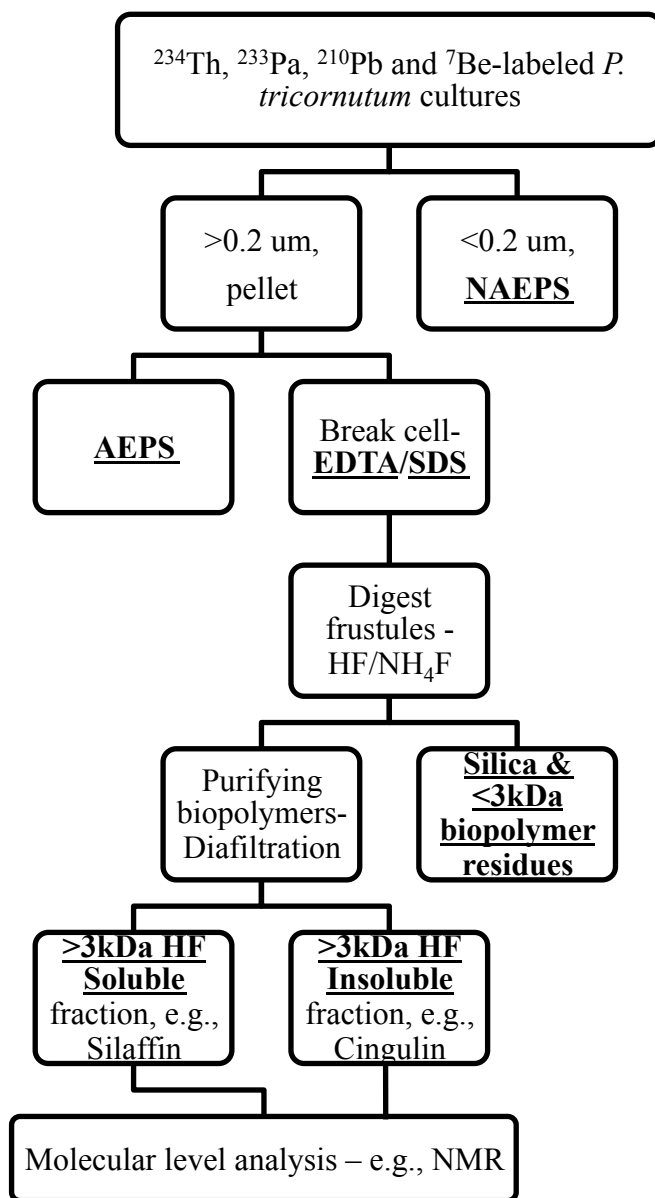


Fig. 4.1 Scheme of chemical separation of individual biopolymers responsible for binding of different radionuclides, from radiolabeled diatom incubations.

The filtrate was collected and defined as the fraction of **digested silica with <3 kDa frustule biopolymer (BP) residues**. The supernatant (defined as **> 3kDa HF soluble**

fraction BP, e.g., silaffin) was concentrated to 250 µl and rinsed with milli-Q water. The pellet from this step was then washed by a 3 ml 200 mM ammonium acetate solution twice with centrifugation at 3000 g for 20 min. The pellet was then resuspended in a 2 ml 100 mM ammonium acetate solution and was sonicated for 20 sec until the mixture solution appeared homogenized. After ultra-centrifuging the mixture solution at 12000 g for 5 min, the pellet (**>3 kDa HF insoluble fraction BP**, e.g, cingulin) was collected and freeze-dried for later use. Combined BP from all three HF fractions represented frustule embedded biopolymers.

To evaluate of the protein size distribution pattern of the collected biopolymer fractions, sodium dodecyl sulfate-polyacrylamide gel electrophoresis (SDS-PAGE, 15% gel) was carried out using standard molecular weight markers (Dual Xtra Standards, Bio-Rad) with a Tris-glycine running buffer (pH=8.3), followed by silver staining (Sambrook et al., 1989).

4.3.4 Partition coefficient of ^{234}Th , ^{233}Pa , ^{210}Pb and ^7Be

Activity concentrations of ^{234}Th , ^{233}Pa , ^{210}Pb and ^7Be were measured by gamma counting the 63.5 keV, 312 keV, 46.5 keV and 477.6 keV lines, respectively, on a Canberra ultra-high purity germanium well type detector. Cells, frustule pellets (with embedded proteins) and separated biopolymer fractions (AEPS, NAEPS, EDTA, SDS, Si & <3 kDa frustule BP residues, >3 kDa HF soluble and insoluble BP fractions)

collected from previous steps were all gamma counted for the determination of activities of ^{234}Th , ^{233}Pa , ^{210}Pb and ^7Be . All reported activities were decay and geometry corrected. ^{233}Pa was added in equilibrium with ^{237}Np , whose activities could be found only in the dissolved phase for all samples, supporting the assumption that ^{237}Np would not adsorb onto particles relevant for the calculation of the decay and in-growth corrections of ^{233}Pa . Traditional partition coefficients (K_d) between dissolved and particulate phases were used to quantify the sorption of radionuclides onto different particles in different experimental systems. K_d was defined here as:

$$K_d = A_p \times (A_d \times C_p)^{-1} \quad (1)$$

where A_p and A_d represent particulate and dissolved activities (Bq l^{-1}) of radionuclides; and C_p is the particle concentration (g ml^{-1}) (Honeyman and Santschi, 1989; Guo and Santschi, 1997b).

4.3.5 Nuclear Magnetic Resonance (NMR) spectroscopy: Solid-state NMR analysis

High-resolution solution state 2D NMR approaches were applied to identify the signatures of biomolecules extracted from diatom frustules. Solid-state 2D-HSQC NMR spectrum of HF insoluble fraction biopolymers were obtained on a Bruker Avance II 400 MHz NMR spectrometer using Topspin 2.0 software (Bruker-biospin, Billerica, MA) at Old Dominion University. Optimized procedures and settings are as listed below: freeze-dried sample was dissolved in $\text{DMSO-}d_6$ in a dry atmosphere and was transferred to a 4

mm NMR tube for analysis (to prevent a large water peak that is often centered at 3.3 ppm that can obscure sample signals); the sample was then spun at 7 kHz with an angle of 57.4° to the magnetic field. Spectral simulations were carried out using Advanced Chemistry Development's (ACD/Labs) Spec Manager (version 9.15) software (Xu et al., 2008; Xu et al., 2012).

4.4 Results and discussion

4.4.1 Binding of radionuclides in different biopolymers fractions

In Fig. 4.1, individual biopolymers fractions responsible for binding different radionuclides are named after their chemical separation method and used here to differentiate the source of the biopolymers. The $\log K_d$ values of all selected radionuclides were calculated with the whole diatom cells (with and without Si frustules), whole cells after removing AEPS, frustules with all embedded BP, as well as the intracellular BP fraction (Table 4.1). A comparison of $\log K_d$ values is shown in Fig. 4.2.

$\log K_d$ values ranged from 4.30 to 6.00 for ^{234}Th , 4.50 to 6.03 for ^{233}Pa , 3.76 to 5.76 for ^{210}Pb and 4.01 to 6.15 for ^7Be , respectively. No significant differences in $\log K_d$ values of all selected radionuclides with diatom cells with or without silica frustule were observed. Apparently, the silica was not the main phase responsible for the binding, as was also evident in a previous study (Chuang et al., 2013c). Differences of $\log K_d$ values between the fractions with whole cells (with frustules), with cells after removal of AEPS

indicate stronger radionuclide binding to AEPS; furthermore, the difference between whole frustules (with embedded biopolymers) and silica phases can be attributed to strong complexation by the embedded biopolymers. The importance of frustule related biopolymers in radionuclides binding was thus again confirmed.

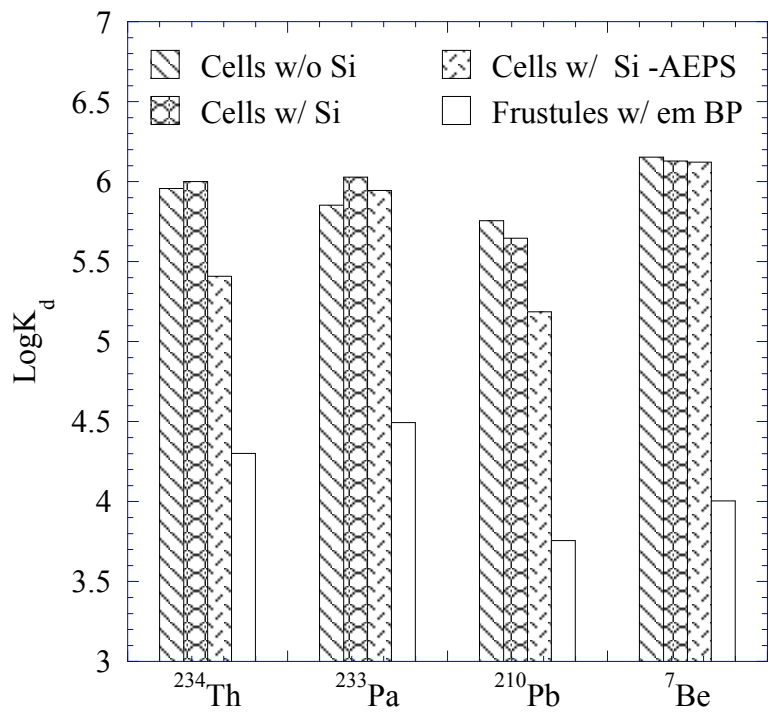


Fig. 4.2 Comparisons of logK_d values of ²³⁴Th, ²³³Pa, ²¹⁰Pb and ⁷Be with different fractions of diatom cells.

Furthermore, the average logK_d values of these radionuclides in the incubation study, 5.42 for ²³⁴Th, 5.58 for ²³³Pa, 5.09 for ²¹⁰Pb, and 5.60 for ⁷Be, followed the order

of $\text{Be} \approx \text{Pa} > \text{Th} > \text{Pb}$ in the water-particle partitioning experiments (Table 4.1). The observed trend, consistent with what was found in the field and laboratory studies (e.g., Chase et al., 2002; Yang et al., 2013b), as well as in our previous studies (Ch 3; Chuang et al., 2013a; Chuang et al., 2013c), showed that Pa and Be had relatively higher preferences bind to biogenic silica particles.

Table 4.1 LogK_d values of ²³⁴Th, ²³³Pa, ²¹⁰Pb and ⁷Be for different diatom cells fractions.

	²³⁴ Th	²³³ Pa	²¹⁰ Pb	⁷ Be
Cells w/o Si	6.00	6.03	5.65	6.13
Cells w/ Si	5.96	5.85	5.76	6.15
Cells w/ Si -AEPS	5.41	5.95	5.19	6.12
Frustules w/ all BP	4.30	4.50	3.76	4.01
Mean	5.42	5.58	5.09	5.60

The percentage of activities of radionuclides in each collected BP fraction extracted from *P. tricornutum* cultured under Si-replete condition are summarized in Table 4.2. Combined NAEPS and AEPS fractions represent extracellular biopolymers; EDTA and SDS extractable fractions represent intracellular biopolymers; and all HF fractions denote the frustule biopolymers. A comparison of the distributions of each radionuclide in these four biopolymer fractions is shown in Fig. 4.3. Affinities to different fractions varied among the different radionuclides (Fig. 4.3). In particular, ²³⁴Th showed highest

affinities to extracellular biopolymers (~45%), followed by intracellular (26%), >3kDa frustule biopolymers (24%), and had the lowest affinity to silica & frustules BP residues phase (<6%); in contrast, more than 50% of ²³³Pa was found in the silica & frustules BP residues fraction, ~26%, ~15% and <4% in the intracellular, extracellular and >3kDa frustule BP fractions, respectively; ²¹⁰Pb was also mostly concentrated in the silica & frustules BP residual phase (~42%), and about evenly distributed in the intracellular and >3kDa frustule BP pools (~20% each), and was least found in the extracellular BP fraction (~15%); ⁷Be was mainly bound to silica & frustules BP residues and intracellular biopolymers (~40% each), and had ~16% and <8% bound to >3kDa frustule BP fraction and extracellular biopolymers, respectively. Overall, more than 50% of selected radionuclides were bound to all biopolymer fractions, again, showing the great importance of these diatom related biopolymers in the scavenging and fractionation of these radionuclides in the ocean.

Table 4.2 Percentages of radionuclide activities in different biopolymer (BP) fractions of diatom cells.

	Extracellular BP		Intracellular BP		Frustules		
	NAEPS	AEPS	EDTA	SDS	Si & >3kDa BP, HF soluble	>3kDa BP, HF soluble	>3kDa BP, HF insoluble
^{234}Th	10.1	35.1	20.8	5.3	5.9	7.3	15.5
^{233}Pa	5.4	10.0	13.2	14.9	53.3	0.0	3.3
^{210}Pb	12.1	2.1	20.1	1.7	42.4	10.3	11.4
^7Be	3.5	4.2	26.2	10.6	38.2	15.6	1.7

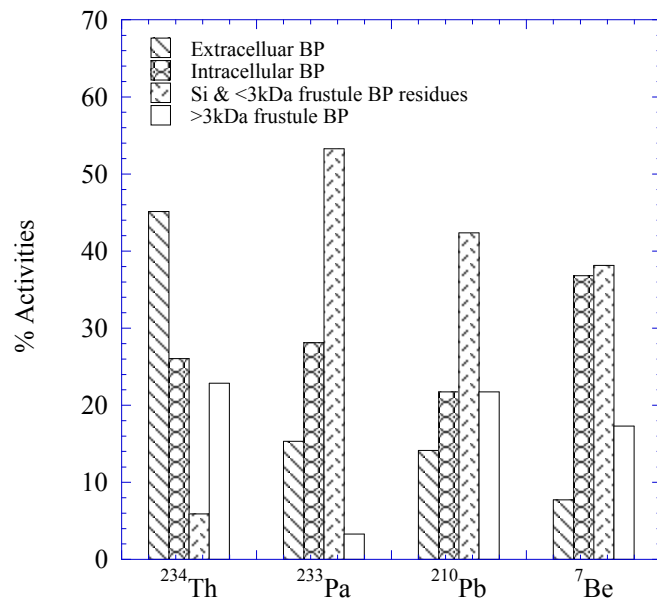


Fig. 4.3 Percentage activities of ^{234}Th , ^{233}Pa , ^{210}Pb and ^7Be in different biopolymer fractions of diatom cell.

4.4.2 Molecular structural studies of frustules embedded biopolymers

Lane 3-6 in SDS-PAGE results (Fig. 4.4) showed patterns in protein size distribution from AEPS and NAEPS extracted from *P. tricornutum* cultured under Si⁺ and Si⁻ conditions. In general, no differences, in terms of size patterns, were observed in the two different Si-supply conditions; NAEPS showed more diverse protein size patterns than AEPS. In terms of amounts, both AEPS and NAEPS samples had higher amounts of proteins in each size section from Si⁺ condition than from Si⁻ conditions. Lane 1 and 2 showed protein size distribution patterns of SDS and EDTA extractable fractions, respectively. More smeared displays of these two fractions might due to possible higher phosphorylated protein contents. And as a result of the sequence of extractions, EDTA fractions had greater amounts of larger proteins than SDS fractions. Overall, the protein size distribution was scattered, ranging from 10 to 150 kDa, in all extracted BP fractions.

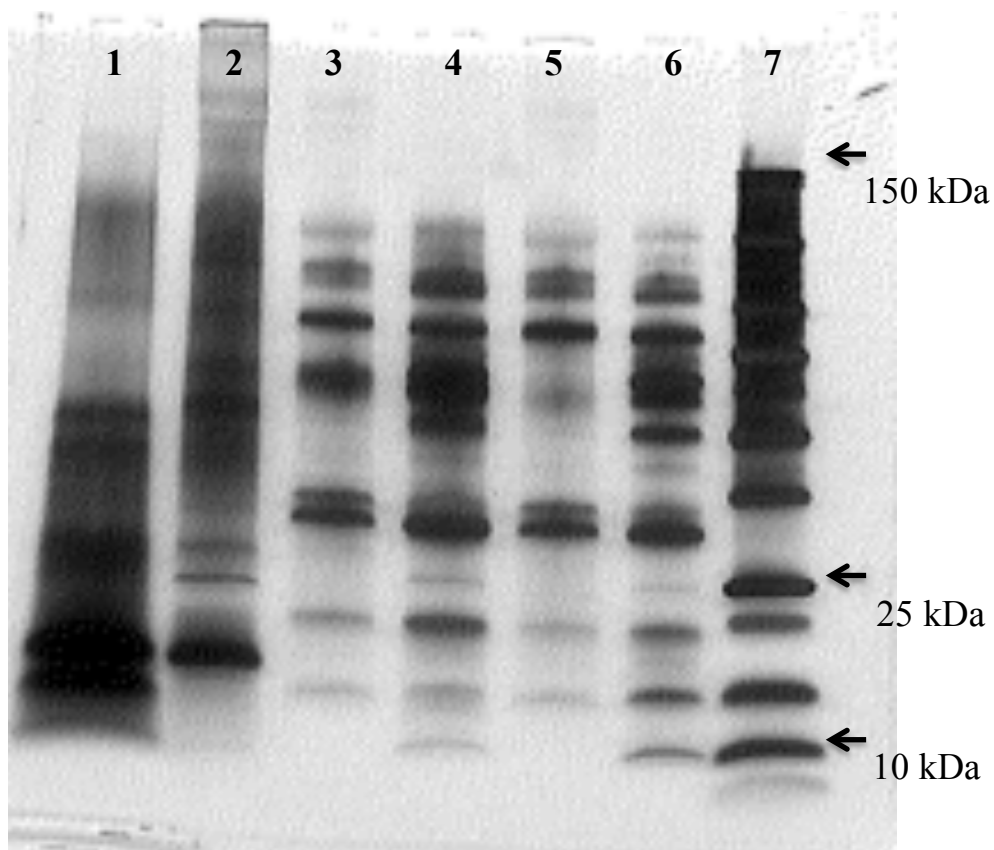


Fig. 4.4 Size distribution pattern of proteins in different biopolymer fractions harvested from *P. tricoratum* grown in seawater media with (L1-4) and without Si (L5, L6) respectively. (Lane 1: SDS extractable fraction, EPS Si+; Lane 2: EDTA extractable fraction, EPS Si+; Lane 3: AEPS Si+; Lane 4: NAEPS Si+; Lane 5: AEPS Si-; Lane 6: NAEPS Si-; Lane 7: standard molecular weight markers).

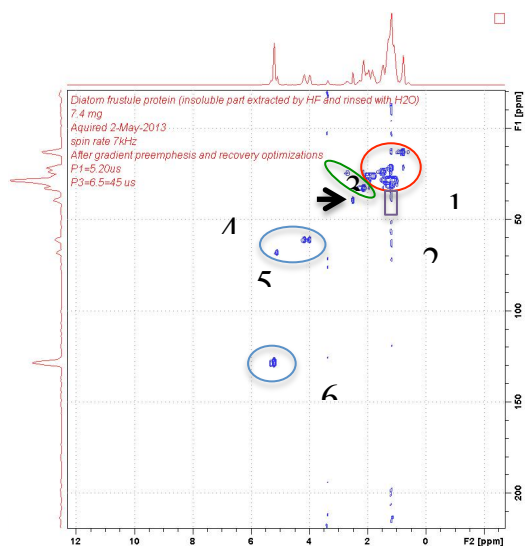
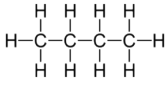
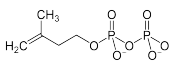
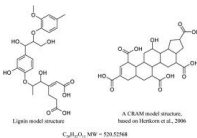
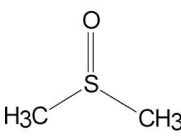
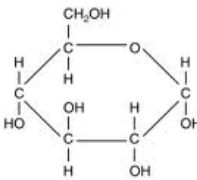
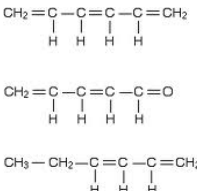


Fig. 4.5 2D HSQC NMR spectrum of the biopolymer residues from HF insoluble fraction in DMSO- d_6 . Assignment of regions: 1. aliphatics; 2. specific methines from intact cyclic terpenoids; 3. Carboxyl-rich alicyclic molecule (CRAM); 4. DMSO- d_6 (NMR solvent); 5. amino-acid α -proton in peptide chains; 6. Non-conjugated double bonds.

Fig. 4.5 showed the 2D HSQC-NMR spectrum of the biopolymer residues from HF insoluble fractions. The HSQC experiment detects the ^1H - ^{13}C bonds in an organic structure. Cross-peaks in an HSQC spectrum represent the chemical shift of both carbon and proton atoms in a C-H unit, forming a specific pattern as the “molecular fingerprint” of specific class of structures. Assignments for the major structural units within corresponding chemical shift ranges were given in Table 4.3 (Kelleher and Simpson, 2006; Xu et al., 2008; Xu et al., 2012).

Table 4.3 2D HSQC NMR spectral assignments in Fig. 5.5.

	^1H (ppm)	^{13}C (ppm)	Example structures	Assigned molecular moieties
1	0.72-2.09	11.44-33.06		aliphatics
2	1.14-1.21	33.69-40.50		Specific methines from intact cyclic terpenoids
3	2.07-2.22	31.07-34.57		CRAM (carboxyl-rich alicyclic molecule)
4	2.47-2.53	37.99-40.85		DMSO (Dimethylsulfoxide, NMR solvent)
5	3.94-5.14	59.71-69.56		Methylene and methine from carbohydrates; amino acid α -protons in peptide chains
6	5.14-5.33	126.1-130.71		Non-conjugated double bonds

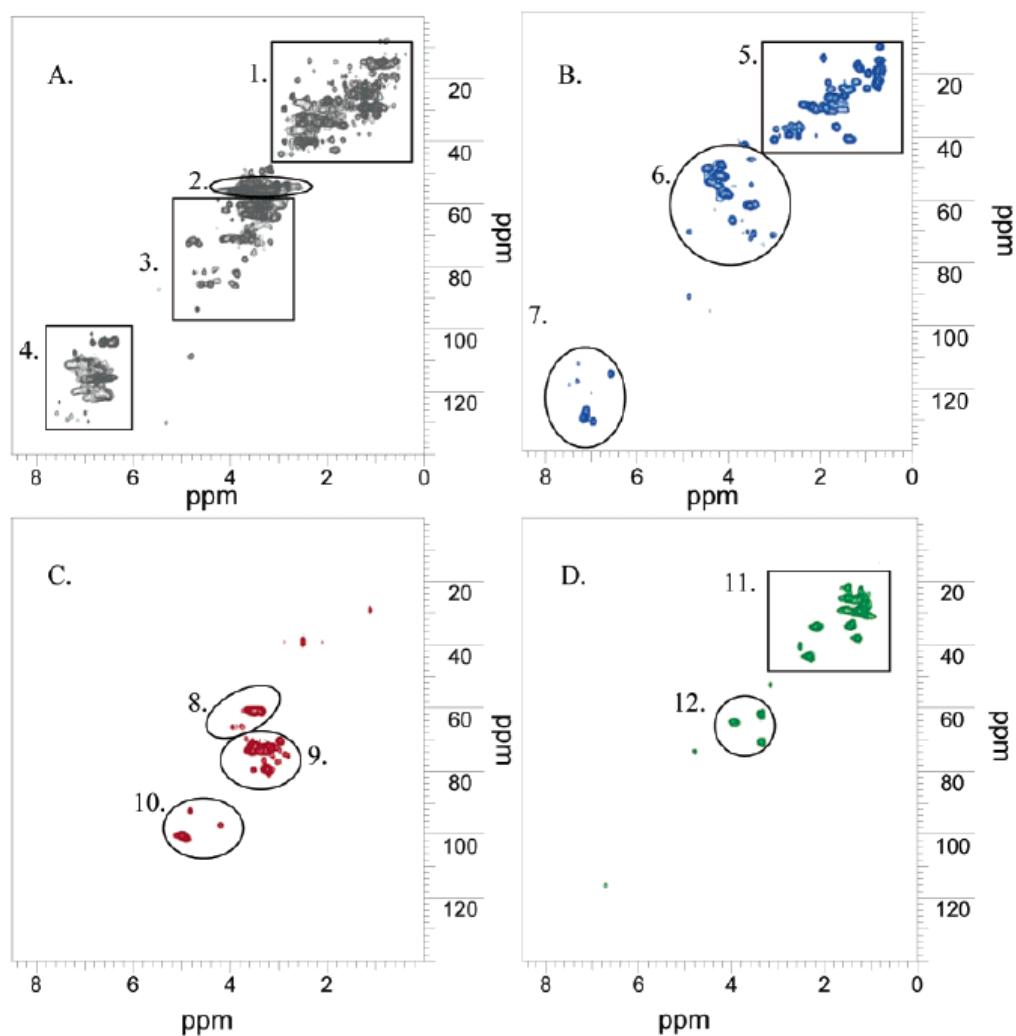


Fig. 4.6 2D HSQC NMR spectra of biopolymer representatives: (A) lignin (aromatic biopolymer), (B) albumin bovine serum (protein), (C) amylopectin (carbohydrate), and (D) tomato cuticle (aliphatic biopolymer). Assignments of the major structural classes as follows: (1) aliphatic linkers (and aliphatic coproducts extracted from wood in lignin isolation), (2) methoxyl, (3) linkers between aromatic rings, (4) aromatic rings, (5) aliphatic side chain residues, (6) amino acid α -protons in peptide chains, (7) aromatic side chain residue, (8) CH_2 in carbohydrate, (9) CH in carbohydrate, (10) anomeric units,

(11) residues in main aromatic chain, and (12) esters and ethers linkers. *Reprinted from Sambrook et al. (1989).

Five major functional groups were identified from the biopolymers in the HF insoluble fraction: aliphatics, specific methines from intact cyclic terpenoids, carboxyl-rich alicyclic molecules (CRAM), methylene and methane from carbohydrates/amino acid α -protons in peptide chains and non-conjugated double bonds. Fig 4.6 (reprinted from Sambrook et al., 1989) represented the 2D HSQC spectra of four classes of major biopolymers: lignin (Fig. 4.6a), protein (Fig. 4.6b), polysaccharides (Fig. 4.6c) and cutins (Fig. 4.6d). The highlighted regions outlined in the four spectra represent the general assignments of the major structural classes as follows: (1) aliphatic linkers (and aliphatic coproducts extracted from wood in lignin isolation), (2) methoxyl, (3) linkers between aromatic rings, (4) aromatic rings, (5) aliphatic side chain residues, (6) amino acid α -protons in peptide chains, (7) aromatic side chain residues, (8) CH₂ in carbohydrates, (9) CH in carbohydrates, (10) anomeric units, (11) residues in main aromatic chains, and (12) esters and ethers linkers. Comparing HSQC spectra of HF insoluble fraction biopolymers with these four reference biopolymers, there is good agreement between the signature observed from the HF insoluble fraction and the pattern produced by proteins, partially by polysaccharides. Hence, the biopolymers in the HF

insoluble fraction are mainly composed of carboxyl-rich, aliphatic-phosphoprotein molecules. Notably, no molecular fingerprint of aromatic functional groups was found in the HF insoluble fraction biopolymers. Nonetheless, as the HSQC experiment detects only ^1H attached to ^{13}C , exchangeable protons (OH, NH, etc.) that are detected in the ^1H spectrum could not be observed.

4.5 Conclusions

To the best of our knowledge, this is the first time the binding of ^{234}Th , ^{233}Pa , ^{210}Pb and ^7Be incubated together with cultured diatom cells, were comprehensively examined, at the molecular level, for their binding ability to different biopolymers released to the medium. In the ternary sorption system (biogenic silica-biopolymers-radionuclides), it is clear that not the mineral phases, biogenic silica, but the biopolymers associated with biogenic SiO_2 , provide the strong binding sites for the radionuclides, accounting for the majority of binding of these radionuclides. 2D HSQC NMR results showed that the biopolymers in the HF insoluble fraction were mainly composed of carboxyl-rich, aliphatic-phosphoproteins, providing strong binding sites for some of the radionuclides (e.g., Pa, Be). These extensive and comprehensive molecular-level analyses of carrier macromolecules of radionuclides were thus of great help to resolve some of the controversial observations on the scavenging and fractionation of radionuclides in the ocean.

CHAPTER V

**ROLE OF BIOPOLYMERS AS MAJOR CARRIER PHASES OF Th, Pa, Pb, Po,
AND Be RADIONUCLIDES IN SETTLING PARTICLES FROM THE
ATLANTIC OCEAN**

5.1 Overview

The concentrations of potential organic (e.g., proteins, polysaccharides, uronic acids, hydroquinones, hydroxamates- and catechol-type siderophores) and inorganic (Fe, Mn, Si, and CaCO₃) carrier phases for radionuclides (²³⁴Th, ²³³Pa, ²¹⁰Po, ²¹⁰Pb and ⁷Be) and their particle-water partition coefficients (K_d) were determined for particles collected by sediment traps deployed at the Oceanic Flux Program (OFP) site off Bermuda (500, 1500 and 3200 m). The purpose was to better understand the mechanisms that control the chemical composition of sinking particles as well as the scavenging and fractionation behaviour of those five radionuclides. Different components contributed differently to the scavenging of different radionuclides at the three depths. Chemical considerations (e.g., ionic potential, ionization energy, multifunctional groups structures), as well as factor analysis (FA) and correlations of logK_d values with chemical parameters, indicate that hydroxamate-siderophores are major classes of biopolymers that have a role in binding Po and Pa. MnO₂ and FeO₂, whose presence is closely related to that of hydroxamate siderophores (HS), are also involved in binding of Pa and Po. The

carbonate and biogenic silica phases are identified to be important in predicting removal and fractionation of Th and Be in the ocean.

5.2 Introduction

Natural particle-reactive radionuclides, such as $^{230,234}\text{Th}$, ^{231}Pa , ^{210}Po , ^{210}Pb and $^{7,10}\text{Be}$, have been widely used for decades as important proxies to understand oceanic processes, such as boundary scavenging, particle flux, paleo-circulation and water mass residence times (Broecker and Peng, 1982). However, the interactions and binding relationships between radionuclides and components of marine particles as well as the molecular level bonding mechanisms remain poorly understood (Santschi et al., 2006). Though radioisotopic tracers can be applied without knowledge of specific mechanisms, the lack of a fundamental understanding of radionuclide scavenging and partitioning can fuel heated scientific controversies over the interpretations of tracer data (e.g., Li, 2005).

Generally, speciation and transport of the low concentrations of natural radionuclides (at ~pico- to femto- or atto- molar concentrations) in the ocean are governed by thermodynamic and kinetic processes in adsorptive uptake and transport by organic or inorganic particles. Given that the concentrations of the ions of natural radionuclides are in the sub-picomolar range, while concentrations of organic and inorganic colloids and particles in surface waters are in the micromolar range (Santschi et al., 1995, 2002), most radionuclide ions are unlikely to form their own hydrolytic

species but tend to associate with a carrier phase by binding to certain functional groups in colloidal and particulate surfaces. There is considerable evidence to support this contention, for example, the associated particles containing hydrolized aluminosilicates and Fe-Mn oxides (Doucet et al., 2001; Kim et al., 2003b; Panak et al., 2003), Fe-organic colloids (Santschi et al., 2002), and polysaccharide-rich exopolymeric substances (Guo et al., 2002a, b; Quigley et al., 2002; Roberts et al., 2009; Xu et al., 2009, 2011).

Most natural radionuclides have metal characteristics and are subject to chelation by organic ligands such as siderophores are the major class of metal chelators in the aquatic environment. Siderophores, a group of high-affinity metal-binding ligand compounds, are secreted by microorganisms in response to the need for soluble Fe, which is present at very low concentrations in oceanic waters (Reid et al., 1993; Neilands, 1995; Winkelmann, 2002). The structural features and chemical composition of siderophores are diverse. The functional groups contain oxygen atoms of hydroxamate, catecholate, α -hydroxy carboxylic and salicylic acids, or nitrogen atoms of oxazoline and thiazoline. In seawater, it has been well documented that 99% or more of water-soluble Fe, especially the ferric ion, Fe(III), is bound to dissolved organic ligands, including siderophores (Gledhill and Van Den Berg, 1994; Rue and Bruland, 1995; Boye et al., 2001; Mawji et al., 2008; Kondo et al., 2012). In the particle phase, however, the existence of

siderophores has, so far, not been documented. Additionally, siderophores could also complex metals other than Fe(III), including natural radionuclides such as Pu(IV) and Th(IV) (Neu et al., 2000; Keith-Roach et al., 2005), which have similar physicochemical properties as the ferric iron.

To evaluate potential carrier phases controlling the speciation and scavenging of particle-reactive radionuclides in the ocean, we have comprehensively examined the composition of sinking particles collected by the Oceanic Flux Program (OFP) sediment traps deployed in the northern Sargasso Sea off Bermuda. The abundance of potential organic carriers, including proteins, total polysaccharides, uronic acids, hydroquinones, and hydroxamate-type and catechol-type siderophores, as well as inorganic phases (Mn, Fe, Si, and CaCO₃) in the particles was quantified. The purpose was to examine their possible correlation with the particle-water partitioning coefficients of ²³⁴Th, ²³³Pa, ²¹⁰Po, ²¹⁰Pb and ⁷Be. To the best of our knowledge, this is the first time that the functionalities of hydroxamate siderophores (HS) in marine particles are studied and implicated to be important for radionuclide binding. The chemical relationships and statistical analyses reported here provide new insights into the relative importance of organic and inorganic carrier phases for different radionuclides with clear evidence that HS is involved in a major way in the binding and removal of specific radionuclides in marine particles.

5.3 Methods

5.3.1 Sediment trap sampling

The Bermuda Oceanic Flux Program (OFP) time-series site is located at 31° 50' N, 64° 10' W with water depth of 4500 m. Sediment trap mooring system, sample processing and analytical protocols have been previously described (Conte et al., 2001; Huang and Conte, 2009). McLane Parflux sediment traps (0.5 m² surface area; McLane Labs, Falmouth, MA, USA) are positioned at 500, 1500 and 3200 m depths and programmed at about 2-week sampling resolution. Sample cups are filled with high purity seawater brine (Salinity of 40) that is prepared by freezing Sargasso Sea deep water (3000 m depth). The trap cup brine is preserved using ultra-high purity HgCl₂ (200 mg/L) to arrest biological degradation during sample collection.

5.3.2 Chemical analysis of sediment trap samples

Sediment trap samples were analyzed for dry weight, carbonate and organic carbon/nitrogen contents using methods detailed in Conte et al. (2001) and Huang and Conte (2009). Carbonate was determined by coulometry (Coulometrics). Organic carbon and nitrogen concentrations and isotopic composition were measured on a mass spectrometer (Europa 20-20 CF-IRMS interfaced with the Europa ANCA-SL elemental analyzer), after acidification of the samples by sulfurous acid to remove carbonates.

Elemental composition was determined using a small sample LiBO₂ fusion/ICPMS method (Huang et al., 2007).

Subsamples of archived OFP sediment trap materials (<125 μm size fraction) were transferred to the Texas A&M University at Galveston for additional analyses for select organic and inorganic phases, and for the determination of partition coefficients of radionuclides between particle and water phases in laboratory. Sixty one samples collected between the years 2004 to 2006 were analyzed: 14 samples from 500 m depth, 22 samples from 1500 m depth and 25 samples from 3200 m depth.

Mn and Fe contents in subsamples (<125 μm) were measured by an atomic absorption spectrometer (Varian) after overnight digestion with 12 N HNO₃ at 85°C. Silica content of OFP sample was analyzed, after digestion, by a colorimetric method adopted from Strickland and Parsons (1972). The digestion method was modified from Hauptkorn et al. (2001). In brief, a mixture of 250 μl of Milli-Q and a 200 μl of 25% TMAH was added to ~1 mg OFP subsample followed by 30 min sonication. The solution was heated to 95°C for overnight. The silicate concentration was determined in the supernatant fraction after centrifuging the solution at 3200g for 10 min. Additional data on the elemental concentrations in the OFP samples has been reported in Huang and Conte (2009).

Total carbohydrate concentrations of OFP subsamples (TCHO) were determined by the TPTZ (2, 4, 6-tripyridyl-s-triazine, Sigma) method using glucose as the standard (Hung and Santschi, 2001). Proteins were analyzed by a modified Lowry protein assay, using bovine serum albumin (BSA) as the standard (Pierce, Thermo Scientific). Uronic acids (URA) were determined by the meta-hydroxyphenyl method, using glucuronic acid as the standard (Filisetti-Cozzi and Carpita, 1991; and modified by Hung and Santschi, 2001). Hydroquinone (HQ) determination was modified from Sirajuddin et al. (2007), using hydroquinone as the standard. Thirty samples were selected to measure particulate hydroquinone. In brief, 300 μ l of Milli-Q water was added to \sim 1 mg particulate sample, and the solution was sonicated for an hour. The solution was then centrifuged (3500g, 5 min) to separate the particles from the supernatant. A 300 μ l aliquot of 100 mM KMnO_4 was added to 100 μ l of the particle-water mixture and reacted for 15 min under room temperature. The hydroquinone concentration was then determined by UV-Vis spectrophotometry at 288 nm.

Hydroxamate siderophore (HS) concentrations were measured by the Csaky's method (1948), using acetohydroxamic acid (AHA) as the standard. Catechol siderophores were analyzed by Arnow's method, using catechol as the standard (Arnow, 1937). However, no catechol siderophores were detected in all OFP samples. Separate measurements of hydroxamate siderophores were carried out on three different sample

fractions, namely, the water/methanol extract, the supernatant after 6N HCl digestion (110°C, 24 hrs), and refractory particulate material remaining after acid digestion.

To assess potential artifacts and interferences in the colorimetric methods (e.g, potential interference of HS on TPTZ analysis; effects of polysaccharides concentration on HS determination), many in-depth cross-calibration experiments were also conducted. AHA standards with different concentrations was applied for the TPTZ method to examine whether there is any absorbance at the characteristic wavelength for polysaccharides. These experiments did identify AHA interference in the spectrophotometric determination of TCHO. An appropriate correction was therefore applied to the raw TCHO concentrations data to eliminate the effects of AHA. No other interferences or artifacts were found.

5.3.3 Sorption experiments

Natural seawater (Salinity of 35) collected from the Gulf of Mexico with background low molecular weight DOC was used for all sorption experiments. The seawater was prepared by sequentially filtering seawater through a 0.4 µm polycarbonate cartridge, followed by filtering through a 1 kDa ultrafiltration membrane to remove particulate and colloidal organic matter (Guo et al., 1995; Roberts et al., 2009).

The ^{234}Th tracer was purified and extracted from a ^{238}U stock solution (Quigley et al., 2002; Alvarado Quiroz et al., 2006). ^{233}Pa , in equilibrium with ^{237}Np , was obtained

from Pacific Northwest National Laboratory was used. ^{210}Pb and ^{210}Po , in 2 N HCl, were purchased from Eckert & Ziegler Isotope Products. The ^7Be tracer solution (in 0.5 N HCl) was manufactured at the Paul Scherrer Institute, Switzerland (Schumann et al., 2013).

^{233}Pa was added in equilibrium with ^{237}Np , whose activities could be found only in the dissolved phase for all samples, supporting the assumption that ^{237}Np would not adsorb onto particles during the experiment, thus justifying the decay and in-growth corrections of ^{233}Pa in solution only.

The design of the sorption experiment was modified from that of Roberts et al. (2009). Specifically, a non-complexing 20mM/10mM Tris-HCl buffer was transferred into acid cleaned experimental tubes to precondition the container walls for at least 24 h to reduce tracer adsorption. The reason for using Tris-HCl is that its buffer capacity also can neutralize the acidic radionuclide tracer solutions to avoid pseudo colloids generation by normally used NaOH, and maintains the pH at 8.0 ± 0.5 . A small drop in pH was only occurring right at the beginning after the addition of the acidic tracer solution due to a limited buffer capacity, but the pH stayed constant throughout the experiment.

Each experiment was performed in duplicate. Ten ml of seawater was added to the preconditioned tube, and then between 10 to 15 Bq of radionuclide tracers (at

equilibrium) was added. Solutions were then gently shaken and left to equilibrate overnight. The next morning trap particles were added to the seawater, resulting in a final particulate concentration of 10 mg/L. This concentration is within the range of suspended particulate matter concentrations in natural seawaters (National Research Council, 1972), which ranges from <1 mg/L in open ocean waters (Guo et al., 1997), to tens to >100 mg/L in the nearshore marine environment and estuarine waters (e.g., Baskaran and Santschi, 1993; Woźniak et al., 2010). This amount also allowed accurate weighing and quantitative recovery of particulate matter from our small experimental system. An equilibrium time of 48 h was used for our adsorption experiments. Based on our kinetic experiments (Chuang et al., unpublished results), particle adsorption of these nuclides after 48 h had reached 81%, 95%, 98%, 92% and 100% for ^{210}Pb , ^{234}Th , ^{233}Pa , ^7Be and ^{210}Po , respectively, of their maximum particle sorption after 120 h. The disadvantage of using a longer experimental/equilibrium time is that it would have resulted in more loss of these isotopes onto the reservoir walls, especially for ^7Be and ^{234}Th . Wall-adsorption of these nuclides after 120 h accounted for 4%, 38%, 18%, 26% and 0% of ^{210}Pb , ^{234}Th , ^{233}Pa , ^7Be and ^{210}Po , respectively, of the total amount that adsorbed to particles after 48 h. Therefore, an equilibrium time of 48 h was consistently used for all adsorption experiments. At the end of the experiment, the solution was filtered through 0.2 μm MicrosepTM polyethersulfone centrifugal filters (Pall Life

Sciences), and the particulate ($>0.2 \mu\text{m}$) and dissolved ($<0.2 \mu\text{m}$) fractions retained for measurements of radionuclide activity. Before filtration, both filter and filtration tubes were pretreated with ultrafiltered seawater to reduce the tracer adsorption.

Release of tracers adsorbed to container walls was assessed by conducting a 2-day sorption test using solutions with and without the presence of particles (SiO_2 , Sigma-Aldrich® S5631, $0.5\text{-}10 \mu\text{m}$, 40 mg/L). The acid recoverable tracer from the container walls was usually less than 10% of the total adsorbed tracer. Therefore, the tracer fraction that was lost to container walls was irreversibly lost, and could thus be ignored from the calculations, as it did not participate in the solution reactions any more. This behavior justified using the sum of the measured fractions as the total amounts participating in the reactions that were studied.

5.3.4 Measurements of radionuclides and their partition coefficients

Activity concentrations of ^{234}Th , ^{233}Pa , ^{210}Pb and ^7Be were measured by gamma counting the 63.5keV , 312keV , 46.5keV and 477.6keV lines, respectively, on a Canberra ultra-high purity germanium well type detector. The ^{210}Po activity was analyzed by liquid scintillation counting (Beckman Model 8100 Liquid Scintillation Counter). All activities of selected radionuclides were corrected for decay (and ingrowth in case of ^{233}Pa) and normalized to the same geometry for ease of comparison and further evaluation.

Partition coefficients (K_d) between dissolved and particulate phases were determined to quantify the interactions between radionuclides and particles in experimental systems. K_d is defined as:

$$K_d = A_p / (A_d * C_p) \quad (1)$$

where A_p and A_d represents particulate and dissolved activities of radionuclides (Bq/L), respectively, and C_p is the particle concentration (g/ml) (Honeyman and Santschi, 1989).

As described before, a small fraction of each radionuclides sorbed to walls appeared to be irreversibly sorbed onto container walls, and therefore, was not considered in the K_d calculations.

5.3.5 Statistical analysis

The whole data set obtained from OFP particle composition analysis and partition coefficient experiments of all selected radionuclides (n=61 for all 16 variables) is summarized in Table 5.1. A serial statistical analysis was performed on this unique data matrix, using the IBM SPSS software® package\

Table 5.1 LogK_d values for ²³⁴Th, ²³³Pa, ²¹⁰Pb, ²¹⁰Po and ⁷Be, as well as chemical composition of the <125 μm fraction of OFP sediment trap samples.

Sample ID	Year	Mid Sampl ing Date	Dept h (m)	Flux mg/m ² / d	CaC O ₃ (%)	Si (%)	OC (%)	TCH O mg/g	Protein mg/g	URA mg/g	HS mg/g	HQ mg/g	Mn mg/g	Fe mg/g	Log K _d (T h)	Log K _d (P a)	Log K _d (P b)	Log K _d (P o)	Log K _d (B e)
% 4/05-5	2005	2/8	500	30.3	62.3	4.92	10.1	36.1	51.1	46.7	16.4		0.179	1.82	5.29	4.83	3.32	5.12	4.14
% 4/05-6	2005	2/22	500	51.7	61.7	5.17	10.1	76.0	45.6	35.2	20.8		0.634	4.23	5.34	4.66	4.07	5.12	4.55
% 4/05-7	2005	3/7	500	67.0	67.5	4.68	8.3	80.7	43.8	39.0	25.2	1.05	0.413	2.19	5.23	4.90	4.12	5.14	4.10
% 4/05-8	2005	3/21	500	100.4	76.3	3.48	5.6	57.5	49.7	46.5	22.9	0.87	0.298	1.80	5.72	4.86	4.19	5.09	4.29
% 8/05-1	2005	4/8	500	38.5	57.3	4.36	12.6	71.2	86.7	47.0	28.4	1.50	0.029	1.40	4.60	5.15	4.28	5.39	3.84
% 11/05-4	2005	9/22	500	24.0	60.2	4.73	10.1	60.6	76.8	53.5	38.2	0.70	0.911	5.96	6.17	4.90	-	5.79	4.42
% 4/06-5	2006	1/26	500	58.1	54.5	6.40	12.1	101.9	52.8	54.0	27.6	2.24	0.049	8.63	-	4.78	4.08	5.02	4.11
% 4/06-7	2006	2/27	500	56.6	59.9	4.87	13.9	76.1	57.7	44.0	26.5	1.22	0.090	3.32	5.18	4.79	3.41	5.09	4.32
% 4/06-10	2006	4/13	500	59.4	71.0	7.22	7.7	39.3	66.3	33.1	24.8		0.041	1.58	4.87	4.93	3.72	4.99	4.22
% 8/06-3	2006	5/31	500	21.5	50.7	7.15	12.3	68.0	41.7	39.9	20.4	0.82	0.041	3.81	5.38	4.81	3.98	4.99	4.36
% 8/06-5	2006	7/1	500	11.5	29.4	9.14	12.7	151.4	59.7	120.8	17.5		0.035		4.17	4.90	4.30	5.25	4.04
% 8/06-6	2006	7/17	500	11.1	-	5.58	16.0	123.6	62.1	63.6	23.0	1.40	0.045	8.62	5.04	4.57	3.79	5.34	4.48
% 12/06-2	2006	9/18	500	16.4	44.9	6.75	12.6	125.1	82.9	73.2	24.4	1.58	0.126	7.02	4.21	4.96	4.14	5.13	3.73
% 12/06-3	2006	10/3	500	18.4	49.0	5.10	11.0	86.4	57.7	56.5	27.5	1.52	0.114	8.83	4.85	4.90	-	5.3	4.04

Table 5.1 "continued.

Sample ID	Year	Mid Sampl ing Date	Dept h (m)	Flux mg/ m ² /d	CaCO ₃ (%)	Si (%)	OC (%)	TCH O mg/g	Protein mg/g	URA mg/g	HS mg/g	HQ mg/g	Mn mg/g	Fe mg/g	Log K _d (T h)	Log K _d (P a)	Log K _d (P b)	Log K _d (P o)	Log K _d (B e)
% 4/05-4	2005	1/25	1500	24.7	62.2	6.48	7.7	38.5	57.9	30.2	24.5	0.54	1.21	5.15	5.79	5.57	4.02	5.48	4.68
% 4/05-5	2005	2/8	1500	46.7	64.8	4.93	7.7	63.9	71.9	50.2	28.9		0.96	4.26	5.76	5.54	4.01	5.67	3.99
% 4/05-6	2005	2/22	1500	47.1	69.2	6.14	7.2	93.2	58.9	28.2	27.9	0.55	1.76	6.91	5.46	4.75	4.60	5.59	4.71
% 4/05-7	2005	3/7	1500	42.2	68.5	5.43	6.7	35.0	94.0	37.7	35.0		1.03	4.13	5.33	5.46	3.74	5.74	4.28
% 4/05-8	2005	3/21	1500	86.5	75.8	5.02	4.8	59.6	65.9	30.6	24.2	0.49	0.76	4.18	7.08	5.15	3.67	5.37	4.46
% 8/05-1	2005	4/8	1500	46.3	72.2	5.20	6.4	64.8	84.8	37.5	17.2	0.50	0.55	2.46	6.03	4.65	3.99	5.38	4.40
% 11/05-2	2005	8/24	1500	20.1	60.4	6.14	7.1	45.3	59.8	34.3	29.3	0.58	1.40	5.53	6.06	5.42	3.98	5.68	4.74
% 11/05-4-2	2005	9/22	1500	30.6	60.5	7.30	6.8	48.8	92.9	39.7	27.2	0.78	1.91	7.78	5.77	5.41	3.60	-	4.19
% 8/06-2	2006	5/16	1500	38.9	59.8	8.00	5.9	55.0	81.9	21.7	32.5	0.44	1.12	5.51	5.82	5.17	3.88	5.31	
% 8/06-3	2006	5/31	1500	25.9	59.1	6.56	5.8	60.9	64.2	27.0	18.1		1.80	8.68	6.26	5.20	4.01	5.39	3.98
% 8/06-5	2006	7/1	1500	32.2	60.5	7.21	7.1	28.2	51.9	55.5	33.7	0.57	1.03	6.16	5.33	5.23	4.11	5.44	4.78
% 8/06-6	2006	7/17	1500	34.3	63.1	8.41	6.9	76.1	35.8	14.7	22.0	0.78	1.00	5.92	5.93	5.12	-	5.2	4.81
% 8/06-7	2006	8/2	1500	21.1	59.4	6.92	8.2	105.4	45.5	29.5	16.7		1.25	6.17	4.62	5.32	3.53	5.26	4.71
% 8/06-8	2006	8/17	1500	26.9	65.1	6.02	6.6	57.4	38.4	25.2	26.6	0.58	2.09	6.34	5.37	5.21	3.95	5.31	4.57
% 12/06-1	2006	9/3	1500	13.1	55.7	6.25	8.6	62.1	37.5	37.7	34.4	0.79	1.66	6.81	6.19	5.31	3.78	5.46	4.36
% 12/06-2	2006	9/18	1500	21.4	62.0	3.51	6.9	37.8	64.0	20.7	45.3		1.48	7.15	5.71	5.44	3.42	5.75	4.37
% 12/06-3	2006	10/3	1500	23.9	60.3	6.51	6.2	54.6	50.0	20.4	36.6	0.63	1.71	7.48	5.48	5.43	4.18	5.69	3.90
% 12/06-4	2006	10/19	1500	28.7	63.5	5.96	6.3	15.6	82.7	34.9	42.7	0.59	1.46	6.65	5.28	5.55	3.68	5.83	4.60
% 12/06-6	2006	11/18	1500	25.2	56.2	4.98	6.7	50.1	45.9	19.2	31.0		1.31	6.82	5.36	5.62	4.49	5.73	3.94
% 8/07-4	2007	5/19	1500	29.7	61.5	4.91	5.6	57.8	44.5	14.7	28.9	0.47	1.17	6.19	5.72	4.99	4.04	5.67	4.53
% 4/07-2	2006	1/4	1500	37.7	59.5	7.47	6.9	52.8	71.7	39.3	43.6	0.52	1.28	6.88	4.57	5.21	3.77	5.88	4.17
% 4/07-3	2007	1/20	1500	35.6	65.7	7.17	6.7	47.7	74.3	34.9	37.1	0.77	1.09	6.34	5.57	5.49	3.95	5.55	4.47

Table 5.1 continued.

Sample ID	Year	Mid Samplin g Date	Dept h (m)	Flux mg/ m ² /d	CaCO ₃ (%)	Si (%)	OC (%)	TCH O mg/g	Protein mg/g	URA mg/g	HS mg/g	HQ mg/g	Mn mg/g	Fe mg/g	Log K _d (T h)	Log K _d (P a)	Log K _d (P b)	Log K _d (P o)	Log K _d (B e)
% 4/05-4	2005	1/25	3200	22.4	56.2	6.80	5.4	27.8	48.9	8.5	31.4		1.75	8.12	5.44	5.21	4.20	5.63	4.34
% 4/05-5	2005	2/8	3200	32.4	57.5	8.05	6.3	17.2	43.1	7.3	37.2	0.54	1.38	8.36	5.85	5.32	4.23	5.65	4.54
% 4/05-6	2005	2/22	3200	58.3	67.4	7.48	5.5	50.7	36.2	6.1	40.6		1.26	7.01	5.69	5.48	3.85	5.43	4.60
% 4/05-7	2005	3/7	3200	45.4	59.4	9.31	5.7	35.3	33.2	4.0	40.4		1.40	7.23	5.49	5.26	3.96	5.49	4.51
% 4/05-8	2005	3/21	3200	55.7	65.7	6.84	5.3	46.2	48.3	4.3	34.3		0.93	7.04	5.74	5.11	3.81	5.58	4.42
% 8/05-1	2005	4/8	3200	39.2	70.0	5.78	5.1	49.5	59.7	7.2	22.6		0.49	3.30	5.20	5.13	3.99	5.41	4.32
% 11/05-2	2005	8/24	3200	24.9	55.6	6.76	4.7	12.3	42.6	6.7	30.4		1.41	7.59	6.21	5.42	4.41	5.68	4.18
% 11/05-4	2005	9/22	3200	30.1	57.8	8.21	4.3	28.5	48.9	7.2	27.3		1.35	8.83	5.72	5.27	4.03	5.7	4.32
% 4/06-5	2006	1/26	3200	60.3	61.3	5.33	5.2	33.9	57.8	5.8	28.3		1.26	7.77	5.88	5.30	4.32	5.55	4.17
% 4/06-7	2006	2/27	3200	60.7	61.5	7.23	5.7	38.9	49.1	5.1	30.8		1.31	8.01	5.29	5.33	3.88	5.83	4.46
% 4/06-10	2006	4/13	3200	67.8	65.9	7.07	4.1	46.4	45.5	6.3	27.5		0.97	6.10	5.63	5.01	3.68	5.61	
% 8/06-2	2006	5/16	3200	39.5	61.6	7.06	4.5	29.3	37.6	9.6	19.4	0.27	1.17	7.74	4.89	5.32	4.43	5.42	4.58
% 8/06-3	2006	5/31	3200	34.4	58.6	5.20	4.7	41.7	30.2	9.4	16.3		1.29	7.66	5.08	5.13	4.16	5.38	4.28
% 8/06-5	2006	7/1	3200	41.7	62.0	5.23	4.7	24.2	31.5	8.4	25.4		1.51	8.37	5.17	4.84	4.10	5.42	4.70
% 8/06-6	2006	7/17	3200	34.4	60.2	7.67	4.3	41.6	29.1	6.2	20.4		1.20	7.44	5.44	5.27	4.07	5.64	4.67
% 8/06-7	2006	8/2	3200	32.4	64.2	5.85	4.8	19.9	60.2	6.7	36.2	0.49	1.18	7.13	5.49	5.07	3.52	5.76	4.34
% 8/06-8	2006	8/17	3200	24.7	61.5	7.38	4.8	25.3	39.1	6.4	27.5		1.68	7.94	5.29	4.94	4.45	5.72	4.62
% 12/06-1	2006	9/2	3200	8.2	57.5	7.87	5.9		41.1	4.8					5.91	5.49	4.05	5.73	4.43
% 12/06-2	2006	9/17	3200	13.4	54.5	6.07	5.1	20.4	41.7	5.9	30.8		1.57	7.50	5.37	5.14	4.17	5.87	3.86
% 12/06-3	2006	10/2	3200	30.8	63.6	6.59	4.7	28.9	38.3	4.6	26.1		1.63	7.72	5.27	4.98	4.20	5.85	4.51
% 12/06-4	2006	10/18	3200	19.2	62.4	5.95	5.2	11.1	41.9	9.0	32.3		1.35	7.69	5.78	5.25	3.96	5.84	4.42

Table 5.1 continued.

Sample ID	Year	Mid Samplin g Date	Dept h (m)	Flux mg/ m ² /d	CaCO ₃ (%)	Si (%)	OC (%)	TCH O mg/g	Protein mg/g	URA mg/g	HS mg/g	HQ mg/g	Mn mg/g	Fe mg/g	Log K _d (T h)	Log K _d (P a)	Log K _d (P b)	Log K _d (P o)	Log K _d (B e)
% 12/06-6	2006	11/17	3200	22.9	61.6	6.87	4.8	31.3	51.3	5.7	27.8		1.44	8.23	5.47	5.38	4.29	5.84	4.60
% 4/07-2	2006	1/4	3200	31.4	62.0	7.93	5.8	64.2	47.8	5.5	20.7	0.59	1.33	7.95	5.88	5.67	4.35	5.72	4.58
% 4/07-3	2007	1/20	3200	46.3	62.3	7.99	4.9	38.0	66.7	5.4	26.0		1.51	7.87	5.40	5.34	3.67	5.84	4.55
% 8/07-4	2007	5/19	3200	32.2	57.8	7.12	4.2	19.3	59.2	8.2	23.6		1.28	7.55	5.69	5.28	3.94	5.84	4.62

Two-tailed Pearson Product Moment Correlation analysis was executed to determine the significant correlations between each of two variables. Factor analysis (varimax) was performed to evaluate relationships among the compositional variables and the partition coefficients (K_d), using all samples. All chemical components determined in this study were used except hydroquinone content, due to the limited number of analyses ($n=30$). In a generalized adsorption/desorption reaction: $C \leftrightarrow X$, where X = concentration of a given species in solid phase (g or mole per gram of solid), and C = concentration of a given species in liquid phase (g or mole per cm^3 of liquid), the equilibrium constant K_d is $K_d = X/C = \exp(-\Delta G_r/(RT))$. $\log K_d$ is proportional to $-\Delta G_r$, which is the Gibbs free energy change of the sorption reaction. Therefore, $\log K_d$ values were used for all statistical analyses to evaluate the possible carrier phases for radionuclides. The adequacy of our data for factor analysis was evaluated by the Kaiser-Meyer-Olkin (KMO) measure of the sampling adequacy method. Factors were extracted by principle component analysis, and rotated by the varimax method with Kaiser Normalization. For Pearson correlation tests, pair-wise deletion was used when there were missing data; and for factor analysis, list-wise deletion was used when there were missing data.

5.4 Results

5.4.1 Average composition of the OFP trap particles (<125µm)

The organic (organic carbon, proteins, total carbohydrates, uronic acids, hydroquinones and hydroxamate siderophores), and inorganic (Si, Fe, Mn, CaCO₃) compositions of sediment trap samples, and the logK_d values for radionuclides (²³⁴Th, ²³³Pa, ²¹⁰Po, ²¹⁰Pb and ⁷Be) are given in Table 5.1 and their averages in Table 5.2. Our measured average Si, Fe and Mn values for <125µm trap particles are comparable with those for <1000µm particles analyzed by Huang and Conte (2009); and the differences are within 20% or better.

In terms of overall particle composition, CaCO₃ is the most abundant component in OFP samples, ranging from 29.4% to 76.3% (Table 5.2), with an average value of 61.0% over the whole water column. The average content of CaCO₃ shows a fairly stable distribution without any decreasing or increasing trends in samples from the three different depths (Table 5.2). In contrast, the average content of Si, Mn and Fe in the sediment trap samples shows a significant increase with increasing depth (Table 5.2). For organic components in the OFP samples, total organic carbon (OC) comprised 4.1% to 16.0% of the total weight, showing a significant decrease with depth (Table 5.2).

Table 5.2 Averages of $\log K_d$ values of radionuclides, particulate organic and elemental concentrations and the total particle fluxes at three depths at the Oceanic Flux Program (OFP) site off Bermuda.

		Depth					
		500 m (n=14)		1500 m (n=22)		3200 m (n=25)	
		Mean	std	Mean	std	Mean	std
LogK _d (Th)		5.08	0.56	5.66	0.53	5.53	0.31
LogK _d (Pa)		4.85	0.14	5.28	0.25	5.24	0.19
LogK _d (Pb)		3.95	0.32	3.92	0.29	4.07	0.25
LogK _d (Po)		5.20	0.21	5.54	0.2	5.66	0.16
LogK _d (Be)		4.19	0.24	4.41	0.29	4.44	0.19
Flux	mg/m ² /d	40.3	26.1	33.6	15.0	36.4	15.3
CaCO ₃	%	57.3	12.1	63.0	4.9	61.1	3.8
Si	%	5.68	1.48	6.21	1.17	6.95	1.03
OC	%	11.08	2.69	6.76	0.85	5.03	0.57
TCHO	mg/g	82.4	33.1	55.0	19.8	32.6	13.2
Protein	mg/g	59.6	14.2	62.5	17.8	45.2	10.1
URA	mg/g	53.8	22.2	31.1	10.5	6.57	1.58
HS	mg/g	24.5	5.4	30.2	8.1	28.5	6.4
HQ	mg/g	1.29	0.46	0.60	0.12	0.47	0.14
Mn	mg/g	0.21	0.27	1.32	0.39	1.32	0.27
Fe	mg/g	4.55	2.90	6.07	1.40	7.51	1.05

Similar to OC, the concentrations of TCHO, URA and HQ were relatively high for surface samples and decreased with depth. Results showed that HS was only detectable in the acid digestible fraction, indicating that HS moieties are strongly bound to materials that are solubilized only under more extremely acidic conditions. Particulate

HS concentrations, however, were lower in the 500m-depth samples than in the deeper water column samples (Table 5.2).

5.4.2 Partitioning of ^{234}Th , ^{233}Pa , ^{210}Po , ^{210}Pb and ^7Be between dissolved and particulate phases

Log K_d values derived from OFP sinking particulate samples after 2 days equilibration ranged from 4.17 to 7.08 for ^{234}Th , 4.57 to 5.67 for ^{233}Pa , 4.99 to 5.88 for ^{210}Po , 3.32 to 4.60 for ^{210}Pb and 3.73 to 4.81 for ^7Be , respectively (Table 5.1 and 5.3).

While it is possible that K_d values would have been higher after longer equilibration times (e.g., Nyffeler et al., 1984), potential problems from colloids generation and wall adsorption limited equilibration times to 2 days.

The average log K_d values of these radionuclides, 5.5 for ^{234}Th , 5.2 for ^{233}Pa , 5.5 for ^{210}Po , 4.0 for ^{210}Pb , and 4.4 for ^7Be , followed the order of $\text{Po} \geq \text{Th} > \text{Pa} > \text{Be} > \text{Pb}$ in the water-particle partitioning experiments (Table 5.2). Moreover, log K_d values of Po, Pa and Be show increasing trends with depth (From here on, we adopt symbol log $K_d(\text{X}, \text{Y}, \text{Z})$ to represent log K_d values of X, Y and Z). The log $K_d(\text{Th})$ of deep water samples (1500m and 3200m) are significantly higher than those of the 500m samples; however, log $K_d(\text{Pb})$ shows relatively constant values among three depths (Table 5.2).

Table 5.3 Comparisons of logK_d values among ²³⁴Th, ²³³Pa, ²¹⁰Po, ²¹⁰Pb and ⁷Be from different aquatic environments.

Nuclides	Study areas	logK _d range	References
²³⁴ Th	OFP	4.17 - 7.08	<i>This study</i>
	AESOPS, EqPac, MAB and others**	5.59 - 6.95	Chase et al., 2002
	OFP	4.64 - 6.86	Roberts et al., 2009
	Gulf of Mexico	5.22 - 6.62	Roberts et al., 2009
	Controlled experiments		
	SiO ₂	3.98	Guo et al., 2002a
	CaCO ₃	5.60	
	SiO ₂	5.90 - 6.23	Geibert and Usbeck, 2004
	CaCO ₃	5.04 - 5.18	
	SiO ₂	5.54	Roberts et al., 2009
	CaCO ₃	5.70	
²³³ Pa	OFP	4.57 - 5.67	<i>This study</i>
	AESOPS, EqPac, MAB and others**	5.34 - 6.15	Chase et al., 2002
	OFP	3.90 - 7.12	Roberts et al., 2009
	Gulf of Mexico	3.96 - 4.66	Roberts et al., 2009
	Controlled experiments		
	SiO ₂	5.09	Guo et al., 2002a
	CaCO ₃	3.68	
	SiO ₂	5.60 - 6.00	Geibert and Usbeck, 2004
	CaCO ₃	5.23 - 7.79	
	SiO ₂	4.39	Roberts et al., 2009
	CaCO ₃	5.11	
²¹⁰ Po	OFP	4.99 - 5.88	<i>This study</i>
	Southern North Sea	4.41-6.01*	Zuo and Eisma, 1993
	Northwestern Mediterranean Sea	5.08-6.30	Masqué et al., 2002b
	Northwestern Mediterranean margin	3.84-7.06*	Tateda et al., 2003
	Controlled experiments	3.02 - 5.48	Yang et al., 2013
	²¹⁰ Pb	OFP	3.32 - 4.60
Southern North Sea		4.34-6.82*	Zuo et al., 1993
Northwestern Mediterranean Sea		4.56-6.22	Masqué et al., 2002b
Gulf of Mexico		5.08-6.89	Baskaran et al., 2002
Northwestern Mediterranean margin		4.23-6.99*	Tateda et al., 2003
Controlled experiments		3.22 - 6.49	Yang et al., 2013

Table 5.3 continued.

Nuclides	Study areas	logK _d range	References
⁷ Be	OFP	3.73 - 4.81	<i>This study</i>
	Sabine-Neches estuary, Texas	3.18-4.94	Baskaran et al., 1997
	Loire estuary	4.57-4.91	Ciffroy et al., 2003
	Tampa Bay, Florida	3.00-5.19*	Baskaran et al., 2007
	Controlled experiments	3.57 - 4.65	Yang et al., 2013

*The logK_d values were calculated according to the reported dissolved, and particulate activities of radionuclides, and the concentrations of suspended particulate matter.

**SW Pacific sector of the Southern Ocean (AESOPS), the equatorial Pacific (EqPac) and the Mid Atlantic Bight (MAB).

Table 5.4 R-values for each two crossed factors by 2-tailed Pearson Product Moment Correlation (pair-wise deletion for missing data).

	LogK _d (Th)	LogK _d (Pa)	LogK _d (Pb)	LogK _d (Po)	LogK _d (Be)	CaCO ₃	OC	Si	Mn	Fe	TCHO	Protein	URA	HS	HQ
LogK _d (Th)	1.00	0.26	-0.07	0.25	0.26	.45**	-.44**	-0.08	.38**	0.05	-.39**	-0.05	-.39**	0.15	-.54**
LogK _d (Pa)	0.26	1.00	0.03	.57**	0.08	0.02	-.48**	0.26	.57**	0.28	-.45**	0.04	-.38**	.40**	-0.46
LogK _d (Pb)	-0.07	0.03	1.00	0.13	-0.07	-0.23	-0.15	0.13	0.15	0.24	0.03	-0.30	-0.10	-0.17	-0.01
LogK _d (Po)	0.25	.57**	0.13	1.00	0.16	0.06	-.57**	0.13	.69**	.51**	-.57**	0.03	-.50**	.51**	-.57**
LogK _d (Be)	0.26	0.08	-0.07	0.16	1.00	.36**	-0.33	0.27	0.34	0.16	-0.26	-.33**	-.37**	0.00	-.60**
CaCO ₃	.45**	0.02	-0.23	0.06	.36**	1.00	-.48**	-.35**	0.15	-.47**	-.39**	0.07	-.42**	0.08	-.50**
OC	-.44**	-.48**	-0.15	-.57**	-0.33	-.48**	1.00	-0.21	-.70**	-0.29	.74**	0.29	.79**	-0.17	.79**
Si	-0.08	0.26	0.13	0.13	0.27	-.35**	-0.21	1.00	0.24	.43**	-0.03	-0.20	-0.18	0.02	-0.26
Mn	.38**	.57**	0.15	.69**	0.34	0.15	-.70**	0.24	1.00	.59**	-.55**	-0.23	-.62**	.34**	-.70**
Fe	0.05	0.28	0.24	.51**	0.16	-.47**	-0.29	.43**	.59**	1.00	-0.18	-0.29	-.40**	0.23	0.05
TCHO	-.39**	-.45**	0.03	-.57**	-0.26	-.39**	.74**	-0.03	-.55**	-0.18	1.00	0.19	.73**	-.37**	.72**
Protein	-0.05	0.04	-0.30	0.03	-.33**	0.07	0.29	-0.20	-0.23	-0.29	0.19	1.00	.47**	0.18	0.12
URA	-.39**	-.38**	-0.10	-.50**	-.37**	-.42**	.79**	-0.18	-.62**	-.40**	.73**	.47**	1.00	-0.17	.68**
HS	0.15	.40**	-0.17	.51**	0.00	0.08	-0.17	0.02	.34**	0.23	-.37**	0.18	-0.17	1.00	-0.17
HQ	-.54**	-0.46	-0.01	-.57**	-.60**	-.50**	.79**	-0.26	-.70**	0.05	.72**	0.12	.68**	-0.17	1.00

(Bold value with ** denotes correlations significance level <0.01)

5.4.3 Effects of particle composition on the partitioning of ^{234}Th , ^{233}Pa , ^{210}Po , ^{210}Pb and ^7Be between dissolved and particulate phases

Relationships among the concentrations of particle components and $\log K_d$ values of radionuclides were obtained as a correlation matrix (Table 5.4) by applying the Pearson Product Moment Correlation method on all data (Table 5.1). Different components or phases varied in their correlation with the $\log K_d$ values of the radionuclides. We arbitrarily call a weak correlation when the correlation coefficient $\gamma = 0.3-0.39$, a moderate correlation when $\gamma = 0.4-0.49$, and a strong correlation when $\gamma \geq 0.5$ in the following discussion using this approach. The most abundant component CaCO_3 is moderately correlated with $\log K_d(\text{Th})$ and weakly with $\log K_d(\text{Be})$; Mn is strongly correlated with $\log K_d(\text{Po}, \text{Pa})$ and weakly with $\log K_d(\text{Th}, \text{Be})$; Fe is strongly correlated to $\log K_d(\text{Po})$; and HS is strongly correlated with $\log K_d(\text{Po})$ and moderately with $\log K_d(\text{Pa})$ (Table 5.4). In terms of the bulk organic material, OC shows a moderate to strong negative correlation with $\log K_d(\text{Th}, \text{Po}, \text{Pa})$ and a weak negative correlation with $\log K_d(\text{Be})$. Among all radionuclides, only $\log K_d(\text{Pb})$ shows a weak negative correlation with protein.

Table 5.5 Rotated structure matrix derived from the covariance matrix with logK_d of selected radionuclides with data from all three depths.

	Component			
	1	2	3	4
% of variance	36.46	13.49	13.03	7.89
LogK_d(Po)	<i><u>0.90</u></i>	0.07	-0.06	-0.11
LogK_d(Pa)	<i><u>0.74</u></i>	-0.04	-0.15	0.10
Mn	<i><u>0.72</u></i>	0.36	-0.11	-0.29
HS	<i><u>0.67</u></i>	-0.11	-0.08	0.40
Fe	<i><u>0.64</u></i>	<i><u>0.43</u></i>	-0.36	-0.34
LogK_d(Th)	0.34	0.07	<i><u>0.54</u></i>	-0.14
Si	0.24	<i><u>0.61</u></i>	<i><u>-0.40</u></i>	0.04
Protein	0.08	<i><u>-0.65</u></i>	0.08	<i><u>0.51</u></i>
LogK_d(Be)	0.07	<i><u>0.80</u></i>	0.21	0.19
LogK_d(Pb)	0.06	-0.07	-0.11	<i><u>-0.82</u></i>
CaCO ₃	-0.07	0.03	<i><u>0.91</u></i>	0.18
Flux	-0.32	-0.06	<i><u>0.76</u></i>	0.08
URA	<i><u>-0.50</u></i>	<i><u>-0.56</u></i>	-0.13	<i><u>0.43</u></i>
OC	<i><u>-0.62</u></i>	<i><u>-0.41</u></i>	<i><u>-0.41</u></i>	0.38
TCHO	<i><u>-0.63</u></i>	-0.31	-0.19	0.09

(Bold and italic value denotes loadings at a significance level of ± 0.4)

Factor analysis (varimax) was used to further explore the effects of particle composition on radionuclide partitioning and find the most likely carrier phase(s) for radionuclide binding in the sediment trap samples. The KMO values obtained were with a high significance level ($p < 0.001$). Four factors with eigenvalues greater than one were extracted.

With all samples analyzed, four extracted factors explained 70.9% of the total variance present in the original data set (Table 5.5). Factor loadings (fl) of $-0.4 \geq fl \geq 0.4$ are considered here to be significant (bold numbers in Table 5.5). The factor loadings of variables on factors 1 to 4 (F1 to F4) are plotted in Fig. 5.1. For clarity, some variables are omitted in Fig. 5.1 when their factor loadings were $-0.4 \leq fl \leq 0.4$ in the two plotted factors. In Fig. 5.1, variables within one dotted oval have significant correlation (either $\gamma \geq 0.4$ or $\gamma \leq -0.4$) between any pair of them in the correlation matrix (Table 5.4). Two variables connected by straight lines are also significantly correlated. According to Fig. 1a, factor 1 (F1) is represented by $\log K_d(\text{Po}, \text{Pa})$, HS, Mn and Fe. However, HS alone does not correlate significantly with Mn and Fe. The negative factor 1 (-F1) is represented by TCHO, OC, and URA. Members of F1 and -F1 groups are inversely correlated. F2 is represented by $\log K_d(\text{Be})$ and Si. However, the correlation coefficient between Si and $\log K_d(\text{Be})$ pair is very low ($\gamma = 0.27$). Instead, Si is moderately correlated with Fe ($\gamma = 0.43$). -F2 represents protein which is partially correlated with

URA. F3 is represented by carbonate, particle flux and $\log K_d(\text{Th})$, and $-F3$ by Si and OC (Fig. 5.1b). The high correlation between carbonate and particle flux implies that the observed seasonal variation of particle flux is mainly caused by the change in the surface production rate of carbonate in the study area. Si and OC may have a dilution effect on the content of carbonate in the trap sediments. F4 is represented by protein, URA and partially by OC, and $-F4$ by $\log K_d(\text{Pb})$ alone. Also, it should be mentioned that in Table 5.5, HS had a F4 loading of 0.4 but is not shown in Fig. 5.1b, because it is likely an artifact caused by the varimax operation. According to the correlation matrix (Table 5.4), HS does not correlate with protein, URA, and OC, nor negatively with $\log K_d(\text{Pb})$.

In complement to the results of the factor analysis, Fig. 5.2 and 5.3 provide the x-y correlation plots of the concentrations or ratios of selected variables in sediment trap samples to illustrate in detail the variation patterns of variables among the samples obtained at three different sampling depths (500m, 1500m and 3200m). Relevant features of those figures are highlighted in the following discussion section.

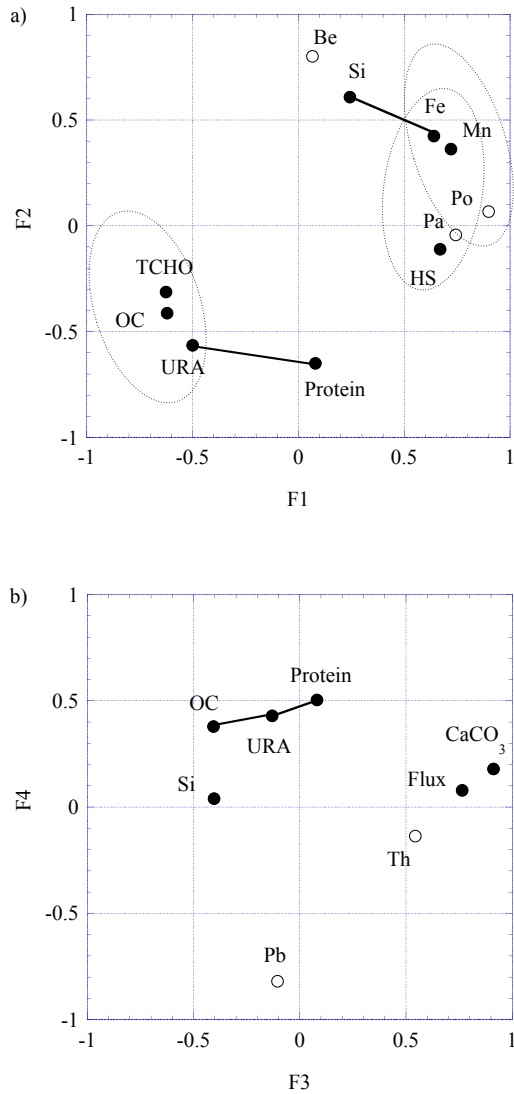


Fig. 5.1 Graphic representation of Factor Analysis (FA) carried out with all three depths samples (open circle: radionuclides; filled circle: possible carrier phases/proxies). a) Distribution of factors according to their loadings of F1 and F2; b) Distribution of factors according to their loadings of F3 and F4.

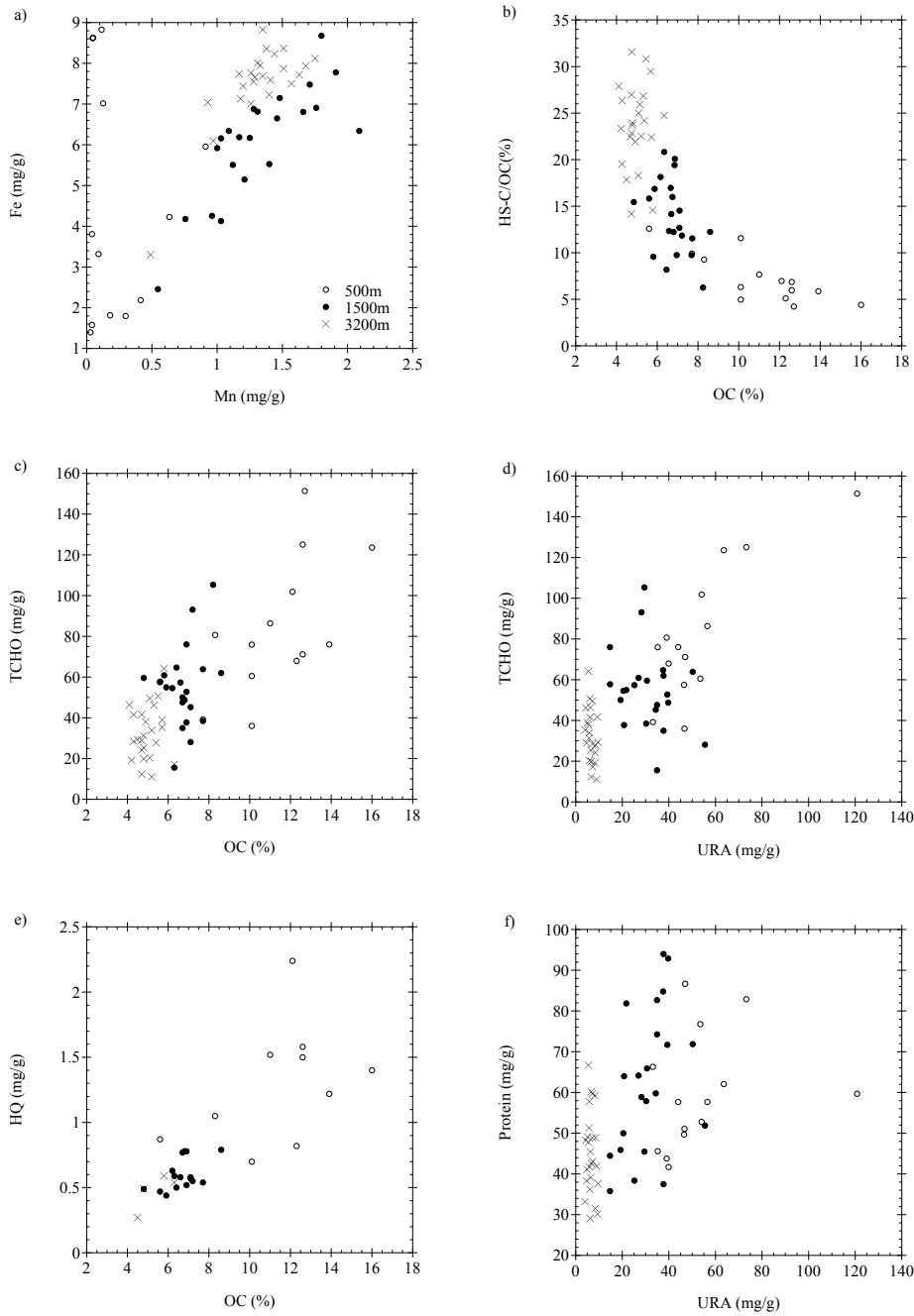


Fig. 5.2 Correlations of particulate concentration (in wt/wt unit) of a) Mn with Fe; b) OC with HS-C/OC; c) OC with TCHO; d) URA with TCHO; e) OC with HQ; f) URA with Protein; in three different depths.

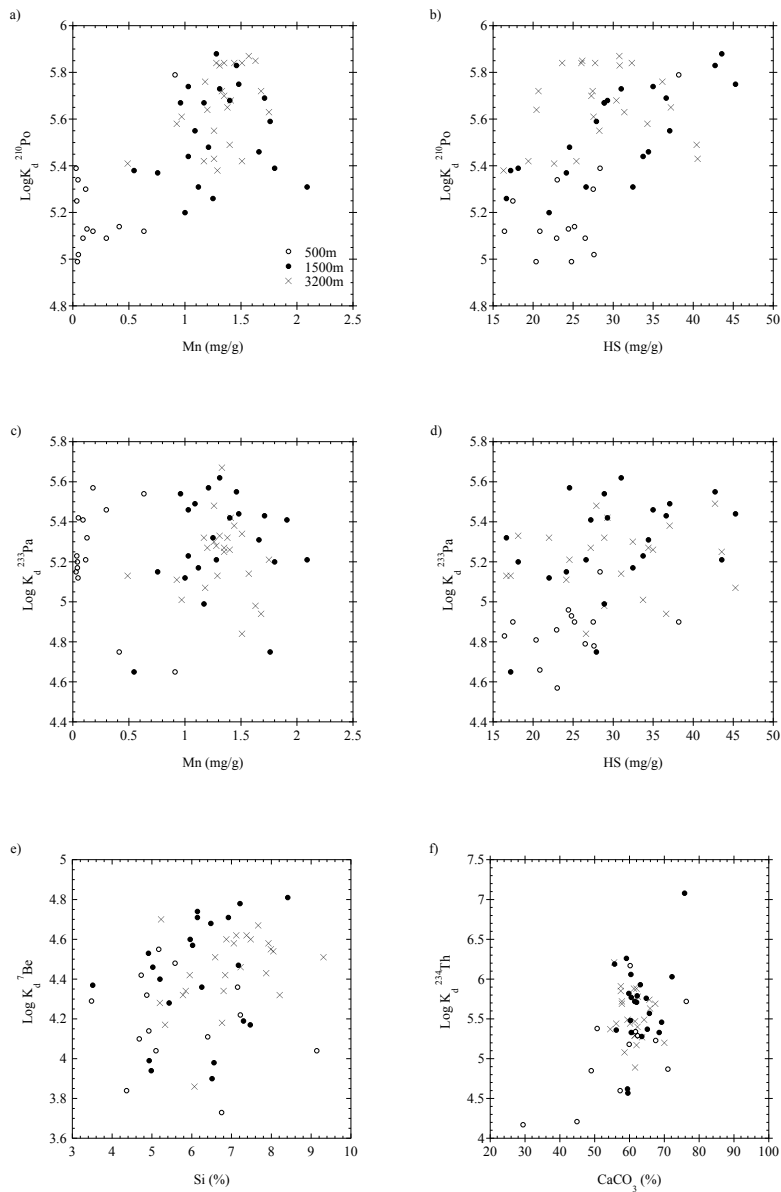


Fig. 5.3 Correlations of a) particulate Mn concentration with $\log K_d^{210}\text{Po}$; b) particulate HS concentration with $\log K_d^{210}\text{Po}$; c) particulate Mn concentration with $\log K_d^{233}\text{Pa}$; d) particulate HS concentration with $\log K_d^{233}\text{Pa}$; e) particulate Si concentration with $\log K_d^{7}\text{Be}$; f) particulate CaCO_3 concentration with $\log K_d^{234}\text{Th}$; in three different depths.

5.5 Discussion

5.5.1 Hydroxamate siderophores in marine particulate organic materials

So far, very little attention has been paid to the presence of siderophores in particulate organic matter (suspended or sinking particles $>0.2\mu\text{m}$) in the marine environment. Even less attention has been paid to the molecular-level mechanisms regulating the interactions between natural radionuclides and siderophores. Surprisingly, strongly Fe(III) complexing hydroxamate siderophores (HS) were found to contribute a relatively high percentage (1.57 to 5.25%) of the total particulate weight in the sediment trap samples (Table 5.2) but catecholate siderophores were below the detection limit. The catecholate siderophores, which are also known to form very stable complexes with Fe are also very efficient in dissolving Fe bearing minerals (Albrecht-Gary and Crumbliss, 1998). Furthermore, they can shift the redox potential to such a low region that it does not allow biological reductants to reduce the complex (Albrecht-Gary and Crumbliss, 1998). However, the reasons why we did not detect any particulate catecholate siderophores but find high concentration of HS in OFP particles are still unclear. Further molecular level structural analysis of siderophore moieties in different extracted solutions would be needed to resolve these questions.

The average HS flux at OFP site off Bermuda was about $1 \text{ mg-C m}^{-2} \text{ day}^{-1}$, staying relatively constant over the 3500 m water column (data derived from Table 5.1, the

fluxes of various parameters = total particle flux × concentrations of various parameters in particles). Compared to the average gross primary productivity in the Sargasso Sea off Bermuda ($160 \text{ g-C m}^{-2} \text{ yr}^{-1}$, or $440 \text{ mg-C m}^{-2} \text{ day}^{-1}$; Menzel and Ryther, 1959), this flux is about 0.23 % of the primary productivity, or compared to an organic carbon downward export flux of $9 \text{ g-C m}^{-2} \text{ yr}^{-1}$, or $25 \text{ mg-C m}^{-2} \text{ day}^{-1}$ (Kim et al., 2003a), the HS flux is about 4% of the average OC flux. Moreover, the HS flux remained fairly constant over all depths, suggesting that HS is likely a refractory organic component, at least on the time scale of particle sinking. This is also supported by FA results in F1 loadings, where HS is shown to be negatively correlated with OC, TCHO and URA. As shown in Fig. 5.2b, HS-C/OC ratio is relatively high for samples from 1500m and 3200m depths as compared with those from 500m. Figures 5.2c to 5.2e show systematic decreases of TCHO, URA and HQ concentrations with sampling depth, indicating their labile nature. The stability of protein probably lies between HS and URA (Fig. 5.2f).

The contribution of HS to the particulate organic carbon (POC) flux at depth is below that of the uncharacterized organic carbon fraction in the same depth range. Lee et al. (2004) found that the percentage of uncharacterized carbon in the particle flux in the equatorial Pacific Ocean at 105m, 1000m and in >3500m was ~20%, 70% and >70%, respectively. Similarly, (Hirose and Tanoue, 2001) found that approximately 40% of deep POC at 2000-m depth in the North Pacific Ocean and Bering Sea was refractory

POC, with the strong organic ligand (SOL) to POC ratio in the per mil range. Results from Hirose (1995) furthermore suggest that the Th complexation capacity of suspended particulates in the surface ocean is about 10 nM. Given that suspended particle concentrations are of the order of 100 $\mu\text{g/L}$, the estimated strong organic Th ligand (SOL) concentrations can be in the order of 100 $\mu\text{mole/g}$. Such a value is similar to the HS and Fe concentrations measured in our OFP subsamples. A later study from the same group (Hirose and Tanoue, 2001), suggested that the main source of the SOL is marine bacteria, because the concentration of the chelator in phytoplankton and zooplankton is more than one order of magnitude lower than that of bacteria. It is quite likely that SOL or uncharacterized carbon is mainly composed of HS molecules. Further studies are needed to confirm this hypothesis.

The relatively high ratio of siderophore moieties to OC in the deep water particles (Fig. 5.2b) may indicate that siderophore moieties become more stable through Fe(III) chelation. Available chemical speciation data of particulate iron from the oceanic literature using EXAFS/XANES and microXAS did not clearly differentiate organo-Fe from inorganic Fe (Lam et al., 2002; Duckworth et al., 2008). These methods, however, documents that the majority of open ocean particulate iron is tri-valent Fe (Lam et al., 2012), even though a number of researchers also documented Fe(II) phases (e.g., Fe-sulfides) near upwelling sites or hydrothermal plumes (Lam et al., 2012; Toner et al.,

2012). However, at the OFP site, one could expect that most of the Fe would be organo-Fe(III) (hydroxamate-bound Fe), as a significant fraction of OC is composed of hydroxamate-C. Nonetheless, our results would need to be confirmed by other methods, e.g., by EXAFS/XANES and/or micro-XAS.

In Huang and Conte (2009), some direct evidence for the relative partitioning of Fe with organic matter and inorganic materials is presented. These authors reported a crustal enrichment factor of 1.3-1.4 for Fe in OFP sediment trap particles, suggesting some enrichment of Fe in organic phases. Similarly, the relative factor loadings of Fe from PMF (Positive Matrix Factorization) analysis indicated that at 500m depth ~20% of the Fe is associated with organic matter and 20% with oxy-hydroxides; at 1500 and 3200 m Fe is more evenly distributed among possible carrier phases, including shale particles.

Besides, it is possible that physicochemical properties of siderophores are changing with depth, due to bacterial reworking (Jiao et al., 2010), change in relative hydrophobicity, and subsequent chemical modifications (cross-linking) of particulate organic matter. Thus, siderophores may play a more important role in the biogeochemical cycle of trace metals (e.g., Fe) and natural radionuclides (e.g., Po and Pa, in this study) than previously thought. There is also a direct evidence from flow injection electrospray ionization mass spectrometry, which showed that the cation Th(IV) can replace Fe(III) to form a a strong and soluble Th-hydroxamate siderophores complex in

terrestrial environments (Keith-Roach et al., 2005). The implication is that hydroxamate siderophores can enhance the mobility of actinides (IV) in such environments.

Laboratory experiments have shown that, after deprotonation, monohydroxamic acids, such as acetohydroxamic acids $\text{CH}_3\text{CONHOH} = \text{AHA}$ (the standard used to determine the HS concentration in this study), act as bidentate ligands to form octahedral complexes with Fe(III). Fe(III) is coordinated through two ketonic oxygen atoms of the $-\text{CONHO}-$ group, which exhibit octahedral configuration both in the solid state and in solution (Kurzak et al., 1992). This is confirmed by X-ray diffraction studies (Brown et al., 1979). In addition, the stabilities of the chelating compound increases with increasing size of the substituent of R in the monohydroxamic acids, such as R-COHNOH (Brown et al., 1979). In a Fe(III)-hydroxamate complex, at least three units of monohydroxamic acids are required for Fe chelation. In OFP particles, the HS/Fe molar ratio averages 3.92 (ranging from 1.54 to 14.86, derived from Table 5.1), indicating sufficient hydroxamate binding sites for Fe and other metals such as Pa and Po.

According to another structural study of the marine hydroxamate siderophore exochelin MS (the extracellular siderophore from *Mycobacterium smegmatis*, Dhungana et al., 2004), there are seven protonation sites for metal binding, one on a carboxylic acid, three on hydroxamate sites, and three on primary amine groups. The binding of radionuclides with natural hydroxamate siderophores might also form a similar

configuration. As a consequence of the heterogeneity of the binding sites, the isoelectric point, pH_{IEF} , of any extracted radionuclide-binding molecule would be expected to show different pH_{IEF} patterns due to the different pK_a values of different binding sites, as was found in Ch2 and Ch3.

5.5.2 Effects of particle composition on the scavenging and fractionation of radionuclides

K_d values comparable to ours can be found in the literature (e.g., Zuo and Eisma, 1993; Baskaran et al., 1997; Baskaran and Santschi, 2002; Chase et al., 2002; Guo et al., 2002a; Masque et al., 2002; Ciffroy et al., 2003; Tateda et al., 2003; Geibert and Usbeck, 2004; Baskaran and Swarzenski, 2007; Roberts et al., 2009; Yang et al., 2013), ranging from 10^3 to 10^7 for different radionuclides in marine environments (Table 5.3). However, because of the well documented particle-concentration effect (Li et al., 1984; Honeyman and Santschi, 1989) on $\log K_d$ for many of these radionuclides, and since we used a particle concentration of 10 mg/L, typical for near-shore waters (Baskaran and Santschi, 1993; Woźniak et al., 2010), K_d values can be higher at lower particle concentration such as those occurring in the open ocean (typically less than 1mg/L; Guo et al., 1997).

The observed close association among Mn, Fe, HS, $\log K_d$ (Po, Pa) (Fig. 5.1, Tables 5.4 and 5.5) in the trap samples may be explained by the following coupled processes: Mn(II)-oxidizing bacteria are encoded by specific oxidase genes to oxidize Mn(II) and

Mn(III) (Geszvain et al., 2013). HS forms a strong complex with Mn(III) and stabilizes Mn(III), thus enhances the oxidation of Mn(II) to Mn(III) and MnO₂ (Spiro et al., 2009; Geszvain et al., 2011; Madison et al., 2011; Harrington et al., 2012). Therefore, Po and Pa may be incorporated into MnO₂ (Fig. 5.3a and 5.3c), and/or taken up by HS through ion exchange with Fe(III) and Mn(III) (Fig. 5.3b and 5.3d). Another possible explanation is as follows: As shown in Fig. 2a, the most of samples from 500 m have very low Mn content (<0.2 mg/g) but have wide rang in Fe content (1 to 9 mg/g). In contrast, samples from 1500m and 3200m are high in Mn content but the range in Fe content is still similar to that of 500m. Meanwhile Mn and Fe contents are highly correlated. It might be possible then that the oxidation of Mn(II) to Mn(III) and to MnO₂ could also be catalyzed by Fe containing minerals without invoking HS as facilitator. Which of these coupled processes are realized in the ocean is not known, even though one might expect that microbial involvement is more likely. Using the average compositions of OFP sediment trap samples given by Huang and Conte (2009), we roughly estimate the relative abundance of possible carrier phases for radionuclides at different depths. By assuming that all Al in samples is contributed by shale particles (alumino-silicates), the contributions from shale for other elements are calculated and subtracted from the total to obtain the net as shown in Table 5.6. Using the data in the net columns, OC is converted to dry organic matter, Fe to Fe₂O₃, Mn to MnO₂, Ca to CaCO₃, and Si to SiO₂.

Table 5.6 Elemental composition and their possible % shale contribution in OFP sediment trap particles.

Element	Total (ppm)				Contribution from shale			Net (= total - shale contribution)			% Shale contribution		
	Shale	500m	1500m	3200m	500m	1500m	3200m	500m	1500m	3200m	500m	1500m	3200m
OC	12000	171000	74000	54000	675	1514	2090	170325	72486	51910	0.39	2.05	3.87
N	1000	24000	10000	6200	56	126	174	23944	9874	6026	0.23	1.26	2.81
Mg	15000	4474	5641	6128	844	1892	2613	3630	3749	3515	18.86	33.54	42.64
Al	87000	4893	10975	15154	4893	10975	15154	0	0	0	100.00	100.00	100.00
Si	275000	50390	99471	126904	15466	34691	47901	34924	64780	79003	30.69	34.88	37.75
P	700	2249	911	700	39	88	122	2210	823	578	1.75	9.69	17.42
Ca	16000	267341	260918	253605	900	2018	2787	266441	258900	250818	0.34	0.77	1.10
Sc	13	0.70	1.50	2.00	0.73	1.64	2.26	-0.03	-0.14	-0.26	104.45	109.33	113.22
Ti	4600	200	406	599	259	580	801	-59	-174	-202	129	143	134
V	130	7.80	21.20	30.20	7.31	16.40	22.64	0.49	4.80	7.56	93.74	77.36	74.98
Mn	850	191	927	1119	48	107	148	143	820	971	25	12	13
Fe	47200	2943	6651	9367	2655	5954	8221	288	697	1146	90	90	88
Co	19	3.90	11.50	13.20	1.1	2.4	3.3	2.8	9.1	9.9	27.4	20.8	25.1
Ni	50	33	39	42	2.8	6.3	8.7	30.2	32.4	33.6	8.5	16.3	20.6
Cu	45	49	58	73	2.5	5.7	7.8	46.5	52.3	65.2	5.2	9.8	10.7
Zn	95	114	107	84	5.3	12.0	16.5	108.7	95.0	67.5	4.7	11.2	19.7
Sr	170	1743	1831	1759	9.6	21.4	29.6	1733	1810	1729	0.5	1.2	1.7
Cd	0.3	2.7	1	0.51	0.02	0.04	0.05	2.68	0.96	0.46	0.62	3.78	10.25
Ba	580	401	842	818	33	73	101	368	769	717	8	9	12
Pb	20	42	56	75	1.1	2.5	3.5	40.9	53.5	71.5	2.7	4.5	4.6

The shale content in samples is estimated from the ratio of Al contents in the sample and the global average shale (Li, 2000). The results are summarized in Table 5.7 (by normalizing the total wt% as 100%). The contents of shale particles, opal, Mn-Fe oxides increase with depth, while the content of organic matter decreases drastically, and that of carbonate remains nearly constant (Table 5.7). In comparison, $\log K_d(\text{Th, Po, Pa, Be})$ values increase with depth (Table 5.1), while $\log K_d(\text{Pb})$ remains nearly constant. Interestingly, about 10-12 % of Fe is present as iron oxides; 75-88 % Mn as manganese oxides, and 62-69 % of Si as opal; while the remaining fractions are all contributed by shale particles in the OFP samples (Table 5.6).

Table 5.7 Concentration of selected elements in their estimated forms.

	(% wt in total particles)		
	500m	1500m	3200m
Organic matter	32.9	15.4	10.9
Silicate	4.7	11.7	15.9
Opal	6.3	12.8	15.5
Carbonate	56.0	59.9	57.4
MnO ₂	0.02	0.12	0.14
Fe ₂ O ₃	0.03	0.09	0.15
Total	100.0	100.0	100.0

It is not surprising then that OC is not a good predictor for radionuclide scavenging, even though, as our data suggest, sorption to biopolymers likely controls the extent of scavenging. This is due to the fact that these biopolymers are minor components in the particle flux, and co-produced with biogenic silica and CaCO₃ shells, thus hiding their

role when one only determines major components in the sinking or suspended particle assemblage. From F2 and F3 factor loadings (Table 5.5), it is apparent that CaCO₃ and opal (Si) might be good predictors of scavenging of selective radionuclides (CaCO₃ for Th and SiO₂ for Be), as also suggested by Chase et al. (2002). However, in order to get 10 % of a dissolved radionuclide to adsorb onto suspended or sinking particles, this would require logK_d values of 6 or higher for that particle component in the ocean. Typical logK_d values for pure CaCO₃ and SiO₂ phases are, however, only 3 to 5 for these radionuclides (Table 5.3, and summary in Roberts et al., 2009). In addition, our unpublished results (Ch3 and Ch4) show that acid-cleaned silica frustules from diatom *Phaeodactylum tricornutum* give logK_d values similar to commercially available pure SiO₂ for five different radionuclides (²³⁴Th, ²¹⁰Pb, ²³³Pa, ⁷Be and ²¹⁰Po), and are 1-2 orders of magnitude lower than those of untreated whole plankton cells, regardless if cells contained biogenic SiO₂ shells or not.

Though both logK_d(Th) and CaCO₃ are high in F3 loadings (Fig. 5.1b, Table 5.5), they are only moderately correlated ($\gamma = 0.45$) (Table 5.4). As shown in Fig. 5.3f, if one takes out two extreme low points and one high point, the apparent correlation between logK_d(Th) and CaCO₃ content would just disappear. The implication likely is that Th(IV) is evenly distributed to multiple binding moieties on well-documented organic coatings of the sinking particles. Interactive effects between mineral phases and associated biopolymers are thus strongly suggested by our data, a result that would require further study.

Well designed cross- and inter-calibration experiments of different

spectrophotometric methods may resolve the observed apparent correlations among CaCO_3 , percentage of total carbohydrates-C in total organic carbon (TCHO-C/C%) and $\log K_d$ values of Th and Pa found by Roberts et al. (2009). These authors suggested that the carbohydrate content could be used as a proxy parameter for the presence of the strongly chelating compounds or functional groups, since pure carbohydrates are not considered to be effective sorbents for actinides. In our calibration study, the TCHO concentration measured by the TPTZ method was also linearly correlated with AHA (standard for HS determination) concentration from 0 to 500 mM, suggesting that the correlation observed by Roberts et al. (2009) could also have resulted from the contribution of hydroxamates in the particle samples to the total polysaccharides pool.

Overall, all selected radionuclides, except Pb, showed specific carrier phase(s) in the sorption experiments. These radionuclides are all A-type metals, except for Pb, which is a B-type metal that is expected to prefer to bind to sulfur-containing sites on organic ligands rather than to oxygen-sites. As a consequence of the addition of ultra-high purity HgCl_2 (200 mg/L) preservative in the trap cup brine that arrests biological degradation during sample collection, the sulfur-binding sites on those organic ligands in the particles might all have been occupied by Hg^{2+} , another B-type metal. Hence, carrier phase(s) for Pb are not resolved with our approach, and thus, remain uncertain. And this might have also led to relatively lower K_d values of Pb in this study compared with values found in the literatures (Table 5.3).

5.5.3 Postulated binding mechanisms

In natural systems, Fe(III) has to compete not only with protons for the siderophore binding sites, but also with other metal ions having similarly strong binding energy. Binding energies for various natural metal ions are dependent on charge, Lewis acidity (hardness), size, d-electron configuration and electronegativity (Albrecht-Gary and Crumbliss, 1998), as well as the ionic potential (z/r) or ionization energy of the binding ions (I_z) (Li, 1991). The special Fe-HS binding structure reflects all these properties, leading to the high binding energy of Fe and high propensity for mobilization by siderophores. From the observed correlations and chemical considerations, we propose that Po(IV) and Pa(IV) are bound to siderophores by replacing Fe(III) with these four-valent ions, which have similar ionic potential (z/r) or ionization energy (I_z). In seawater, the most common oxidation state for Po is indeed the particle-reactive IV state (Hussain et al., 1995).

Some radionuclides have more than one possible oxidation state in natural waters. For example, Pa, its predominant form in seawater is likely Pa(V) (Choppin, 1983), which is more soluble and sorbs to particle surfaces to a lower extent than its four-valent counterpart, Pa(IV), in broad analogy to Pu and Np. Thus, it is likely that Pa(V) must first be reduced to Pa(IV) before adsorption can take place, as has been observed for Np(V), which is reduced by humic substances in natural waters (Zeh et al., 1999). According to the redox potentials listed in Ahrland et al. (1973), Pa should more easily be reduced from V to IV state than Pu and Np from V to IV. The redox potential for Pa(V \rightarrow IV) reduction is 0.29V in 6M HCl, while that of Pu in 1M HClO₄ is given as -

1.17V, and that of Np as -0.74V. Since hydroquinones, commonly present in humic substances (e.g., Kalmykov et al., 2008, and references therein), have been documented to reduce Pu and Np to their IV state (Zeh et al., 1999; Kalmykov et al., 2008), one could expect that the same should happen to Pa. While Marquardt et al. (2004) have documented the lability and propensity to oxidation of Pa(IV) in pure, highly acidic solutions (but not at neutral pH), they also documented that Pa(IV) is forming very strong complexes to common ligands that could be expected to stabilize the IV oxidation state at neutral pH.

$\log K_d(\text{Be})$ is only weakly correlated with Ca ($\gamma = 0.36$) and Mn ($\gamma = 0.34$), and very weakly with Si ($\gamma = 0.27$) and Fe ($\gamma = 0.16$) (Table 5.4). The apparent association between $\log K_d(\text{Be})$, Si and Fe shown in Fig. 5.1a and Table 5.5 could again be an artifact of varimax operation. Thus, Be is likely evenly distributed among different carriers. As mentioned before, about 62 to 69% of Si is in the form of opal and the rest in shale. While the Si-OH group on pure silica surfaces is a relatively weak ligand, with a seawater $\log K_d$ value for metal ions of only 3 to 5 (Schindler, 1975; Schindler et al., 1976; Schindler and Stumm, 1987; Stumm and Morgan, 1996; e.g., Guo et al., 2002b; Santschi et al., 2006; Roberts et al., 2009), biogenic silica surface appears to form stronger bonds to Be and other metals (e.g., Rutgers van der Loeff and Berger, 1993; Chase et al., 2002; Moran et al., 2002; Scholten et al., 2005; Kretschmer et al., 2011). This stronger bonding could likely be due to the inclusions of templating organic residues, e.g., silaffins (Kröger et al., 2002; Poulsen et al., 2003; Wieneke et al., 2011). Thus, the apparent association between Be and Si could also be considered as a

contribution from the binding of a specific organic phase embedded onto the biogenic silica as well as on carbonate shells. Further isolation and identification of the organic molecules/compounds are needed to confirm such an organic binding phase and the potential binding mechanisms.

5.6 Conclusions

Hydroxamate siderophores (HS) appear to be a main component of recalcitrant organic carbon in the sinking particles and to play an important role in the fractionation and scavenging of Po and Pa in the water column. Based on our results, we propose the following mechanism: Mn(II)-oxidizing bacteria are encoded by specific oxidase genes to oxidize Mn(II) to Mn(III) and to MnO₂. The function of HS is to form strong HS-Fe(III)-Mn(III) complexes to also stabilize Mn(III). The radionuclides of Po and Pa may be directly incorporated into MnO₂, and/or taken up by HS through exchange with Fe(III) and Mn(III) in their 4-valent states. It is also possible that the oxidation of Mn(II) to Mn(III) and to MnO₂ could be catalyzed by Fe containing minerals without invoking HS as a facilitator. However, microbial involvement is more likely. The apparent associations between Si and logK_d(Be) and between CaCO₃ and logK_d(Th) in factor analysis are likely artifacts. The radionuclides of Be and Th are probably evenly distributed among the different major mineral carrier phases, many of which are covered by various biopolymers. This close association between carrier phases and associated biopolymers may obscure the direct bonding of radionuclide to organic biopolymers.

The finding that hydroxamate siderophores are likely important carriers for some radionuclides warrants a more in-depth evaluation of organic carrier phases at the

molecular level, as previously carried out for other radionuclides (e.g., $^{239, 240}\text{Pu}$ and $^{127, 129}\text{I}$) (Xu et al., 2008, 2013). Unequivocal identification of the functionalities and binding selectivities of those radionuclides' carrier phases are needed for better data interpretation and understanding of biogeochemical cycles of carbon, iron and natural radionuclides. This information would also be crucial if we are to construct better radioisotopes-based models of the carbon flux and particle dynamics in the ocean.

CHAPTER VI

SUMMARY

Laboratory experiments had been conducted to investigate the binding mechanism of ^{234}Th , ^{233}Pa , ^{210}Pb , ^{210}Po and ^7Be radionuclides to different particles types (silica, diatom frustules, diatom cells with and without frustules, sediment trap particles), colloidal organic materials (marine colloids and exopolymeric substances) and its related biopolymers.

Combined results from factor analysis of radionuclide partitioning and chemical composition as well as isoelectric focusing data provide a basis to evaluate possible biopolymeric macromolecular carrier phases for the selected radionuclides. It becomes evident that specific organic biomolecules in marine colloids and EPS are the main carrier phases for selected radionuclides in the ocean, consistent with results from previous field and laboratory studies. In particular, acid polysaccharides and uronic acids appear to be the organic ligands for ^{234}Th binding; hydroxamate siderophores and organic sulfur containing biomolecules are important in the binding of ^{233}Pa ; ^{210}Pb -binding is associated to acid polysaccharides- and/or Fe-related protein-containing biomolecules; proteins-containing biomolecules are shown to be major classes of ^{210}Po binding biopolymers; for ^7Be , the strongest binding biomolecules seem to contain hydroquinone and/or Fe-containing biomolecules, and silaffins in diatoms.

Sorption experiments were also conducted with silica frustules from cells of diatom *Phaeodactylum tricornutum* were extensively acid-washed to remove both surface organic coatings and accessible tightly-bound templating biomolecules embedded in the

silica shell (e.g., silaffin) until the final OC concentration was <0.1%,. These silica frustules showed similar $\log K_d$ values to a commercially available pure silica, for all five radionuclides (^{234}Th , ^{210}Pb , ^{233}Pa , ^7Be and ^{210}Po). Most importantly, $\log K_d$ values of radionuclides on pure silica particles were significantly, by 1-2 orders of magnitude, lower than those of whole diatom frustules in the presence of the templating biomolecules. No significant difference in the $\log K_d$ values of each radioisotope between diatom cells with or without silica frustule was found, providing further evidence that silica cannot be the main carrier phase, as is traditionally assumed, for these selected radionuclides in the ocean.. Moreover, activity distributions of different radionuclide-carrying biomolecules along a pH gradient in the electric field revealed that isoelectric points are unique for the different radionuclides, suggesting that specific organic carrier phases are responsible for the binding of different radionuclides.

To the best of our knowledge, this is the first time the binding of ^{234}Th , ^{233}Pa , ^{210}Pb and ^7Be incubated together with cultured diatom cells, were comprehensively examined, at the molecular level, for their binding ability to different biopolymers released to the medium. In the ternary sorption system (biogenic silica-biopolymers-radionuclides), it became clear that it is not the mineral phases, e.g., biogenic silica, but the biopolymers associated with biogenic SiO_2 , that is providing the strongest binding sites for the different radionuclides, accounting for the majority of binding of these radionuclides. 2D HSQC NMR results showed that the biopolymers in the HF insoluble fraction were mainly composed of carboxyl-rich, aliphatic-phosphoproteins, providing strong binding sites for some of the radionuclides (e.g., Pa, Be). These extensive and comprehensive

molecular-level analyses of carrier macromolecules of radionuclides were thus of great help to resolve some of the controversial observations on the scavenging and fractionation of radionuclides in the ocean.

From the results of studies that examined the effects of particle composition on the scavenging of radionuclides with settling particles from the Atlantic Ocean, hydroxamate siderophores (HS) appeared to be a main component of recalcitrant organic carbon and to play an important role in the bindings of Po and Pa in the water column. Based on our results, we could propose the following mechanism: Mn(II)-oxidizing bacteria are encoded by specific oxidase genes to oxidize Mn(II) to Mn(III) and to MnO₂. The function of HS might be to form strong HS-Fe(III)-Mn(III) complexes that also stabilize Mn(III) in its three-valent state. The radionuclides of Po and Pa, in their 4-valent states, may be directly incorporated into MnO₂, and/or taken up by HS through exchange with Fe(III) and Mn(III). It is also possible that the oxidation of Mn(II) to Mn(III) and to MnO₂ could be catalyzed by Fe containing minerals without invoking HS as facilitator. However, microbial involvement might be more likely. The radionuclides of Be and Th are probably evenly distributed among the different major mineral carrier phases, many of which are covered by various biopolymers. This close association between carrier phases and associated biopolymers may obscure the direct bonding of radionuclide to organic biopolymers.

Overall, the findings that biopolymers are likely important carriers for radionuclides warrant a more in-depth evaluation of organic carrier phases at the molecular level. Unequivocal identification of the functionalities and binding selectivities of those

radionuclides' carrier phases are needed for better data interpretation and understanding of biogeochemical cycles of carbon, iron and natural radionuclides. This information would also be crucial if we are to construct better radioisotopes-based models of the carbon flux and particle dynamics in the ocean.

REFERENCES

- Ahrland, S., Liljenzin, J.O. and Rydberg, J., 1973. Solution Chemistry. In: J.C. Bailar and A.F. Trotman-Dickenson (Editors), Comprehensive inorganic chemistry. Oxford Pergamon exclusive distributors in Western Hemisphere, Compendium Publishers, Oxford.
- Albrecht-Gary, A.M. and Crumbliss, A.L., 1998. Coordination chemistry of siderophores: thermodynamics and kinetics of iron chelation and release. *Metal Ions in Biological Systems*, 35, 239-327.
- Alhassanieh, O., Abdul-Hadi, A., Ghafar, M., Aba, A., 1999. Separation of Th, U, Pa, Ra and Ac from natural uranium and thorium series. *Applied Radiation and Isotopes* 51, 493-498.
- Alvarado Quiroz, N.G., Hung, C.-C., Santschi, P.H., 2006. Binding of thorium(IV) to carboxylate, phosphate and sulfate functional groups from marine exopolymeric substances (EPS). *Marine Chemistry* 100, 337-353.
- Anderson, R. F., M. P. Bacon, and P. G. Brewer. 1983. Removal of ^{230}Th and ^{231}Pa at ocean margins. *Earth and Planetary Science Letters* 66, 73-90.
- Arce, F.T.n., Avci, R., Beech, I.B., Cooksey, K.E., Wigglesworth-Cooksey, B., 2004. A live bioprobe for studying diatom-surface interactions. *Biophysical Journal* 87, 4284-4297.
- Armbrust, E. V. 2009. The life of diatoms in the world's oceans. *Nature* 459, 185-192.

- Arnow, L.E., 1937. Colorimetric determination of the components of 3,4-dihydroxyphenylalaninetyrosine mixtures. *Journal of Biological Chemistry* 118, 531-537.
- Bacon, M.P., Spencer, D.W., Brewer, P.G., 1976. $^{210}\text{Pb}/^{226}\text{Ra}$ and $^{210}\text{Po}/^{210}\text{Pb}$ disequilibria in seawater and suspended particulate matter. *Earth and Planetary Science Letters* 32, 277-296.
- Baines, S.B., Pace, M.L., 1991. The production of dissolved organic-matter by phytoplankton and its importance to bacteria - patterns across marine and fresh-water systems. *Limnology and Oceanography* 36, 1078-1090.
- Baskaran, M. and Santschi, P.H., 1993. The role of particles and colloids in the transport of radionuclides in coastal environments of Texas. *Marine Chemistry* 43, 95-114.
- Baskaran, M. and Santschi, P.H., 2002. Particulate and dissolved Pb-210 activities in the shelf and slope regions of the Gulf of Mexico waters. *Continental Shelf Research* 22, 1493-1510.
- Baskaran, M., 2011. Po-210 and Pb-210 as atmospheric tracers and global atmospheric pb-210 fallout: A review. *Journal of Environmental Radioactivity* 102, 1126-1126.
- Baskaran, M., Ravichandran, M., Bianchi, T.S., 1997. Cycling of Be-7 and Pb-210 in a high DOC, shallow, turbid estuary of south-east Texas. *Estuarine Coastal and Shelf Science* 45, 165-176.

- Baskaran, M., Santschi, P.H., Benoit, G., Honeyman, B.D., 1992. Scavenging of thorium isotopes by colloids in seawater of the Gulf of Mexico. *Geochimica Et Cosmochimica Acta* 56, 3375-3388.
- Baskaran, M., Swarzenski, P.W., 2007. Seasonal variations on the residence times and partitioning of short-lived radionuclides (Th-234, Be-7 and Pb-210) and depositional fluxes of Be-7 and Pb-210 in Tampa bay, Florida. *Marine Chemistry* 104, 27-42.
- Benner, R., Biddanda, B., Black, B., McCarthy, M., 1997. Abundance, size distribution, and stable carbon and nitrogen isotopic compositions of marine organic matter isolated by tangential-flow ultrafiltration. *Marine Chemistry* 57, 243-263.
- Bhaskar, P.V., Grossart, H.P., Bhosle, N.B., Simon, M., 2005. Production of macroaggregates from dissolved exopolymeric substances (EPS) of bacterial and diatom origin. *Fems Microbiology Ecology* 53, 255-264.
- Boye, M., van den Berg, C.M.G., de Jong, J.T.M., Leach, H., Croot, P. and de Baar, H.J.W., 2001. Organic complexation of iron in the Southern Ocean. *Deep-Sea Research Part I-Oceanographic Research Papers* 48, 1477-1497.
- Broecker, W.S., Peng, T., 1982. *Tracers in the sea*. 690.
- Brown, D.A., McKeith, D. and Glass, W.K., 1979. Transition metal complexes of monohydroxamic acids. *Inorganica Chimica Acta* 35, 5-10.
- Bruno, J., 1990. The influence of dissolved carbon dioxide on trace metal speciation in seawater. *Marine Chemistry* 30, 231-240.

- Brzezinski, M.A., Villareal, T.A., Lipschultz, F., 1998. Silica production and the contribution of diatoms to new and primary production in the central north pacific. *Marine Ecology Progress Series* 167, 89-104.
- Buesseler, K.O., 1998. The decoupling of production and particulate export in the surface ocean. *Global Biogeochemical Cycles* 12, 297-310.
- Burnett, W.C., Corbett, D.R., Schultz, M., Horwitz, E.P., Chiarizia, R., Dietz, M., Thakkar, A., Fern, M., 1997. Pre-concentration of actinide elements from soils and large volume water samples using extraction chromatography. *Journal of Radioanalytical and Nuclear Chemistry* 226, 121-127.
- Carr, M.-E., Friedrichs, M.A.M., Schmeltz, M., Aita, M.N., Antoine, D., Arrigo, K.R., Asanuma, I., Aumont, O., Barber, R., Behrenfeld, M., Bidigare, R., Buitenhuis, E.T., Campbell, J., Ciotti, A., Dierssen, H., Dowell, M., Dunne, J., Esaias, W., Gentili, B., Gregg, W., Groom, S., Hoepffner, N., Ishizaka, J., Kameda, T., Quéré, C.L., Lohrenz, S., Marra, J., Mélin, F., Moore, K., Morel, A., Reddy, T.E., Ryan, J., Scardi, M., Smyth, T., Turpie, K., Tilstone, G., Waters, K., Yamanaka, Y., 2006. A comparison of global estimates of marine primary production from ocean color. *Deep-Sea Research Part II-Topical Studies in Oceanography* 53, 741-770.
- Chase, Z., Anderson, R.F., 2004. Comment on "on the importance of opal, carbonate, and lithogenic clays in scavenging and fractionating Th-230, Pa-231 and Be-10 in the ocean" by S. Luo and T.-L. Ku. *Earth and Planetary Science Letters* 220, 213-222.

- Chase, Z., Anderson, R.F., Fleisher, M.Q., Kubik, P.W., 2002. The influence of particle composition and particle flux on scavenging of Th, Pa and Be in the ocean. *Earth and Planetary Science Letters* 204, 215-229.
- Chen, C.-S., Anaya, J.M., Zhang, S., Spurgin, J., Chuang, C.-Y., Xu, C., Miao, A.-J., Chen, E.Y.T., Schwehr, K.A., Jiang, Y., Quigg, A., Santschi, P.H., Chin, W.-C., 2011. Effects of engineered nanoparticles on the assembly of exopolymeric substances from phytoplankton. *PLoS ONE* 6, e21865.
- Cherrier, J., Burnett, W.C., Larock, P.A., 1995. Uptake of polonium and sulfur by bacteria. *Geomicrobiology Journal* 13, 103-115.
- Choppin, G.R., 1983. Comparison of the solution chemistry of the actinides and lanthanides. *Journal of The Less-Common Metals* 93, 323-330.
- Choppin, G.R., 1989. Soluble rare earth and actinide species in seawater. *Marine Chemistry* 28, 19-26.
- Chuang, C.-Y., Ho, Y.-F., Santschi, P.H., 2013a. Is biogenic silica responsible for scavenging of radionuclides, ^{234}Th , ^{233}Pa , ^{210}Pb , ^{210}Po , ^7Be , in the ocean? A case study with *Phaeodactylum tricornutum*, ASLO 2013 Aquatic Sciences Meeting, New Orleans, Louisiana, USA.
- Chuang, C.-Y., Santschi, P.H., Ho, Y.-F., Conte, M.H., Guo, L.D., Schumann, D., Ayranov, M., Li, Y.-H., 2013b. Role of biopolymers as major carrier phases of Th, Pa, Pb, Po, and Be radionuclides in settling particles from the atlantic ocean. *Marine Chemistry* (In Press).

- Chuang, C.-Y., Santschi, P.H., Jiang, Y., Ho, Y.-F., Quigg, A., Guo, L.D., Ayranov, M., Schumann, D., 2013c. Role of diatoms in the scavenging of particle reactive radionuclides, thorium, protactinium, lead, polonium and beryllium, in the ocean: A case study with *Phaeodactylum tricoratum*. *Limnology and Oceanography* (submitted).
- Ciffroy, P., Reyss, J.-L. and Siclet, F., 2003. Determination of the residence time of suspended particles in the turbidity maximum of the Loire estuary by ^7Be analysis. *Estuarine, Coastal and Shelf Science* 57, 553-568.
- Coale, K.H., Johnson, K.S., Chavez, F.P., Buesseler, K.O., Barber, R.T., Brzezinski, M.A., Cochlan, W.P., Millero, F.J., Falkowski, P.G., Bauer, J.E., Wanninkhof, R.H., Kudela, R.M., Altabet, M.A., Hales, B.E., Takahashi, T., Landry, M.R., Bidigare, R.R., Wang, X.J., Chase, Z., Strutton, P.G., Friederich, G.E., Gorbunov, M.Y., Lance, V.P., Hilting, A.K., Hiscock, M.R., Demarest, M., Hiscock, W.T., Sullivan, K.F., Tanner, S.J., Gordon, R.M., Hunter, C.N., Elrod, V.A., Fitzwater, S.E., Jones, J.L., Tozzi, S., Koblizek, M., Roberts, A.E., Herndon, J., Brewster, J., Ladizinsky, N., Smith, G., Cooper, D., Timothy, D., Brown, S.L., Selph, K.E., Sheridan, C.C., Twining, B.S., Johnson, Z.I., 2004. Southern ocean iron enrichment experiment: Carbon cycling in high- and low-Si waters. *Science* 304, 408-414.
- Cochran, J.K., Bacon, M.P., Krishnaswami, S., Turekian, K.K., 1983. Po-210 and Pb-210 distributions in the central and eastern Indian-ocean. *Earth and Planetary Science Letters* 65, 433-452.

- Conte, M.H., Ralph, N. and Ross, E.H., 2001. Seasonal and interannual variability in deep ocean particle fluxes at the Oceanic Flux Program (OFP)/Bermuda Atlantic Time Series (BATS) site in the western Sargasso Sea near Bermuda. *Deep Sea Research Part II: Topical Studies in Oceanography* 48, 1471-1505.
- Csáky, T.Z., 1948. An estimation of bound hydroxylamine in biological materials. *Acta Chemica Scandinavica* 2, 450-454.
- Das, S.K., Marsili, E., 2011. Bioinspired metal nanoparticle: Synthesis, properties and application, nanomaterials, in: Rahman, M. (Ed.). InTech.
- Decho, A.W., Lopez, G.R., 1993. Exopolymer microenvironments of microbial-flora multiple and interactive effects on trophic relationships. *Limnology and Oceanography* 38, 1633-1645.
- Dhungana, S., Ratledge, C., Crumbliss, A.L., 2004. Iron chelation properties of an extracellular siderophore exochelin *MS*. *Inorganic Chemistry* 43, 6274-6283.
- Doucet, F.J., Lead, J.R., Santschi, P.H., 2007. Environmental colloids and particles: Behaviour, separation and characterisation, in: Wilkinson, K., Lead, J.R. (Eds.), *Colloid-trace element interactions in aquatic systems.*, 3 ed. John Wiley & Sons Ltd., pp. 95-158.
- Doucet, F.J., Schneider, C., Bones, S.J., Kretchmer, A., Moss, I., Tekely, P., Exley, C., 2001. The formation of hydroxyaluminosilicates of geochemical and biological significance. *Geochimica Et Cosmochimica Acta* 65, 2461-2467.
- Du, J.Z., Zhang, J., Baskaran, M., 2011. Applications of short-lived radionuclides (^7Be , ^{210}Pb , ^{210}Po , ^{137}Cs and ^{234}Th) to trace the sources, transport pathways and

- deposition of particles/sediments in rivers, estuaries and coasts, in: Baskaran, M. (Ed.), Handbook of environmental isotope geochemistry. Springer Berlin Heidelberg, pp. 305-329.
- Duan, S., Bianchi, T.S., 2007. Particulate and dissolved amino acids in the lower mississippi and pearl rivers (USA). *Marine Chemistry* 107, 214-229.
- Duckworth, O.W., Bargar, J.R. and Sposito, G., 2008. Sorption of ferric iron from ferrioxamine B to synthetic and biogenic layer type manganese oxides. *Geochimica Et Cosmochimica Acta* 72, 3371-3380.
- Falkowski, P.G., Barber, R.T., Smetacek, V., 1998. Biogeochemical controls and feedbacks on ocean primary production. *Science* 281, 200-206.
- Fanghänel, T., Neck, V., 2002. Aquatic chemistry and solubility phenomena of actinide oxides/hydroxides. *Pure and Applied Chemistry* 74, 1895-1907.
- Feng, H., Cochran, J.K., Hirschberg, D.J., 1999. Th-234 and Be-7 as tracers for the transport and dynamics of suspended particles in a partially mixed estuary. *Geochimica Et Cosmochimica Acta* 63, 2487-2505.
- Field, C.B., Behrenfeld, M.J., Randerson, J.T., Falkowski, P., 1998. Primary production of the biosphere: Integrating terrestrial and oceanic components. *Science* 281, 237-240.
- Filisetti-Cozzi, T.M.C.C. and Carpita, N.C., 1991. Measurement of uronic acids without interference from neutral sugars. *Analytical Biochemistry* 197, 157-162.

- Fisher, N.S., Burns, K.A., Cherry, R.D., Heyraud, M., 1983. Accumulation and cellular-distribution of Am-241, Po-210, and Pb-210 in two marine-algae. *Marine Ecology-Progress Series* 11, 233-237.
- Fisher, N.S., Cochran, J.K., Krishnaswami, S., Livingston, H.D., 1988. Predicting the oceanic flux of radionuclides on sinking biogenic debris. *Nature* 335, 622-625.
- Fisher, N.S., Reinfelder, J.R., 1995. The trophic transfer of metals in marine systems. *Metal speciation and bioavailability in aquatic systems*, 363-406.
- Fogg, G.E., 1983. The ecological significance of extracellular products of phytoplankton photosynthesis. *Botanica Marina* 26, 3-14.
- Frigeri, L. G., T. R. Radabaugh, P. A. Haynes, and M. Hildebrand. 2006. Identification of Proteins from a Cell Wall Fraction of the Diatom *Thalassiosira pseudonana* : Insights into Silica Structure Formation. *Molecular and Cellular Proteomics* 5, 182-193.
- Geibert, W. and Usbeck, R., 2004. Adsorption of thorium and protactinium onto different particle types: Experimental findings. *Geochimica Et Cosmochimica Acta* 68, 1489-1501.
- Geszvain, K., McCarthy, J.K. and Tebo, B.M., 2013. Elimination of Manganese(II,III) Oxidation in *Pseudomonas putida* GB-1 by a Double Knockout of Two Putative Multicopper Oxidase Genes. *Applied and Environmental Microbiology* 79, 357-366.

- Geszvain, K., Yamaguchi, A., Maybee, J. and Tebo, B., 2011. Mn(II) oxidation in *Pseudomonas putida* GB-1 is influenced by flagella synthesis and surface substrate. *Archives of Microbiology* 193, 605-614.
- Gledhill, M. and Van Den Berg, C.M.G., 1994. Determination of Complexation of Iron(III) with Natural Organic Complexing Ligands in Seawater Using Cathodic Stripping Voltammetry. *Marine Chemistry* 47, 41-54.
- Greenwood, N.N., Earnshaw, A., 1998. *Chemistry Of The Elements*.
- Guo, L.D., Hung, C.C., Santschi, P.H., Walsh, I.D., 2002a. ^{234}Th scavenging and its relationship to acid polysaccharide abundance in the Gulf of Mexico. *Marine Chemistry* 78, 103-119.
- Guo, L.D., Santschi, P.H., 1997a. Composition and cycling of colloids in marine environments. *Reviews of Geophysics* 35, 17-40.
- Guo, L.D., Santschi, P.H., 1997b. Isotopic and elemental characterization of colloidal organic matter from the Chesapeake Bay and Galveston Bay. *Marine Chemistry* 59, 1-15.
- Guo, L.D., Santschi, P.H., Baskaran, M., 1997. Interactions of thorium isotopes with colloidal organic matter in oceanic environments. *Colloids and Surfaces a-Physicochemical and Engineering Aspects* 120, 255-271.
- Guo, L.D., Santschi, P.H., Baskaran, M., Zindler, A., 1995. Distribution of dissolved and particulate ^{230}Th and ^{232}Th in seawater from the Gulf of Mexico and off Cape Hatteras as measured by SIMS. *Earth and Planetary Science Letters* 133, 117-128.

- Guo, L.D., Santschi, P.H., Ray, S.M., 2002b. Metal partitioning between colloidal and dissolved phases and its relation with bioavailability to american oysters. *Marine Environmental Research* 54, 49-64.
- Harrington, J.M., Parker, D.L., Bargar, J.R., Jarzecki, A.A., Tebo, B.M., Sposito, G. and Duckworth, O.W., 2012. Structural dependence of Mn complexation by siderophores: Donor group dependence on complex stability and reactivity. *Geochimica Et Cosmochimica Acta* 88, 106-119.
- Hauptkorn, S., Pavel, J. and Seltner, H., 2001. Determination of silicon in biological samples by ICP-OES after non-oxidative decomposition under alkaline conditions. *Fresenius' Journal of Analytical Chemistry* 370, 246-250.
- Hirose, K. and Tanoue, E., 2001. Strong ligands for thorium complexation in marine bacteria. *Marine Environmental Research* 51, 95-112.
- Hirose, K., 1995. The relationship between particulate uranium and thorium-complexing capacity of oceanic particulate matter. *Science of the Total Environment* 173, 195-201.
- Honeyman, B.D., Santschi, P.H., 1989. A Brownian-pumping model for oceanic trace-metal scavenging - evidence from Th-isotopes. *Journal of Marine Research* 47, 951-992.
- Honeyman, B.D., Santschi, P.H., 1991. Coupling adsorption and particle aggregation - laboratory studies of colloidal pumping using ⁵⁹Fe labeled hematite. *Environmental Science & Technology* 25, 1739-1747.

- Huang, S. and Conte, M.H., 2009. Source/process apportionment of major and trace elements in sinking particles in the Sargasso sea. *Geochimica Et Cosmochimica Acta* 73, 65-90.
- Huang, S., Sholkovitz, E.R. and Conte, M.H., 2007. Application of high-temperature fusion for analysis of major and trace elements in marine sediment trap samples. *Limnology and Oceanography: Methods* 5, 13-22.
- Hung, C.-C., Gong, G.-C., Santschi, P.H., 2012. ^{234}Th in different size classes of sediment trap collected particles from the Northwestern Pacific Ocean. *Geochimica Et Cosmochimica Acta* 91, 60-74.
- Hung, C.C., Guo, L.D., Roberts, K.A., Santschi, P.H., 2004a. Upper ocean carbon flux determined by the ^{234}Th approach and sediment traps using size-fractionated poc and ^{234}Th data from the Gulf of Mexico. *Geochemical Journal* 38, 601-611.
- Hung, C.C., Guo, L.D., Santschi, P.H., Alvarado-Quiroz, N., Haye, J.M., 2003a. Distributions of carbohydrate species in the Gulf of Mexico. *Marine Chemistry* 81, 119-135.
- Hung, C.C., Guo, L.D., Schultz, G.E., Pinckney, J.L., Santschi, P.H., 2003b. Production and flux of carbohydrate species in the Gulf of Mexico. *Global Biogeochemical Cycles* 17.
- Hung, C.C., Santschi, P.H., 2001. Spectrophotometric determination of total uronic acids in seawater using cation-exchange separation and pre-concentration by lyophilization. *Analytica Chimica Acta* 427, 111-117.

- Hung, C.C., Warnken, K., Santschi, P.H., 2004b. Degradation of carbohydrates and persistence of uronic acids in the Trinity River, Texas. Abstracts of Papers of the American Chemical Society 227, U1051-U1052.
- Hung, C.C., Xu, C., Santschi, P.H., Zhang, S.J., Schwehr, K.A., Quigg, A., Guo, L.D., Gong, G.C., Pinckney, J.L., Long, R.A., Wei, C.L., 2010. Comparative evaluation of sediment trap and ^{234}Th -derived POC fluxes from the upper oligotrophic waters of the Gulf of Mexico and the subtropical Northwestern Pacific Ocean. *Marine Chemistry* 121, 132-144.
- Hurd, D.C., Spencer, D.W., 1991. Marine particles: Analysis and characterization. AGU, Washington, DC.
- Hussain, N., Ferdelman, T.G., Church, T.M. and Luther, G., III, 1995. Bio-volatilization of Polonium: Results from laboratory analyses. *Aquatic Geochemistry* 1, 175-188.
- Issartel, J. P., A. Dupuis, C. Moral, and J. L. Girardet. 1991. Fluoride, Beryllium and ADP combine as a ternary complex in aqueous solution as revealed by a multinuclear NMR study. *European Biophysics Journal* 20, 115-126.
- Jiang, Y., Yoshida, T., Quigg, A., 2012. Photosynthetic performance, lipid production and biomass composition in response to nitrogen limitation in marine microalgae. *Plant Physiology and Biochemistry* 54, 70-77.
- Jiao, N., Herndl, G.J., Hansell, D.A., Benner, R., Kattner, G., Wilhelm, S.W., Kirchman, D.L., Weinbauer, M.G., Luo, T., Chen, F. and Azam, F., 2010. Microbial

production of recalcitrant dissolved organic matter: long-term carbon storage in the global ocean. *Nature Reviews Microbiology* 8, 593-599.

Kalmykov, S.N., Schäfer, T., Claret, F., Perminova, I.V., Petrova, A.B., Shcherbina, N.S., Teterin, Y.A., 2008. Sorption of neptunium onto goethite in the presence of humic acids with different hydroquinone group content. *Radiochimica Acta* 96, 685-690.

Kaste, J.M., Baskaran, M., 2011. Meteoric ^7Be and ^{10}Be as process tracers in the environment. *Handbook of Environmental Isotope Geochemistry*, 61-85.

Keith-Roach, M.J., Buratti, M.V. and Worsfold, P.J., 2005. Thorium complexation by hydroxamate siderophores in perturbed multicomponent systems using flow injection Electrospray Ionization Mass Spectrometry. *Analytical Chemistry* 77, 7335-7341.

Kelleher, B.P., Simpson, A.J., 2006. Humic substances in soils: Are they really chemically distinct? *Environmental Science & Technology* 40, 4605-4611.

Kim, G., Hussain, N., Scudlark, J.R., Church, T.M., 2000. Factors influencing the atmospheric depositional fluxes of stable Pb, Pb-210, and Be-7 into Chesapeake Bay. *Journal of Atmospheric Chemistry* 36, 65-79.

Kim, M.A., Panak, P.J., Yun, J.I., Kim, J.I., Klenze, R., Kohler, K., 2003. Interaction of actinides with aluminosilicate colloids in Statu Nascendi part I: Generation and characterization of actinide(III)-pseudocolloids. *Colloids and Surfaces A- Physicochemical and Engineering Aspects* 216, 97-108.

- Kondo, Y., Takeda, S. and Furuya, K., 2012. Distinct trends in dissolved Fe speciation between shallow and deep waters in the Pacific Ocean. *Marine Chemistry* 134–135, 18-28.
- Kretschmer, S., Geibert, W., van der Loeff, M.M.R., Schnabel, C., Xu, S., Mollenhauer, G., 2011. Fractionation of ^{230}Th , ^{231}Pa , and ^{10}Be induced by particle size and composition within an opal-rich sediment of the Atlantic Southern Ocean. *Geochimica Et Cosmochimica Acta* 75, 6971-6987.
- Kröger, N., Deutzmann, R., Sumper, M., 1999. Polycationic peptides from diatom biosilica that direct silica nanosphere formation. *Science* 286, 1129-1132.
- Kröger, N., Lorenz, S., Brunner, E., Sumper, M., 2002. Self-assembly of highly phosphorylated Silaffins and their function in biosilica morphogenesis. *Science* 298, 584-586.
- Kröger, N., Poulsen, N., 2008. Diatoms—from cell wall biogenesis to nanotechnology. *Annual Review of Genetics* 42, 83-107.
- Kröger, N., Sandhage, K.H., 2010. From diatom biomolecules to bioinspired syntheses of silica- and titania-based materials. *MRS Bulletin* 35, 122-126.
- Kumar, M.D., Sarma, V.V.S.S., Ramaiah, N., Gauns, M., de Sousa, S.N., 1998. Biogeochemical significance of transport exopolymer particles in the Indian Ocean. *Geophysical Research Letters* 25, 81-84.
- Kumar, N., Anderson, R.F., Mortlock, R.A., Froelich, P.N., Kubik, P., Dittrich-Hannen, B., Suter, M., 1995. Increased biological productivity and export production in the Glacial Southern Ocean. *Nature* 378, 675-680.

- Kurzak, B., Kozlowski, H. and Farkas, E., 1992. ChemInform Abstract: Hydroxamic and Aminohydroxamic Acids and Their Complexes with Metal Ions. ChemInform, 23(40).
- Lam, P.J., Bishop, J.K., Waychunas, G.A., Sutton, S.R. and Newville, M., 2002. Characterization of Fe in Marine Particulates via Micro-XAS: Possibilities and Limitations. APS Activity Report 2001. Argonne National Lab Laboratory, Argonne, IL; ANL-02/06.
- Lam, P.J., Ohnemus, D.C. and Marcus, M.A., 2012. The speciation of marine particulate iron adjacent to active and passive continental margins. *Geochimica Et Cosmochimica Acta* 80, 108-124.
- Langmuir, D., Herman, J.S., 1980. The mobility of thorium in natural waters at low temperatures. *Geochimica Et Cosmochimica Acta* 44, 1753-1766.
- LaRock, P., Hyun, J.H., Boutelle, S., Burnett, W.C., Hull, C.D., 1996. Bacterial mobilization of polonium. *Geochimica Et Cosmochimica Acta* 60, 4321-4328.
- Lee, C., Wakeham, S. and Arnosti, C., 2004. Particulate Organic Matter in the Sea: The Composition Conundrum. *Ambio* 33, 565-575.
- Leppard, G.G., West, M.M., Flannigan, D.T., Carson, J., Lott, J.N.A., 1997. A classification scheme for marine organic colloids in the adriatic sea: Colloid speciation by transmission electron microscopy. *Canadian Journal of Fisheries and Aquatic Sciences* 54, 2334-2349.
- Li, Y.-H., 1991. Distribution patterns of the elements in the ocean: A synthesis. *Geochimica Et Cosmochimica Acta* 55, 3223-3240.

- Li, Y.-H., 2000. A compendium of geochemistry: From solar nebula to the human brain. Princeton University Press.
- Li, Y.-H., 2005. Controversy over the relationship between major components of sediment-trap materials and the bulk distribution coefficients of ^{230}Th , ^{231}Pa , and ^{10}Be . *Earth and Planetary Science Letters* 233, 1-7.
- Li, Y.-H., Burkhardt, L., Buchholtz, M., Ohara, P. and Santschi, P.H., 1984. Partition of radiotracers between suspended particles and seawater. *Geochimica Et Cosmochimica Acta* 48, 2011-2019.
- Lieser, K.H., Gleitsmann, B., Peschke, S., Steinkopff, T., 1986. Colloid formation and sorption of radionuclides in natural systems. *Radiochimica Acta* 40, 39-47.
- Longhurst, A., Sathyendranath, S., Platt, T., Caverhill, C., 1995. An estimate of global primary production in the ocean from satellite radiometer data. *Journal of Plankton Research* 17, 1245-1271.
- Madison, A.S., Tebo, B.M. and Luther Iii, G.W., 2011. Simultaneous determination of soluble manganese(III), manganese(II) and total manganese in natural (pore)waters. *Talanta* 84, 374-381.
- Mann, D.G., 1999. The species concept in diatoms. *Phycologia* 38, 437.
- Marquardt, C.M., Panak, P.J., Apostolidis, C., Morgenstern, A., Walther, C., Klenze, R. and Fanghänel, T., 2004. Fluorescence spectroscopy on protactinium(IV) in aqueous solution. *Radiochimica Acta* 92, 445-447.

- Masque, P., Sanchez-Cabeza, J.A., Bruach, J.M., Palacios, E. and Canals, M., 2002. Balance and residence times of ^{210}Pb and ^{210}Po in surface waters of the northwestern Mediterranean Sea. *Continental Shelf Research* 22, 2127-2146.
- Matisoff, G., Wilson, C.G., Whiting, P.J., 2005. The Be-7/Pb-210(xs) ratio as an indicator of suspended sediment age or fraction new sediment in suspension. *Earth Surface Processes and Landforms* 30, 1191-1201.
- Mawji, E., Gledhill, M., Milton, J.A., Tarran, G.A., Ussher, S., Thompson, A., Wolff, G.A., Worsfold, P.J. and Achterberg, E.P., 2008. Hydroxamate Siderophores: Occurrence and Importance in the Atlantic Ocean. *Environmental Science & Technology* 42, 8675-8680.
- Menzel, D.W. and Ryther, J.H., 1959. The annual cycle of primary production in the Sargasso Sea off Bermuda. *Deep Sea Research* 6, 351-367.
- Moran, S.B., Shen, C.C., Edmonds, H.N., Weinstein, S.E., Smith, J.N. and Edwards, R.L., 2002. Dissolved and particulate ^{231}Pa and ^{230}Th in the Atlantic Ocean: Constraints on intermediate/deep water age, boundary scavenging, and $^{231}\text{Pa}/^{230}\text{Th}$ fractionation. *Earth and Planetary Science Letters* 203, 999-1014.
- Mort, A.J., Lamport, D.T.A., 1977. Anhydrous hydrogen fluoride deglycosylates glycoproteins. *Analytical Biochemistry* 82, 289-309.
- Murphy, R.J., Lenhart, J.J., Honeyman, B.D., 1999. The sorption of thorium (IV) and uranium (VI) to hematite in the presence of natural organic matter. *Colloids and Surfaces A: Physicochemical and Engineering Aspects* 157, 47-62.

- National Research Council, C.o.W.Q.C., 1972. Suspended particulate materials, Water quality criteria, 1972: a report of the Committee on Water Quality Criteria, Environmental Studies Board, National Academy of Sciences, National Academy of Engineering, Washington, D.C., 1972. Environmental Protection Agency : for sale by the Supt. of Docs., U.S. Govt. Print. Off.
- Neilands, J.B., 1995. Siderophores - structure and function of microbial iron transport compounds. *Journal of Biological Chemistry* 270, 26723-26726.
- Nelson, D.M., Treguer, P., Brzezinski, M.A., Leynaert, A., Queguiner, B., 1995. Production and dissolution of biogenic silica in the ocean - revised global estimates, comparison with regional data and relationship to biogenic sedimentation. *Global Biogeochemical Cycles* 9, 359-372.
- Neu, M.P., Matonic, J.H., Ruggiero, C.E. and Scott, B.L., 2000. Structural characterization of a plutonium(IV) siderophore complex: Single-crystal structure of Pu-desferrioxamine E. *Angewandte Chemie-International Edition* 39, 1442-1444.
- Nozaki, Y., Thomson, J., Turekian, K.K., 1976. The distribution of ^{210}Pb and ^{210}Po in the surface waters of the pacific ocean. *Earth and Planetary Science Letters* 32, 304-312.
- Nyffeler, U.P., Li, Y.-H. and Santschi, P.H., 1984. A kinetic approach to describe trace-element distribution between particles and solution in natural aquatic systems. *Geochimica Et Cosmochimica Acta* 48, 1513-1522.

- Östhols, E., Bruno, J., Grenthe, I., 1994. On the influence of carbonate on mineral dissolution: III. The solubility of microcrystalline ThO₂ in CO₂-H₂O media. *Geochimica Et Cosmochimica Acta* 58, 613-623.
- Panak, P.J., Kim, M.A., Yun, J.I., Kim, J.I., 2003. Interaction of actinides with aluminosilicate colloids in *Statu Nascendi*. Part II: Spectroscopic speciation of colloid-borne actinides(III). *Colloids and Surfaces A-Physicochemical and Engineering Aspects* 227, 93-103.
- Passow, U., Alldredge, A.L., 1994. Distribution, size and bacterial-colonization of transparent exopolymer particles (TEP) in the ocean. *Marine Ecology-Progress Series* 113, 185-198.
- Passow, U., Alldredge, A.L., Logan, B.E., 1994. The role of particulate carbohydrate exudates in the flocculation of diatom blooms. *Deep-Sea Research Part I-Oceanographic Research Papers* 41, 335-357.
- Poulsen, N., Sumper, M. and Kroger, N., 2003. Biosilica formation in diatoms: Characterization of native silaffin-2 and its role in silica morphogenesis. *Proceedings of the National Academy of Sciences of the United States of America* 100, 12075-12080.
- Quigley, M.S., Santschi, P.H., Hung, C.C., Guo, L.D., Honeyman, B.D., 2002. Importance of acid polysaccharides for ²³⁴Th complexation to marine organic matter. *Limnology and Oceanography* 47, 367-377.
- Ragueneau, O., Treguer, P., Leynaert, A., Anderson, R.F., Brzezinski, M.A., DeMaster, D.J., Dugdale, R.C., Dymond, J., Fischer, G., Francois, R., Heinze, C., Maier-

- Reimer, E., Martin-Jezequel, V., Nelson, D.M., Queguiner, B., 2000. A review of the Si cycle in the modern ocean: Recent progress and missing gaps in the application of biogenic opal as a paleoproductivity proxy. *Global and Planetary Change* 26, 317-365.
- Reid, R.T., Live, D.H., Faulkner, D.J., Butler, A., 1993. A siderophore from a marine bacterium with an exceptional ferric ion affinity constant. *Nature* 366, 455-458.
- Reimann, B.E.F., Lewin, J.C., Volcani, B.E., 1965. Studies on biochemistry and fine structure of silica shell formation in diatoms .I. Structure of cell wall of *cylindrotheca fusiformis* reimann and lewin. *Journal of Cell Biology* 24, 39-55.
- Roberts, K.A., Xu, C., Hung, C.C., Conte, M.H., Santschi, P.H., 2009. Scavenging and fractionation of thorium vs. Protactinium in the ocean, as determined from particle-water partitioning experiments with sediment trap material from the Gulf of Mexico and Sargasso Sea. *Earth and Planetary Science Letters* 286, 131-138.
- Robinson, R.S., Brunelle, B.G., Sigman, D.M., 2004. Revisiting nutrient utilization in the glacial antarctic: Evidence from a new method for diatom-bound isotopic analysis. *Paleoceanography* 19, PA3001.
- Rue, E.L. and Bruland, K.W., 1995. Complexation of Iron(III) by Natural Organic-Ligands in the Central North Pacific as Determined by a New Competitive Ligand Equilibration Adsorptive Cathodic Stripping Voltammetric Method. *Marine Chemistry* 50, 117-138.
- Rutgers van der Loeff, M.M., Geibert, W., 2008. U- and Th-series nuclides as tracers of particle dynamics, scavenging and biogeochemical cycles in the oceans, in:

- Krishnaswami, S., Kirk Cochran, J. (Eds.), Radioactivity in the environment. Elsevier, pp. 227-268.
- Sambrook, J., Fritsch, E.F., Maniatis, T., Nolan, C., 1989. Molecular cloning: A laboratory manual. Cold Spring Harbor Laboratory.
- Santschi, P.H., 1997. Colloids in oceanic environments. Composition and importance for trace element cycles. Abstracts of Papers of the American Chemical Society 214, 2-ENVR.
- Santschi, P.H., Burd, A.B., Gaillard, J.F., Lazarides, A.A., 2005. Transport of materials and chemicals by nanoscale colloids and micro- to macro-scale flocs in marine, freshwater, and engineered systems.
- Santschi, P.H., Guo, L.D., Baskaran, M., Trumbore, S., Southon, J., Bianchi, T.S., Honeyman, B., Cifuentes, L., 1995. Isotopic evidence for the contemporary origin of high-molecular weight organic matter in oceanic environments. *Geochimica Et Cosmochimica Acta* 59, 625-631.
- Santschi, P.H., Guo, L.D., Trombore, S., Southon, J., Bianchi, T.S., Cifuentes, L., 1994. Isotopic and biochemical-evidence for the recent origin of colloidal organic-matter in the ocean .1. Carbon partitioning. Abstracts of Papers of the American Chemical Society 207, 146-GEOC.
- Santschi, P.H., Hung, C.C., Schultz, G., Alfarado-Quiroz, N., Guo, L.D., Pinckney, J., Walsh, I., 2003. Control of acid polysaccharide production and Th-234 and POC export fluxes by marine organisms. *Geophysical Research Letters* 30, 16

- Santschi, P.H., Murray, J.W., Baskaran, M., Benitez-Nelson, C.R., Guo, L.D., Hung, C.C., Lamborg, C., Moran, S.B., Passow, U., Roy-Barman, M., 2006. Thorium speciation in seawater. *Marine Chemistry* 100, 250-268.
- Santschi, P.H., Roberts, K.A., Guo, L.D., 2002. Organic nature of colloidal actinides transported in surface water environments. *Environmental Science & Technology* 36, 3711-3719.
- Sapriel, G. and others 2009. Genome-Wide Transcriptome Analyses of Silicon Metabolism in *Phaeodactylum tricornutum* Reveal the Multilevel Regulation of Silicic Acid Transporters. *PLoS ONE* 4, e7458.
- Scheffel, A., Poulsen, N., Shian, S., Kröger, N., 2011. Nanopatterned protein microrings from a diatom that direct silica morphogenesis. *Proceedings of the National Academy of Sciences*.
- Schindler, P.W. and Stumm, W., 1987. The surface chemistry of oxides, hydroxides and oxide minerals. In: W. Stumm (Editor), *Aquatic Surface Chemistry: Chemical Processes at the Particle-Water Interface*. John Wiley & Sons, Inc., pp. 83-110.
- Schindler, P.W., 1975. Removal of trace metals from the oceans: a zero order model. In: C.z.I. Mora and J.a.z.i.u.B. institut (Editors), *Thalassia Jugoslavica*. Center for Marine Research, pp. 101-111.
- Schindler, P.W., Fürst, B., Dick, R. and Wolf, P.U., 1976. Ligand properties of surface silanol groups. I. surface complex formation with Fe^{3+} , Cu^{2+} , Cd^{2+} , and Pb^{2+} . *Journal of Colloid and Interface Science* 55, 469-475.

- Schmitt, J., Nivens, D., White, D.C., Flemming, H.-C., 1995. Changes of biofilm properties in response to sorbed substances - an FTIR-ATR study. *Water Science and Technology* 32, 149-155.
- Scholten, J.C., Fietzke, J., Mangini, A., Stoffers, P., Rixen, T., Gaye-Haake, B., Blanz, T., Ramaswamy, V., Sirocko, F., Schulz, H. and Ittekkot, V., 2005. Radionuclide fluxes in the Arabian Sea: the role of particle composition. *Earth and Planetary Science Letters* 230, 319-337.
- Schumann, D., Ayranov, M., Stowasser, T., Gialanella, L., Leva, A.d., Romano, M., Schuermann, D., 2013. Radiochemical separation of ^7Be from the cooling water of the neutron spallation source sinq at PSI. *Radiochimica Acta* 101, 509-514.
- Scott, B. L., T. M. McCleskey, A. Chaudhary, E. Hong-Geller, and S. Gnanakaran. 2008. The bioinorganic chemistry and associated immunology of chronic beryllium disease. *Chemical Communications* 7, 2837-2847.
- Sigleo, A.C., Means, J.C., 1990. Organic and inorganic components in estuarine colloids: Implications for sorption and transport of pollutants, in: Ware, G. (Ed.), *Reviews of environmental contamination and toxicology*. Springer New York, pp. 123-147.
- Sirajuddin, Bhangar, M.I., Niaz, A., Shah, A., Rauf, A., 2007. Ultra-trace level determination of hydroquinone in waste photographic solutions by UV-VIS spectrophotometry. *Talanta* 72, 546-553.
- Spiro, T.G., Bargar, J.R., Sposito, G. and Tebo, B.M., 2009. Bacteriogenic Manganese Oxides. *Accounts of Chemical Research* 43, 2-9.

- Steinmann, P., Billen, T., Loizeau, J.I., Dominik, J., 1999. Beryllium-7 as a tracer to study mechanisms and rates of metal scavenging from lake surface waters. *Geochimica Et Cosmochimica Acta* 63, 1621-1633.
- Stewart, G., Kirk Cochran, J., Xue, J., Lee, C., Wakeham, S.G., Armstrong, R.A., Masqué, P., Carlos Miquel, J., 2007. Exploring the connection between ^{210}Po and organic matter in the Northwestern Mediterranean. *Deep Sea Research Part I: Oceanographic Research Papers* 54, 415-427.
- Stewart, G.M., Fisher, N.S., 2003a. Bioaccumulation of polonium-210 in marine copepods. *Limnology and Oceanography* 48, 2011-2019.
- Stewart, G.M., Fisher, N.S., 2003b. Experimental studies on the accumulation of polonium-210 by marine phytoplankton. *Limnology and Oceanography* 48, 1720-1720.
- Stewart, G.M., Fowler, S.W., Teyssie, J.L., Cotret, O., Cochran, J.K., Fisher, N.S., 2005. Contrasting transfer of polonium-210 and lead-210 across three trophic levels in marine plankton. *Marine Ecology-Progress Series* 290, 27-33.
- Strickland, J.D.H. and Parsons, T.R., 1972. A practical handbook of seawater analysis, Bulletin 167. Fisheries Research Board of Canada, Ottawa.
- Stumm, W., Morgan, J.J., 1996. Chemical equilibria and rates in natural waters, *Aquatic chemistry*, 3rd ed. John Wiley & Sons, Inc., , New York, p. 1022.
- Šulcek, Z., Povondra, P., 1989. *Methods of decomposition in inorganic analysis*. CRC Press.

- Tateda, Y., Carvalho, F.P., Fowler, S.W. and Miquel, J.-C., 2003. Fractionation of ^{210}Po and ^{210}Pb in coastal waters of the NW Mediterranean continental margin. *Continental Shelf Research* 23, 295-316.
- Thakur, U.K., Shah, D., Sharma, R.S., Sawant, R.M., Ramakumar, K.L., 2006. Studies on protonation and Th(IV) complexation behaviour of dihydroxybenzenes in aqueous 1 M NaClO_4 medium. *Radiochimica Acta* 94, 859-864.
- Toner, B.M., M.A. Marcus, K.J. Edwards, O. Rouxel and German., C.R., 2012. Measuring the form of iron in hydrothermal plume particles. *Oceanography* 25, 209-212.
- Van Loon, J.C., 1985. Selected methods of trace metal analysis: Biological and environmental samples. Wiley.
- Verdugo, P., 2012. Marine microgels. *Annual Review of Marine Science* 4, 375-400.
- Verdugo, P., Alldredge, A.L., Azam, F., Kirchman, D.L., Passow, U., Santschi, P.H., 2004. The oceanic GEL phase: A bridge in the dom-pom continuum. *Marine Chemistry* 92, 67-85.
- Verdugo, P., Santschi, P.H., 2010. Polymer dynamics of DOC networks and GEL formation in seawater. *Deep-Sea Research Part II-Topical Studies in Oceanography* 57, 1486-1493.
- Vraspir, J.M., Butler, A., 2009. Chemistry of marine ligands and siderophores. *Annual Review of Marine Science* 1, 43-63.
- Walter, H. J., M. M. R. Vanderloeff, and H. Hoeltzen. 1997. Enhanced scavenging of Pa-231 relative to Th-230 in the south Atlantic south of the Polar front:

- Implications for the use of the Pa-231/Th-230 ratio as a paleoproductivity proxy. *Earth and Planetary Science Letters* 149, 85-100.
- Wells, L., Goldberg, E.D., 1994. The distribution of colloids in the North Atlantic and Southern Oceans.
- Wells, M.L., 1998. Marine colloids: A neglected dimension. *Nature* 391, 530-531.
- Wells, M.L., Goldberg, E.D., 1992. Marine submicron particles. *Marine Chemistry* 40, 5-18.
- Wen, L.-S., Santschi, P., Gill, G., Paternostro, C., 1999. Estuarine trace metal distributions in Galveston Bay: Importance of colloidal forms in the speciation of the dissolved phase. *Marine Chemistry* 63, 185-212.
- Wen, L.S., Santschi, P.H., Gill, G.A., Paternostro, C.L., Lehman, R.D., 1997a. Colloidal and particulate silver in river and estuarine waters of Texas. *Environmental Science & Technology* 31, 723-731.
- Wen, L.S., Santschi, P.H., Gill, G.A., Tang, D.G., 2002. Silver concentrations in Colorado, USA, watersheds using improved methodology. *Environmental Toxicology and Chemistry* 21, 2040-2051.
- Wen, L.S., Santschi, P.H., Tang, D.G., 1997b. Interactions between radioactively labeled colloids and natural particles: Evidence for colloidal pumping. *Geochimica Et Cosmochimica Acta* 61, 2867-2878.
- Wen, L.S., Santschi, P.H., Warnken, K.W., Davison, W., Zhang, H., Li, H.P., Jiann, K.T., 2011. Molecular weight and chemical reactivity of dissolved trace metals

- (Cd, Cu, Ni) in surface waters from the mississippi river to Gulf of Mexico. *Estuarine Coastal and Shelf Science* 92, 649-658.
- Wen, L.S., Stordal, M.C., Tang, D.G., Gill, G.A., Santschi, P.H., 1996. An ultraclean cross-flow ultrafiltration technique for the study of trace metal phase speciation in seawater. *Marine Chemistry* 55, 129-152.
- Wen, L.S., Warnken, K.W., Santschi, P.H., 2008. The role of organic carbon, iron, and aluminium oxyhydroxides as trace metal carriers: Comparison between the Trinity River and the Trinity River estuary (Galveston Bay, Texas). *Marine Chemistry* 112, 20-37.
- Wieneke, R., Bernecker, A., Riedel, R., Sumper, M., Steinem, C. and Geyer, A., 2011. Silica precipitation with synthetic Silaffin peptides. *Organic & Biomolecular Chemistry* 9, 5482-5486.
- Winkelmann, G., 2002. Microbial siderophore-mediated transport. *Biochemical Society Transactions* 30, 691-696.
- Woźniak, S.B., Stramski, D., Stramska, M., Reynolds, R.A., Wright, V.M., Miksic, E.Y., Cichocka, M. and Cieplak, A.M., 2010. Optical variability of seawater in relation to particle concentration, composition, and size distribution in the nearshore marine environment at Imperial Beach, California. *Journal of Geophysical Research: Oceans* 115, C08027.
- Xu, C., Chen, H., Sugiyama, Y., Zhang, S., Li, H.-P., Ho, Y.-F., Chuang, C.-Y., Schwehr, K.A., Kaplan, D.I., Yeager, C., Roberts, K.A., Hatcher, P.G. and Santschi, P.H., 2013. Novel molecular-level evidence of iodine binding to natural

organic matter from Fourier Transform Ion Cyclotron Resonance Mass Spectrometry. *Science of the Total Environment* 449, 244-252.

Xu, C., Santschi, P.H., Hung, C.C., Zhang, S.J., Schwehr, K.A., Roberts, K.A., Guo, L.D., Gong, G.C., Quigg, A., Long, R.A., Pinckney, J.L., Duan, S.W., Amon, R., Wei, C.L., 2011a. Controls of ^{234}Th removal from the oligotrophic ocean by polyuronic acids and modification by microbial activity. *Marine Chemistry* 123, 111-126.

Xu, C., Santschi, P.H., Schwehr, K.A., Hung, C.C., 2009. Optimized isolation procedure for obtaining strongly actinide binding exopolymeric substances (EPS) from two bacteria (*sagittula stellata* and *pseudomonas fluorescens* biovar II). *Bioresource Technology* 100, 6010-6021.

Xu, C., Santschi, P.H., Zhong, J.Y., Hatcher, P.G., Francis, A.J., Dodge, C.J., Roberts, K.A., Hung, C.C., Honeyman, B.D., 2008. Colloidal cutin-like substances cross-linked to siderophore decomposition products mobilizing plutonium from contaminated soils. *Environmental Science & Technology* 42, 8211-8217.

Xu, C., Zhang, S.J., Chuang, C.-Y., Miller, E.J., Schwehr, K.A., Santschi, P.H., 2011b. Chemical composition and relative hydrophobicity of microbial exopolymeric substances (EPS) isolated by anion exchange chromatography and their actinide-binding affinities. *Marine Chemistry* 126, 27-36.

Xu, C., Zhong, J.Y., Hatcher, P.G., Zhang, S.J., Li, H.P., Ho, Y.F., Schwehr, K.A., Kaplan, D.I., Roberts, K.A., Brinkmeyer, R., Yeager, C.M., Santschi, P.H., 2012. Molecular environment of stable iodine and radioiodine (I-129) in natural

- organic matter: Evidence inferred from nmr and binding experiments at environmentally relevant concentrations. *Geochimica Et Cosmochimica Acta* 97, 166-182.
- Yang, W., Guo, L., Chuang, C.-Y., Santschi, P.H., Schumann, D., Ayrarov, M., 2013a. Influence of macromolecular organic matter on the adsorption of ^{210}Pb , ^{210}Po and ^7Be on nanoparticles in seawater. *Geochimica et Cosmochimica Acta* (submitted).
- Yang, W., Guo, L., Chuang, C.-Y., Schumann, D., Ayrarov, M., Santschi, P.H., 2013b. Adsorption characteristics of ^{210}Pb , ^{210}Po and ^7Be onto micro-particle surfaces and the effects of macromolecular organic compounds. *Geochimica Et Cosmochimica Acta* 107, 47-64.
- Zeh, P., Kim, J.I., Marquardt, C.M., Artinger, R., 1999. The reduction of Np(V) in groundwater rich in humic substances. *Radiochimica Acta* 87, 23-28.
- Zhang, S., Jiang, Y., Chen, C.-S., Creeley, D., Schwehr, K.A., Quigg, A., Chin, W.-C., Santschi, P.H., 2013. Ameliorating effects of extracellular polymeric substances excreted by *Thalassiosira pseudonana* on algal toxicity of CdSe quantum dots. *Aquatic Toxicology* 126, 214-223.
- Zhang, S.J., Santschi, P.H., 2009. Application of cross-flow ultrafiltration for isolating exopolymeric substances from a marine diatom (*amphora* sp.). *Limnology and Oceanography-Methods* 7, 419-429.
- Zhang, S.J., Xu, C., Santschi, P.H., 2008. Chemical composition and $^{234}\text{Th}(\text{IV})$ binding of extracellular polymeric substances (EPS) produced by the marine diatom *amphora* sp. *Marine Chemistry* 112, 81-92.

Zuo, Z. and Eisma, D., 1993. ^{210}Pb and ^{210}Po distributions and disequilibrium in the coastal and shelf waters of the southern North Sea. *Continental Shelf Research* 13, 999-1022.